

University of Texas at Arlington

MavMatrix

Biology Dissertations

Department of Biology

Spring 2024

CORALS IN CRISIS: A TRANSCRIPTOMIC INVESTIGATION OF STONY CORAL TISSUE LOSS DISEASE

Kelsey M. Beavers

University of Texas at Arlington

Follow this and additional works at: https://mavmatrix.uta.edu/biology_dissertations



Part of the [Bioinformatics Commons](#), [Cell Biology Commons](#), [Computational Biology Commons](#), [Genomics Commons](#), [Immunology of Infectious Disease Commons](#), [Integrative Biology Commons](#), and the [Marine Biology Commons](#)

Recommended Citation

Beavers, Kelsey M., "CORALS IN CRISIS: A TRANSCRIPTOMIC INVESTIGATION OF STONY CORAL TISSUE LOSS DISEASE" (2024). *Biology Dissertations*. 1.

https://mavmatrix.uta.edu/biology_dissertations/1

This Dissertation is brought to you for free and open access by the Department of Biology at MavMatrix. It has been accepted for inclusion in Biology Dissertations by an authorized administrator of MavMatrix. For more information, please contact leah.mccurdy@uta.edu, erica.rousseau@uta.edu, vanessa.garrett@uta.edu.

CORALS IN CRISIS: A TRANSCRIPTOMIC INVESTIGATION OF STONY CORAL
TISSUE LOSS DISEASE

by

KELSEY MARIE BEAVERS

DISSERTATION

Submitted in partial fulfillment of the requirements
for the degree of Doctor of Philosophy at
The University of Texas at Arlington
May 2024

Arlington, Texas

Supervising Committee:

Laura Mydlarz (Supervising Professor)
Amy Apprill
Joseph Boll
Todd Castoe
Kayunta Johnson-Winters

Abstract

CORALS IN CRISIS: A TRANSCRIPTOMIC INVESTIGATION OF STONY CORAL
TISSUE LOSS DISEASE

Kelsey Marie Beavers

The University of Texas at Arlington, 2024

Supervising Professor: Laura Mydlarz

Coral reefs face existential threats due to climate change and human activities. The combined effects of ocean warming, overfishing, pollution, and habitat destruction have fundamentally altered the functionality of coral reefs and are driving a drastic increase in the prevalence and severity of coral disease outbreaks. Stony coral tissue loss disease (SCTLD) has emerged one of the most devastating disturbances to Caribbean reef ecosystems on record. Despite notable progress, the cellular mechanisms driving SCTLD pathogenesis remain poorly understood. To address this issue, my dissertation investigates the gene expression, histopathology, immune protein activity, and symbiont community dynamics involved in SCTLD progression and susceptibility. In chapter two, I utilize a multi-species SCTLD transmission experiment to examine the gene expression shifts within the coral host and its algal endosymbiont (family Symbiodiniaceae) in response to SCTLD infection. In chapter three, I correlate histology, immune protein activity, and Symbiodiniaceae community data with constitutive gene expression patterns to identify the factors contributing to disease susceptibility. In chapter four, I present a supervised machine learning framework to examine the gene expression patterns involved in SCTLD progression in a major reef-building coral and its dominant algal endosymbiont. Overall, this work establishes a foundation for integrating host and endosymbiont gene expression patterns with physiological phenotypes into coral disease research and identifies key factors contributing to SCTLD susceptibility and pathogenesis.

Copyright by
Kelsey Marie Beavers

2024

Chapter 2 is *published* under an open-access license in *Nature Communications*.

DOI: <https://doi.org/10.1038/s41467-023-38612-4>

Chapter 3 is currently *under review* at the journal *Integrative and Comparative Biology* and has no current copyright.

Chapter 4 is currently *under review* at the journal *Molecular Ecology* and has no current copyright.

Acknowledgments

I am profoundly grateful to my incredible parents, Lyle and Kelly Beavers, whose unwavering support and encouragement have guided me through every challenge. I am thankful for my wonderful big sister, Devon Lord, who always has and always will inspire me. I am also grateful for my brother-in-law, Dr. Nathan Lord, whose encouragement of my scientific endeavors helped push me to become the researcher that I am today. In addition, I extend my heartfelt gratitude to my boyfriend, Spencer Link, and to my best friends, Annalee Rhodes, Maria Cavazos, and Madison Hockman, whose steadfast love and care sustained me through the rigors of my Ph.D. journey. Their companionship lifted me up when I needed it most, and I surely couldn't have made this body of work without them. I am deeply grateful to my lab cohort, Madison Emery and Emily Van Buren, whose camaraderie and expertise were indispensable to my graduate school experience. It has been a privilege to grow both scientifically and professionally alongside them, and I look forward to witnessing their continued success when our time together at UTA comes to an end. Finally, I extend my sincere gratitude to my dissertation committee, whose guidance has been instrumental in my development as a scientist. I am particularly thankful for my advisor, Dr. Laura Mydlarz. Her mentorship has empowered me to become a capable and confident researcher, and I will always be grateful for the time she has invested in my success.

Table of Contents:

| | |
|--|-------------|
| Abstract | II |
| Acknowledgments | IV |
| Figure List..... | VI |
| Table List..... | VIII |
| Chapter 1: Introductory Material | 1 |
| Chapter 2: Stony coral tissue loss disease induces transcriptional signatures of in situ degradation of dysfunctional Symbiodiniaceae | 6 |
| Chapter 3: Investigating stony coral tissue loss disease susceptibility and progression: insights from gene expression, histology, and physiology | 52 |
| Chapter 4: Classifying gene expression profiles of various tissue states in stony coral tissue loss disease | 91 |
| Chapter 5: Conclusion | 128 |
| References..... | 132 |

Figure List

Chapter 2

- Figure 1 – Overview of experimental design and analysis
- Figure 2 – Expression boxplots of relevant orthologs with significant differential expression between disease states
- Figure 3 – Expression of single-copy coral orthologs significantly correlated to disease phenotypes
- Figure 4 – Single-copy orthologs with significant differences in expression between disease states
- Figure 5 – Dominant symbiont DEGs
- Figure 6 – Single-copy symbiont orthologs with significant differences in expression between disease states
- Figure 7 – *Rab7* correlations
- Figure 8 – Histology and *rab7* correlation analysis

Chapter 3

- Figure 1 – Measured phenotype traits for all samples from two health states from the SCTL D transmission experiment
- Figure 2 – Shortened WGCNA module-trait heatmap
- Figure 3 – Eigengene analysis of modules associated with high relative risk of SCTL D
- Figure 4 – Eigengene analysis of modules associated with low relative risk of SCTL D
- Figure 5 – Eight selected genes with high significance to relative risk of SCTL D
- Figure 6 – Grey module genes with high significance to health status

Chapter 4

- Figure 1 – Experimental design and analysis workflow
- Figure 2 – Functional enrichment of up- and downregulated genes within the top 500 *M. cavernosa* features from each tissue health state
- Figure 3 – Functional enrichment of up- and downregulated genes within the top 500 *C. goreau* features from each tissue health state
- Figure 4 – Top features in HH *M. cavernosa*
- Figure 5 – Top features in HD *M. cavernosa*
- Figure 6 – Top features in LD *M. cavernosa*
- Figure 7 – Selected top features in *C. goreau*
- Figure 8 – Characterization of SCTLD tissue health states in *M. cavernosa* and *C. goreau*

Table List

Chapter 2

- Table 1 – Reference transcriptome sources and assembly metrics

Chapter 4

- Table 1 – Reference transcriptome assembly metrics

Chapter 1: Introductory Material

Coral reefs are one of the most diverse and productive ecosystems on the planet. Often called the rainforests of the sea, coral reefs cover less than 0.1% of the Earth's surface but host a quarter of all known marine species¹. In addition, an estimated 1 billion people worldwide benefit either directly or indirectly from the ecosystem services that reef ecosystems provide, such as food provisioning, income and livelihood opportunities, carbon sequestration, protection from wave energy and erosion, tourism, and cultural value^{2,3}. At least 500 million people reside in the direct vicinity of coral reefs and have a high degree of dependency on these ecosystem services to meet their daily needs^{2,4,5}.

The wealth of biodiversity seen within coral reefs comes from the ability of stony corals (scleractinians) within the Cnidaria phylum to lay the foundation of and build massive three-dimensional reef structures in nutrient-poor waters⁶. Stony corals are predominantly colonial organisms, composed of many interconnected animals called polyps⁷. Each polyp is made up of two cell layers: an epidermis (outer epithelium) facing the environment, and a gastrodermis (inner epithelium) surrounding the gastrovascular cavity⁸. Between these two layers is a mostly acellular connective tissue layer called the mesoglea⁷. The mouth of each polyp is surrounded by stinging tentacles called cnidocytes that help corals capture and ingest planktonic prey⁷. Although stony corals can feed heterotrophically, in order to thrive in oligotrophic waters, they rely on their ability to host autotrophic, single-celled algae of the family Symbiodiniaceae within their gastrodermis^{9,10}. In this symbiosis, the coral host provides a protective habitat and the nutrients necessary for photosynthesis, such as ammonium and carbon dioxide, to its Symbiodiniaceae¹¹. In return, the Symbiodiniaceae produce oxygen and supply its coral host with organic products from photosynthesis, such as glucose, glycerol, and amino acids¹². This intricate symbiosis provides the coral animal with the energy required to build massive structures

that form reef ecosystems through the synthesis and secretion of calcium carbonate (CaCO_3) skeletons¹³.

Both global and local anthropogenic impacts pose a significant threat to marine ecosystems, and have already fundamentally altered the biodiversity and productivity of coral reefs¹⁴. The compounding effects of climate change, overfishing, pollution, and habitat destruction have resulted in a fifty percent loss of global coral cover and the ecosystem services they provide since the 1950s¹⁵. When corals experience prolonged periods of physiological stress, such as elevated sea surface temperatures, the Symbiodiniaceae are expelled or otherwise removed from the coral's gastrodermis, a process known as coral bleaching^{16,17}. Without their endosymbiotic partners, the coral host loses its primary source of energy and is subject to starvation and mortality if the symbiosis is not reestablished. A rapid increase in sea surface temperatures has triggered an increase in the frequency and severity of coral bleaching events^{18–21}. Based on current greenhouse gas emission trends, coral reefs are expected to lose all meaningful functionality by 2050¹⁹, emphasizing the critical importance of meaningful action on climate change.

Unfortunately, in addition to exacerbating coral bleaching events, increased ocean temperatures have also dramatically escalated the frequency and severity of marine disease outbreaks²². Coral disease outbreaks in particular stand out as being driven largely by a changing environment²³. Over the last 25 years, coral disease incidence has tripled and is expected to increase to 75% by 2100 under conservative estimates²⁴. This is particularly concerning given that coral diseases have significantly contributed to population declines and even functional extinction of certain coral species in relatively short periods of time^{23,25}. It is for these reasons that infectious disease has been brought to the forefront of coral biology research.

Caribbean coral reefs are currently experiencing one of the most devastating coral disease outbreaks in recorded history, known as stony coral tissue loss disease (SCTLD). This disease induces rapid tissue loss in over 22 species of scleractinian corals and can lead to complete colony mortality within months²⁶. SCTLD was initially identified off the shores of Miami, Florida in 2014 and has since spread across nearly the entire Caribbean region, affecting reefs in at least 28 countries and territories²⁶. Although research has shown that SCTLD is contagious and waterborne²⁷⁻³², the exact cause of this disease remains elusive. Several studies have documented shifts in the coral microbiome in response to SCTLD^{33,34,34-37}, and that antibiotic treatment can halt or slow lesion progression^{28,38-41}, suggesting bacterial involvement in SCTLD infection. Alternatively, other researchers have proposed viral pathogen involvement, supported by the detection of filamentous viral-like particles linked to endosymbiont pathology using transmission electron microscopy (TEM)⁴² and the assembly of putative filamentous viral genomes from SCTLD-affected coral holobiont metatranscriptomes⁴³.

Despite the unknown etiology of SCTLD, a growing body of evidence suggests that it leads to coral-Symbiodiniaceae dysbiosis. Histopathology indicates that algal endosymbionts in the coral gastrodermis are among the first cells to exhibit pathological changes during SCTLD infection^{44,45}, and that these changes were associated with the presence of viral-like particles localized exclusively within the cytoplasm and chloroplasts of the algal endosymbionts⁴². Additionally, field-based observations have noted a reduction or halting of SCTLD lesion progression in bleached coral colonies^{31,46,47}. However, a direct link between SCTLD activity and seasonal temperature remains elusive^{28,30,32,48}. These findings are noteworthy because other coral diseases tend to show the opposite pattern of increasing in prevalence and severity during warmer summer months⁴⁹⁻⁵¹. The decrease in SCTLD prevalence on reefs experiencing thermal

stress may be attributed to the loss of Symbiodiniaceae from bleached coral tissue²⁶, highlighting the importance of coral-algal symbiosis in the pathology of this disease.

While considerable strides have been made in SCTL D research, our understanding of the cellular mechanisms driving SCTL D susceptibility and pathogenesis remains incomplete. The extensive evolutionary history of scleractinian corals has given rise to variations in disease incidence and severity at both a species and family level^{52,53}, which have been linked to differential investment in immune mechanisms⁵⁴. Stony corals, like all invertebrates, possess an innate immune system and antioxidant enzymes crucial to fending off pathogens and maintaining cellular homeostasis⁵⁵. Understanding the interplay of immune and antioxidant mechanisms and their impact on disease susceptibility remains central to coral disease research.

To address these knowledge gaps, I utilized comparative transcriptomics to investigate the cellular processes underlying both SCTL D pathogenesis and susceptibility. In chapter two, I investigate the gene expression shifts in response to SCTL D infection across multiple species of coral and genera of Symbiodiniaceae and find that this disease triggers the *in situ* degradation of metabolically-dysfunctional Symbiodiniaceae. In chapter three, I link histopathology, immune/antioxidant protein measurements, and Symbiodiniaceae community to constitutive gene expression patterns and identify the factors that distinguish highly susceptible species from their less vulnerable counterparts at the cellular level. In chapter four, I present a novel supervised machine learning framework to describe the cellular processes involved in SCTL D progression in a major reef-building coral, *Montastraea cavernosa*, and its dominant algal endosymbiont, *Cladocopium goreaui*. Overall, these chapters provide strong support for the hypothesis that SCTL D infection results in coral-endosymbiont dysbiosis, and offers insights into the dynamic interplay between immunity, symbiotic relationships, and disease progression

in corals. This work establishes a foundation for integrating host and endosymbiont gene expression patterns into coral disease research, thereby providing valuable information for the development of intervention efforts aimed at preserving coral reef ecosystems in the face of a rapidly changing environment.

Chapter 2: Stony coral tissue loss disease induces transcriptional signatures of in situ degradation
of dysfunctional Symbiodiniaceae

Authors: Kelsey M. Beavers¹, Emily W. Van Buren¹, Ashley M. Rossin², Madison A. Emery¹,
Alex J. Veglia³, Carly E. Karrick³, Nicholas J. MacKnight¹, Bradford A. Dimos¹, Sonora S.
Meiling⁴, Tyler B. Smith⁴, Amy Apprill⁵, Erinn M. Muller⁶, Daniel M. Holstein², Adrienne M. S.
Correa³, Marilyn E. Brandt⁴, Laura D. Mydlarz¹

¹Department of Biology, University of Texas at Arlington, Arlington, TX, USA

²Department of Oceanography and Coastal Sciences, Louisiana State University, Baton Rouge,
LA, USA

³Department of BioSciences, Rice University, Houston, TX, USA

⁴Center for Marine and Environmental Studies, University of the Virgin Islands, St. Thomas,
USVI, USA

⁵Marine Chemistry and Geochemistry Department, Woods Hole Oceanographic Institution,
Woods Hole, MA, USA

⁶Mote Marine Laboratory, Sarasota, FL, USA

Citation: Beavers, K.M., Van Buren, E.W., Rossin, A.M. *et al.* Stony coral tissue loss disease
induces transcriptional signatures of in situ degradation of dysfunctional Symbiodiniaceae. *Nat*
Commun **14**, 2915 (2023). <https://doi.org/10.1038/s41467-023-38612-4>

ABSTRACT

Stony coral tissue loss disease (SCTLD), one of the most pervasive and virulent coral diseases on record, affects over 22 species of reef-building coral and is decimating reefs throughout the Caribbean. To understand how different coral species and their algal symbionts (family Symbiodiniaceae) respond to this disease, we examine the gene expression profiles of colonies of five species of coral from a SCTLD transmission experiment. The included species vary in their purported susceptibilities to SCTLD, and we use this to inform gene expression analyses of both the coral animal and their Symbiodiniaceae. We identify orthologous coral genes exhibiting lineage-specific differences in expression that correlate to disease susceptibility, as well as genes that are differentially expressed in all coral species in response to SCTLD infection. We find that SCTLD infection induces increased expression of *rab7*, an established marker of in situ degradation of dysfunctional Symbiodiniaceae, in all coral species accompanied by genus-level shifts in Symbiodiniaceae photosystem and metabolism gene expression. Overall, our results indicate that SCTLD infection induces symbiophagy across coral species and that the severity of disease is influenced by Symbiodiniaceae identity.

INTRODUCTION

Global climate change has initiated a dramatic increase in the prevalence, frequency, and severity of marine disease outbreaks^{22,56}, and has contributed to whole reef ecosystem regime shifts as well as significant population decreases of certain coral species²³. As a hotspot for coral diseases, the Caribbean is particularly at risk of severe biodiversity loss, exhibiting a 50-80% decline in living coral tissue since the 1970s^{57,58}. Although the etiologic agents of many of these diseases remain elusive, one prevailing hypothesis postulates that a growing number of diseases

result from environmentally induced microbiome imbalances and a subsequent increase in opportunistic or polymicrobial infections^{59,60}. As climate change pressures continue to escalate, emerging and endemic outbreaks in the Caribbean are likely to decimate reef-building coral populations, resulting in reef ecosystem collapse.

Stony coral colonies are holobionts comprised of the coral host and a diverse consortium of symbiotic microorganisms, including Symbiodiniaceae, bacteria, fungi, and viruses^{61,62}. The coral host provides a protective habitat as well as metabolic byproducts to its symbiotic partners and in return receives oxygen and organic compounds from its Symbiodiniaceae, as well as pathogen defense and nutrient cycling from its other microbiota^{61,62}. Symbiodiniaceae and bacteria symbionts are important to colony health, but anthropogenic disturbance can destabilize these associations, initiate bleaching (of Symbiodiniaceae) and ultimately result in colony tissue loss^{23,63}.

The Caribbean is currently experiencing an outbreak of the most pervasive and contagious coral disease on record – stony coral tissue loss disease (SCTLD)⁴⁷. Originating off the coast of southeast Florida in 2014, SCTLD is a waterborne disease known to cause acute tissue loss in more than half of reef-building species in the Caribbean^{30,64}. Although previous work on SCTLD suggests that there may be common secondary bacterial infections^{33–35,65}, and antibiotic treatment has been shown to be 84% effective in stopping tissue loss³⁸, a pathogen responsible for SCTLD has not yet been identified. However, a growing line of evidence implicates viral infection of Symbiodiniaceae in the etiology of this disease based on 1) a reduction or halting of lesion progression in bleached corals⁴⁶, 2) histopathological examination identifying lytic necrosis of host gastrodermal cells where Symbiodiniaceae reside⁴⁴, 3) transmission electron microscopy (TEM) detection of filamentous viral-like particles associated

with endosymbiont pathology⁴², and 4) the assembly of putative filamentous viral genomes from SCTLD-affected coral holobiont metatranscriptomes⁴³.

SCTLD affects over 22 species of coral and previous evidence suggests that coral holobionts vary in their susceptibilities to this disease^{64,66}. In April of 2019, three months after initial cases of SCTLD were observed in the United States Virgin Islands (USVI), Meiling et al.⁶⁶ conducted a controlled SCTLD transmission experiment in which fragments from six species of coral were split in half and placed into control and treatment mesocosms. Colony halves placed into treatment mesocosms were incubated with SCTLD-infected colonies of *Diploria labyrinthiformis*, while corresponding genotype fragments placed into control mesocosms were incubated with visually healthy colonies of *D. labyrinthiformis*. By monitoring lesion appearance over an 8-day experimental period, Meiling et al.⁶⁶ was able to obtain tangible disease phenotype measurements, such as disease prevalence and incidence, relative risk of lesion development, and lesion growth rate. These phenotypes were used to demonstrate microbial community shifts across different coral microhabitats following disease exposure and lesion appearance³⁷. Overall, results presented in Meiling et al.⁶⁶ found that of the six species tested, *Colpophyllia natans* and *Orbicella annularis* showed the greatest susceptibility to SCTLD and the highest lesion growth rates in the USVI compared to *Pseudodiploria strigosa*, *Porites astreoides*, and *Montastraea cavernosa*.

Here, we utilize the spectrum of disease phenotypes obtained by Meiling et al.⁶⁶ and apply comparative transcriptomics to elucidate the biological processes underlying variations in SCTLD susceptibility. Transcriptomics provides an invaluable tool to measure gene expression responses to pathological conditions, and a previous study has linked SCTLD progression in two coral species to the expression of genes involved in immunity, apoptosis, and tissue

rearrangement⁶⁷. However, the cellular mechanisms by which different coral species and symbiont lineages (presented here at the genus-level) respond to this disease remain largely unknown. By linking the gene expression profiles of multiple coral species to quantitative disease phenotypes, we identify coral and Symbiodiniaceae expression shifts in response to SCTLD infection that contribute to variation in disease susceptibility and resistance.

RESULTS

Transmission experiment

At the end of the transmission experiment, 100% of the *C. natans* and *O. annularis* fragments showed signs of active SCTLD lesions, followed by 75% of *P. strigosa* fragments, 62.5% of *P. astreoides* fragments, and 37.5% of *M. cavernosa* fragments. Coral fragments were classified by their treatment outcome as either “controls”, “exposed” or “infected.” Fragments exposed to apparently healthy *D. labyrinthiformis* donor corals were classified as controls. Fragments exposed to SCTLD-infected *D. labyrinthiformis* donor corals but did not develop lesions were classified as exposed, while those that did develop lesions were classified as infected. *C. natans* had the highest median relative risk of infection (12.19), followed by *O. annularis* (12.09), *P. strigosa* (9.30), *P. astreoides* (7.91) and *M. cavernosa* (5.10) (Figure 1, A). *C. natans* also had the fastest average lesion growth rate (0.42 cm²/hr), followed by *O. annularis* (0.20 cm²/hr), *P. strigosa* (0.13 cm²/hr), *M. cavernosa* (0.09 cm²/hr), and *P. astreoides* (0.03 cm²/hr) (Figure 1, A). Full experimental results are presented in Meiling et al.⁶⁶ and can be found in Supplementary Data 1 and 2.

Coral transcriptome assembly and annotation

To determine differential expression, we sequenced 52 transmission experiment coral tissue samples which resulted in a total of 2.82 billion raw reads with an average of 54.3 million reads per sample. Reference *de novo* metatranscriptomes for *C. natans* and *P. astreoides* as well as a genome-guided *M. cavernosa* assembly were sourced from previous Mydlarz lab work⁶⁸. Genome-guided transcriptome assembly of the *O. annularis* cleaned reads produced an assembly of 34,741 contigs with a N50 size of 7,601 bp and *de novo* transcriptome assembly of the *P. strigosa* cleaned, quality-filtered, coral-only reads produced an assembly of 23,116 contigs with a N50 size of 4,970 bp (Table 1).

Isolation and quantification of coral and Symbiodiniaceae reads

From the clean reads, a total of 1.02 billion mapped to the coral host and 887.6 million reads mapped to the sample's dominant symbiont lineage (see Methods – Isolation and quantification of coral and Symbiodiniaceae reads), with an average of 19.58 million and 17.07 million reads per sample mapped to the host and dominant symbiont, respectively (Supplementary Data 1). Mapping of coral host and dominant symbiont reads to their respective transcriptome and subsequent transcript quantification resulted in a total of 13,692 *C. natans*, 13,138 *O. annularis*, 9,796 *P. strigosa*, 13,271 *P. astreoides*, 11,628 *M. cavernosa*, 10,675 *Symbiodinium* spp., 10,072 *Breviolum* spp., 11,939 *Cladocopium* spp., and 10,328 *Durusdinium* spp. length-normalized transcripts with an annotation evalue of $1.0e^{-6}$. Dominant Symbiodiniaceae identified for each sample based on transcripts largely agreed with Symbiodiniaceae lineages identified from each sample via Illumina MiSeq amplicon sequencing of the internal transcribed spacer-2 (ITS-2) region of Symbiodiniaceae rDNA (Supplementary Information – Figure 2, Supplementary Data 3).

Differential expression of coral transcripts

The number of genes significantly expressed ($p_{adj} \leq 0.05$) in response to SCTLD exposure varied among species. The most susceptible species, *C. natans*, had the highest number of differentially expressed genes (DEGs) between exposed and non-exposed treatments at 1,350 followed by *M. cavernosa*, the least susceptible species, at 385 DEGs, *O. annularis* at 229 DEGs, *P. strigosa* at 90 DEGs and *P. astreoides* at 42 DEGs (Figure 1, B). We identified the highest percentage of DEGs involved in immunity and/or the response to viral infection in the highly susceptible species *O. annularis* (7% of DEGs), followed by *C. natans* and *P. astreoides* (5% of DEGs), *M. cavernosa* (4% of DEGs) and *P. strigosa* (2% of DEGs) (Figure 1, B). No DEGs were shared across all 5 species.

Merging of Uniprot Entry IDs across coral species followed by DESeq2 normalization and low average expression removal resulted in 2,147 inferred homologs with measurable expression. Of these, 150 were identified by GO term as involved in immunity and/or the response to viral infection and 17 were identified as involved in extracellular matrix (ECM) structure. The one-way ANOVA identified 16 immune/viral response homologs and 3 ECM homologs with significant differential expression between disease states (TukeyHSD Test; $p \leq 0.05$) (Supplementary Data 7). Among these homologs included the antiviral gene Interferon regulator factor 2 (*IRF2*), two genes putatively involved in symbiont population maintenance, Ras-related protein rab 7 (*rab7*) and Polyunsaturated fatty acid 5-lipoxygenase (*ALOX5*), and a collagen alpha chain fragment (*COA*).

Merging of Orthogroup IDs across coral species followed by DESeq2 normalization and low average expression removal resulted in 4,759 annotated orthologs with measurable

expression. Of these, 212 were identified by GO term as involved in immunity and/or the response to viral infection and 107 were identified as involved in extracellular matrix structure. The one-way ANOVA identified 30 immune/viral response orthologs and 18 ECM orthologs with significant differential expression between disease states (TukeyHSD Test; $p \leq 0.05$) (Supplementary Data 9). Three of these homologs, SMAD family member 6 (*smad6*), Toll-like receptor 6 (*TLR6*), and TNF-receptor-associated factor 3 (*Traf3*), were identified as members of the nuclear factor kappa B (NF- κ B) pathway (Figure 2). Deleted in malignant brain tumors 1 (*Dmbt1*), a gene involved in mucosal innate immunity, was significantly downregulated in infected corals relative to controls ($p = 0.0019$) (Figure 2). *Rab7* was also identified by our ortholog analysis as significantly upregulated in infected corals relative to controls ($p = 0.023$), as well as Charged multivesicular body protein 4b (*Chmp4b*), another gene involved in the same endosome maturation pathway as *rab7* ($p = 0.0017$) (Figure 2). Among the ECM orthologs significantly differentially expressed between control and infected corals included Superoxide dismutase [Cu-Zn] 1 (*sodA*) and Alpha-2 type I collagen (*col2a1*) (Figure 2).

Coral expression variance and evolution model

The differential expression of single-copy orthologs across the five coral species were used to test variation both among and within species by applying the Expression Variance and Evolution (EVE) model⁶⁹. A total of 1,817 single-copy orthologs were identified between the five coral species, 1,766 of which had measurable expression levels across all species and were used as inputs for the EVE model. This model, a phylogenetic ANOVA, parametrizes the ratio (β) of population to evolutionary expression level. A large β is associated with higher variation within versus between species and indicates expression diversity or plasticity. A small β is

associated with higher variation between versus within species and indicates lineage-specific expression diversity. B does not change if there is stabilizing or no selection acting on expression level. Here we use EVE to identify two categories of single-copy orthologous genes: 1) those with small β values ($p \leq 0.05$) exhibiting lineage-specific or adaptive expression and 2) those with large β values ($p \leq 0.05$) exhibiting expression plasticity. EVE identified 84 significant lineage-specific orthologs and 217 significant highly variable orthologs in the coral animal ($p \leq 0.05$) (Figure 1, C).

Of the 84 lineage-specific orthologs, 75 were annotated with a sufficient evalue ($1.0e^{-6}$) and kept for analysis. The expression of those 75 orthologs were averaged across species and tested for linear correlation with: (1) species median relative risk of infection and (2) species average lesion growth rate using Pearson's correlation. Three orthologs were identified as significantly correlated to relative risk ($p \leq 0.05$) and were annotated as Vacuolar protein-sorting-associated protein 35 (*vps25*), Zeta-sarcoglycan (*SGCZ*), and Cytoplasmic dynein 1 light intermediate chain 2 (*DYNC1LI2*) (Figure 3). Additionally, five orthologs were identified as significantly correlated to lesion growth rate ($p \leq 0.05$) and were annotated as Arrestin domain-containing protein 2 (*ARRDC2*), COP9 signalosome complex subunit 8 (*Cops8*), Golgin subfamily A member 7B (*GOLGA7B*), Ribulose-phosphate 3-epimerase (*Rpe*), and PHD finger protein 10 (*phf10*) (Figure 3). *ARRDC2*, located in the cytoplasmic vesicle and plasma membrane and predicted to be involved in protein transport⁷⁰, showed a highly significant positive linear correlation to lesion growth rate ($R = 0.99$, $p = 0.0011$)(Figure 3). Another gene, *Cops8*, a member of the COP9 signalosome, showed significant negative correlation between expression level and lesion growth rate ($R = -0.91$, $p = 0.032$)(Figure 3).

Of the 217 highly variable orthologs, the one-way ANOVA identified 78 with significant differential expression between disease states ($p \leq 0.05$), of which 53 were annotated with a sufficient evalue ($1.0e^{-6}$). The relative expression of those annotated orthologs with the most significant differences in expression ($p \leq 0.01$) were averaged across disease state and plotted in a heatmap (Figure 4, A). Notable orthologs with highly significant differences in expression between control and SCTLD-infected corals were plotted by species as well as disease state (Figure 4, B). Of all the highly variable orthologs, Tropomyosin alpha-4 chain (*Tpm4*) showed the most significant difference in expression between control and infected corals ($p = 2.0e-07$). Additionally, Transmembrane prolyl 4-hydroxylase (*P4HTM*), an enzyme that “senses” hypoxic conditions, was also significantly downregulated in corals infected with SCTLD (Figure 4). Alternatively, two orthologs significantly upregulated between control and SCTLD-infected corals were annotated as Protein BTG1 (*BTG1*) and Parkin coregulated gene protein homolog (*PACRG*) (Figure 4).

***C. natans* differential expression**

PCA of transcriptome-wide gene expression of *C. natans* samples identified dominant symbiont genus as the main driver (PC1) of expression-level differences in this species rather than disease state (Supplementary Information – Figure 4, A). Because *C. natans* samples dominated by *Durusdinium* symbionts experienced greater disease severity as measured by lesion growth rate compared with *Cladocopium*, the top 20 genes driving the differences in expression between *Cladocopium*- and *Durusdinium*-dominated hosts (PC1 loadings) were identified and their rlog expression was plotted (Supplementary Information – Figure 4, B).

Differential expression of Symbiodiniaceae transcripts

The number of genes significantly differentially expressed ($\text{padj} \leq 0.05$) in response to SCTL exposure varied between dominant symbiont genera. *Breviolum* spp. had the highest number of DEGs with 18, followed by *Durusdinium* spp. with 13 DEGs, and *Cladocopium* with 5 DEGs. *Symbiodinium* spp. had no DEGs (Figure 1). No DEGs were shared amongst all three of the genera that had DEGs, but *Breviolum* spp. and *Durusdinium* spp. shared three: Photosystem I P700 chlorophyll a apoprotein A1 (*psaA*), Photosystem II CP43 reaction center protein (*psbC*), and Photosystem II CP47 reaction center protein (*psbB*) (Figure 5). To enumerate the number of DEGs in each genus involved in photosynthesis, DEGs containing the GO term “photosynthesis” were counted. Remarkably, 62% of *Durusdinium* spp. DEGs were involved in photosynthesis, followed by 17% of *Breviolum* spp. DEGs and 0% of *Cladocopium* spp. DEGs (Figure 1, E).

Symbiodiniaceae expression variance and evolution model

The differential expression of single-copy orthologs across the four dominant symbiont genera were used to test variation both among and within species by applying the EVE model⁶⁹. A total of 5,332 single-copy orthologs were identified between the four dominant symbiont genera, 5,125 of which had measurable expression levels across all genera and were used as inputs for the EVE model. EVE identified 292 significant lineage-specific orthologs and 1,212 significant highly variable orthologs ($p \leq 0.05$) (Figure 1). Of the 292 lineage-specific orthologs, 120 were annotated with a sufficient evalue ($1.0e^{-6}$) and kept for analysis. Four of those annotated orthologs were identified as significantly correlated to lesion growth rate ($p \leq 0.01$): Probable protein phosphatase 2C 45 ($R = -0.993$, $p = 0.008$), Charged multivesicular body protein 3 ($R = -0.991$, $p = 0.009$), Zinc finger CCCH domain-containing protein 1 ($R = -0.999$, p

= 0.001), and Serine/threonine protein phosphatase 2A regulatory subunit β ($R = -0.996$, $p = 0.004$).

Of the 1,212 highly variable orthologs, the one-way ANOVA identified 48 with significant differential expression between disease states ($p \leq 0.05$), of which 24 were annotated with a sufficient evalue ($1.0e^{-6}$). 75% (18/24) of these orthologs exhibit a significant transcriptional shift in the SCTL D-exposed (but no lesion) corals relative to controls, while only 4.2% (1/24) exhibit such a shift in the SCTL D-infected (with lesion) corals (Figure 6, A). Relevant orthologs were plotted by species as well as disease state (Figure 6, B). Two orthologs, annotated as Cyclin-dependent kinase 2 (*Cdk2*), a cell cycle regulator that orchestrates the entry into mitosis/meiosis⁷⁰, and 2-alkenal reductase (*DBR*), involved in the degradation of reactive carbonyl species⁷⁰, showed significant downregulation in the SCTL D-exposed corals relative to controls (Figure 6, B). Alternatively, Guanine Deaminase (*GuaD*), a gene involved in the production of xanthine and ammonia from guanine, exhibited a significant increase in expression in the SCTL D-exposed corals relative to controls (Figure 6, B).

Coral *rab7* correlations to Symbiodiniaceae genes

Two photosystem genes in *Symbiodinium* (*psaA* and *psbC*) and in *Durisdinium* (*psaA* and *psbB*) were significantly positively correlated to coral *rab7* expression, an established marker of symbiophagy ($p \leq 0.05$) (Figure 7). Although not statistically significant, the expression of Superoxide dismutase and Heat shock protein 70 were also positively correlated to coral *rab7* expression in these symbiont genera. Alternatively, in *Cladocopium* symbionts the expression of Heat shock protein 70 was significantly negatively correlated to coral *rab7*

expression ($p \leq 0.01$) (Figure 7). No *Breviolum* genes were significantly correlated to coral *rab7* expression.

Coral *rab7* correlations to histology measurements

Rab7 expression was significantly negatively correlated to average symbiont size ($R = -0.48$, $p = 0.00049$), but was not correlated to the ratio of symbiont size to symbiosome size ($R = -0.19$, $p = 0.19$) (Figure 8). There was no significant difference in average symbiont size between disease states, but there was a significant decrease in the ratio of symbiont size to symbiosome size in both the disease-exposed and disease-infected fragments relative to the controls ($p = 5.7e-04$ and $p = 3.83e-05$, respectively) (Figure 8).

DISCUSSION

Caribbean coral reefs are currently experiencing the worst disease-related mortality event on record, with several reef-building species suffering massive regional die-offs. Here, we investigated the gene expression responses of five phylogenetically distinct coral species and their dominant Symbiodiniaceae following experimental exposure to SCTL D. Through the combined use of differential expression analyses on immune-related genes and highly variable orthologs, as well as correlation analyses of lineage-specific orthologs to disease phenotypes, we examined the gene expression patterns consistent across species as well as those that may contribute to variations in species susceptibility. First, we found that SCTL D infection induced expression of homologous and orthologous genes involved in immunity, apoptosis, and ECM structure in all five coral species. Second, we showed that species-level SCTL D susceptibility was correlated to lineage-specific differences in expression of single-copy orthologs involved in

vesicular trafficking and signal transduction. Third, we found evidence that SCTLD exposure (without visible lesions) induces major expression shifts in the highly variable Symbiodiniaceae single-copy orthologs, but not in those of the coral animal. Finally, we identified and compared the genes significantly differentially expressed by various Symbiodiniaceae genera in response to SCTLD infection and posit that SCTLD disrupts normal host-symbiont interactions and *in situ* degradation of dysfunctional Symbiodiniaceae.

SCTLD infection induces an immune response across coral species

Consistent with multiple lines of evidence implicating SCTLD as a viral disease, we found transcriptional signatures of antiviral immunity across five coral species experimentally infected with SCTLD. Two members of the interferon antiviral response pathway, *Traf3* and *IRF2*, showed significant differential expression between disease states. *Traf3*, a negative regulator of the nuclear factor kappa B (NF- κ B) pathway and a positive regulator of type I interferon (IFN1) production in humans⁷¹, was significantly upregulated in SCTLD-infected corals relative to control. Similarly, *IRF2*, an antagonist of IFN1 transcriptional activation⁷⁰, was downregulated in SCTLD-infected corals relative to resistant corals. The upregulation of IFN1 production and the concordant downregulation of its antagonist is a strong indication that corals manifesting visible SCTLD lesions are activating an antiviral immune response.

We also found transcriptional evidence of a functional shift in the coral surface mucus layer, the first line of defense against foreign particles and microbes⁷². *Dmbt1*, involved in mucosal innate immunity and microbial homeostasis in humans⁷⁰, exhibited significant overall downregulation in SCTLD-infected corals relative to controls. Wright et al.⁷³ found downregulation of this gene in *Acropora millepora* challenged with *Vibrio* spp., leading them to

the hypothesis that this gene may play a role in maintaining healthy associations with commensal microbes. Our results are consistent with this hypothesis, as downregulation of *Dmbt1* in SCTLD-infected corals was accompanied by significant shifts in mucus microbiome composition towards dysbiosis in specimens from this same study³⁷. Downregulation of *Dmbt1* in SCTLD-infected corals may therefore render corals unable to maintain mucosal microbial homeostasis, leading to a loss of the protective capabilities of their surface mucus layer and making them susceptible to secondary infection by opportunistic bacteria. These results explain why antibiotic treatment is sufficient to arrest treated SCTLD lesions, but ineffective at preventing new lesion appearance on other parts of the same coral colony³⁹.

In addition, our results indicate a significant upregulation of apoptosis and related stress-response processes in SCTLD-infected corals relative to controls. *SMAD6*, a member of the transforming growth factor β (TGF- β) signaling pathway, exhibited a strong decrease in expression between control and infected corals. Knockdown of this protein has been shown to increase apoptosis and inhibit cell cycle progression in human cells⁷⁴. Similarly, *ALOX5*, a proinflammatory gene hypothesized to play a role in the phagocytosis of apoptotic bodies in regenerating *Hydra*⁷⁵, showed a concomitant increase in expression in infected corals. We also found significant upregulation of the antioxidant *sodA*, an established coral immune response antioxidant also involved in symbiosis breakdown^{76,77}. Finally, we observed strong downregulation of multiple collagen genes in infected corals, suggesting a stress-induced decrease in ECM structural proteins not immediately needed for cell survival. These results are highly similar to the expression level shifts of immune, apoptosis, and ECM genes detected in SCTLD-infected corals from Florida⁶⁷.

SCTLD susceptibility is correlated to increased vesicular trafficking and decreased signaling

Our results indicate that species-level variation in SCTLD susceptibility correlates to differential expression of single-copy orthologs involved in vesicular trafficking and signaling. Two orthologs involved in vesicular transport, *DYNC1LI2* and *vps25*, displayed a positive linear correlation between expression level and relative risk of SCTLD infection. *DYNC1LI2* acts as a motor for the retrograde transport of vesicles along microtubules and *vps25* is a component of the endosomal sorting complex required for transport II (ESCRT-II), which functions in the endocytosis of ubiquitinated membrane proteins for lysosomal degradation⁷⁰. Interestingly, some RNA viruses such as HIV-1 hijack the ESCRT pathway to facilitate viral budding and egress from infected cells⁷⁸. In fact, ESCRT-II depletion or elimination in human cells resulted in reduced HIV-1 Gag protein production, visible decreases in budding efficiency, and diminished intracellular levels of virion protein⁷⁹. The increased average expression of *vps25* in highly susceptible coral species may represent an elevated capacity of a SCTLD-associated virus to hijack ESCRT-II to facilitate virion production and export.

Additionally, our results indicate that signal transduction is reduced in coral species exhibiting the most severe forms of SCTLD lesion progression. The expression of one single-copy ortholog annotated as *ARRDC2* showed a strong positive correlation to lesion growth rate. Mammalian β -arrestins are known to regulate G-protein-coupled receptor (GPCR) trafficking and signaling, and proteins with predicted “arrestin-like” domains have been indicated to function similarly⁸⁰. Interestingly, the human bacterial pathogen *Streptococcus pneumoniae*, which binds to a GPCR to enter host cells for transcytosis, can avoid lysosomal degradation in cells exhibiting overexpression of β -arrestin 1⁸¹. Bacterial work on SCTLD suggests that there

may be common secondary bacterial infections^{33–35,65}, and antibiotic treatment has been shown to halt lesion progression^{38,39}. The strong correlation between *ARRDC2* expression and lesion growth rate in SCTL D corals indicates that overexpression of this gene may prevent successful lysosomal degradation of bacteria, potentially opportunistic pathogens invading compromised tissue.

Another single-copy ortholog involved in signaling, annotated as *Cops8*, showed significant negative correlation between expression level and lesion growth rate. *Cops8* is a member of the COP9 signalosome, a conserved multiprotein complex that functions as an important regulator of many signaling pathways through its control over ubiquitin-proteasome-mediated protein degradation⁸². Through the ubiquitin-dependent degradation of the NF- κ B inhibitor IkappaB α , the COP9 signalosome can mediate NF- κ B activation, which in turn triggers an immune response⁸³. Therefore, these results indicate that species of coral exhibiting rapid lesion progression of SCTL D, such as *C. natans* and *O. annularis*, may be unable to mount an effective immune response due to their comparatively low levels of immune signaling.

SCTL D-infected corals are reducing endosymbiont density through *in situ* degradation

One of the most significant findings of this study is the consistent differential expression of genes involved in symbiophagy, the *in situ* degradation of dead or dysfunctional symbionts. This process, triggered by a stress event, transforms the host-derived symbiosome from an arrested state of phagocytosis into a digestive organelle resulting in the consumption of the endosymbiont^{16,17,84,85}. Protein rab7, a recognized marker of autophagy across taxa, is associated with endocytic phagosomes containing dead or dysfunctional zooxanthellae in the anemone *Aiptasia pulchella* and stony coral *Pocillopora damicornis*^{84,85}. In our study, we found *rab7* to

show significant upregulation in infected corals relative to both control and exposed (no lesion) corals, implicating symbiophagy as a common cellular phenotype of SCTL D lesions. Similarly, we observed strong increases in expression of *Chmp4b*, a gene involved in the same endosome-to-lysosome maturation pathway as *rab7*. Additionally, *ALOX5*, a pro-inflammatory gene whose expression was found by Fuess et al.⁸⁶ to be negatively correlated with symbiont density, was also significantly upregulated in infected corals relative to controls. The upregulation of *rab7*, *Chmp4b*, and *ALOX5* in SCTL D-infected corals corroborates strongly with evidence that this disease causes a breakdown of host-symbiont physiology⁴⁴.

Because *in situ* degradation of endosymbionts represents a host innate immune response to compromised symbionts¹⁶, we investigated transcriptional evidence of symbiont impairment. Within the symbiont DEGs, we see evidence of photosynthesis dysfunction in both the downregulation of photosystem genes in *Breviolum* spp., as well as the upregulation of those same genes in *Durusdinium* spp. In fact, all the genes upregulated by *Durusdinium* symbionts are involved in energy production, likely indicative of photosystem overexcitation. Furthermore, the samples dominated by *Durusdinium* spp. displayed the fastest lesion growth rates in our study, indicating that symbiont photosystem overexcitation may lead to worse outcomes for SCTL D infected corals.

Coral *rab7* expression was positively correlated to symbiont photosystem genes in both *Symbiodinium* and *Durusdinium*, as well as the antioxidant gene Superoxide dismutase (*sodA*) and Heat shock 70 kDa protein (*Hsp70*) – two known indicators of symbiont stress and dysfunction^{16,87}. Because coral *rab7* is an established marker of symbiophagy, these correlations indicate that symbiont photosystem overexcitation and stress are associated with higher levels of *in situ* degradation of symbionts by their coral host. This pattern, however, is not ubiquitous

across symbiont genera and potentially contributes to variability in disease susceptibility. Using histology measurements, we found high *rab7* expression associated with small symbiont size, although there was no significant difference in symbiont size across disease states. However, there was a significant decrease in the ratio of symbiont size to symbiosome size in both the disease-exposed and disease-infected corals relative to controls. Taken together, these results indicate that SCTL D exposure triggers symbiont stress and subsequent symbiosome enlargement, a change in morphology indicative of symbiophagy⁸⁵.

Expression-level shifts in the coral single-copy orthologs identified by EVE as highly variable provide evidence as to why diseased corals may be inducing symbiophagy rather than exocytosis to remove dysfunctional symbionts. Of all highly variable orthologs, *Tpm4* showed the most significant difference in expression between control and infected corals. The protein encoded by this gene contributes to most, if not all, functions of the actin cytoskeleton⁷⁰, and has been shown by single-cell sequencing to be localized predominantly within alga-hosting cells in corals⁸⁸. In fact, Mayfield et al.⁸⁹ found decreased expression of a related gene, *tropomyosin*, in the Pacific coral *Seriatopora hystrix* at night, supporting their hypothesis that coral alga-hosting cells experience major cytoskeletal rearrangement as endosymbionts switch from photosynthesis to respiration. Additionally, the strong upregulation in infected corals of *Btg1*, an antiproliferation protein maximal during the G₀/G₁ phase of the cell cycle⁷⁰, indicates that SCTL D infection induces host cell quiescence or senescence, stalling cell growth and proliferation. Cells exposed to environmental stress are thought to enter G₀ due to lack of nutrients necessary for division⁹⁰. Because corals derive up to 100% of their daily metabolic requirements from their Symbiodiniaceae⁹¹, it is likely that the concomitant expression decrease in *Tpm4* and increase in *Btg1* are indicative of coral starvation due to inadequate photosynthate

transfer from symbionts. Taken together with the increased expression of coral immune- and stress-response genes, this provides evidence that SCTLD-infected corals are mounting an autophagic immune response against dysfunctional symbionts and/or their pathogens.

Contrary to the coral EVE results, the majority of the highly variable *Symbiodiniaceae* single-copy orthologs identified by EVE exhibit significant transcriptional changes in the SCTLD-exposed (but not lesioned) symbionts relative to controls. The dramatic shift in symbiont gene expression seen in the exposed corals could represent two things: 1) early symbiont responses to SCTLD infection before the manifestation of visible lesions on the coral, or 2) a successful symbiont response to SCTLD pathogen exposure preventing the onset of disease. Because the expression of many of these orthologs is comparable between control and SCTLD-infected corals, we believe the latter to be true. If so, the downregulation of the cell cycle regulator Cyclin-dependent kinase 2 (*Cdk2*) and upregulation of the ammonium assimilator guanine deaminase (*GuaD*) in SCTLD-exposed algal cells provides evidence that symbiont cell cycle arrest may prevent the onset of visible lesions in the host. This is consistent with results from Huntley et al.³⁷ showing that mucus microbiome alterations occurred even in the corals exposed to SCTLD but did not develop lesions. Up to half of the fixed carbon supplied by *Symbiodiniaceae* to the coral host is expelled as mucus^{92,93}, making it plausible that symbiont cell cycle arrest has metabolic consequences negatively affecting coral mucus production.

The results presented here provide evidence that 1) viral infection of *Symbiodiniaceae* is implicated in SCTLD pathology, and 2) disease manifestation is associated with *in situ* degradation of defective symbionts. Our study provides the underlying mechanisms involved in processes identified by histological observations, such as shrunken and necrosing symbionts, enlarged symbiosomes, and AVLP uniquely localized within algal endosymbiont cells^{42,44,66}. Our

application of innovative bioinformatic methods allows us to consider both coral and algal endosymbiont processes involved in SCTL D infection and brings us closer to understanding the pathogenicity of SCTL D so we may effectively combat this devastating disease.

METHODS

Experimental approach, sample preparation and sequencing

All research conducted in this study complies with all relevant ethical regulations as outlined by the Department of Planning and Natural Resources Coastal Zone Management. The SCTL D transmission experiment was carried out at the University of the Virgin Islands (UVI) in April of 2019 and is published in Meiling et al.⁶⁶. Briefly, one fragment from each of five species of stony coral (*C. natans*, *M. cavernosa*, *O. annularis*, *P. astreoides*, and *P. strigosa*) was placed into a control mesocosm equidistant from a central healthy *D. labyrinthiformis* donor coral colony. Corresponding genet fragments from each species were placed into an experimental mesocosm equidistant from a SCTL D-infected *D. labyrinthiformis* donor coral colony. Eight genets of healthy *D. labyrinthiformis* were used as control donor corals and eight genets of diseased *D. labyrinthiformis* were used as SCTL D donor corals. This paired design was replicated for a total of eight genets per species. Experimental coral fragments that developed lesions were removed when 30% tissue loss was achieved and were stored at -80°C for RNA sequencing. Corresponding control genet fragments were removed and processed at the same time. All fragments regardless of health status were processed at the end of an eight-day experimental period. Upon completion of the experiment, lesion growth rate was determined for each SCTL D-infected fragment and median relative risk of infection was calculated for each species by Meiling et al.⁶⁶ (Supplementary Data 2).

Total RNA was extracted using the RNAqueous-4PCR Total RNA Isolation Kit from Invitrogen (Life Technologies AM1914). First, a sterilized bone cutter was used to scrape off a pea-sized amount of frozen coral tissue from each fragment into a 2 mL microcentrifuge tube. On diseased fragments, tissue was harvested between 2 and 5 cm from the visible lesion. Tissue samples were lysed with a refrigerated Qiagen TissueLyser II at 30 oscillations/sec for 30 seconds during the lysis stage and the elution stage was performed in two steps (30ul elution followed by another 30ul elution). Contaminating DNA and chromatin were removed from each sample of total RNA using the Ambion DNase I (RNase-free) kit from Invitrogen (Life Technologies AM2222). Prior to sequencing, all samples underwent quality assessment using an Agilent Bioanalyzer 2100 at the University of Texas at Arlington Genomics Core Facility (Arlington, TX, USA). The 52 samples that passed quality assessment (RIN numbers ≥ 7) were sent to Novogene Co., LTD (Beijing, China). At Novogene, samples were preprocessed for mRNA enrichment using polyA tail capture and mRNA libraries were prepared using the NEBNext Ultra II RNA Library Prep Kit from Illumina. The resulting cDNA libraries were fed into the Illumina NovaSeq 6000 for 150 bp, paired-end sequencing.

Coral transcriptome assembly and annotation

Raw reads from Novogene were quality filtered using FastP v. 0.20.1⁹⁴ under default parameters. A genome-guided transcriptome for *O. annularis* was generated using the *Orbicella faveolata* genome⁹⁵ and a *de novo* metatranscriptome was assembled for *P. strigosa*, both using Trinity v. 2.11.0⁹⁶. Coral-only transcripts were obtained from the *de novo* metatranscriptomes (*C. natans*, *P. astreoides* and *P. strigosa*) adopting the *in-silico* filtration method outlined by Davies et al⁹⁷. First, the longest transcript isoform was obtained using the

get_longest_isoform_seq_per_trinity_gene.pl script available within the Trinity v. 2.11.0 package⁹⁸. Next, this assembly was blasted against a Master Coral database comprised of both genome-derived predicted gene models and transcriptomes spanning a wide diversity of coral families using BlastX v. 2.2.27^{97,99–101}. Transcripts with less than 95% identity to this Master Coral database and shorter than 150 bp were filtered out. Next, the program TransDecoder v5.5.0 (<https://github.com/TransDecoder/TransDecoder/wiki>) was used to first extract the longest open reading frame (ORF) from each transcript and then to generate a predicted peptide sequence from this ORF, resulting in predicted proteomes for each of these three species. Sequences with high sequence similarity within each proteome were then collapsed using cd-hit v.4.8.1¹⁰² using default parameters. The resulting sequences were extracted from the initial assembly to generate coral-only reference transcriptomes. The completeness of the resulting assemblies was assessed with Benchmarking Universal Single Copy Orthologs (BUSCO) v.5.2.2¹⁰³. Assembly metrics can be found in Table 1. Finally, coral host and dominant symbiont transcripts were annotated with reviewed UniprotKB/Swiss-Prot Entry IDs using BlastX v. 2.2.27¹⁰⁴ using an evaluate cutoff of $1.0e^{-6}$ (Supplementary Data 4).

Isolation and quantification of coral and Symbiodiniaceae reads

BBSplit v. 38.90 was used to separate out coral, Symbiodiniaceae, and non-coral/non-Symbiodiniaceae reads using coral-only and Symbiodiniaceae reference transcriptomes under default parameters. Symbiodiniaceae transcriptomes representing the genera *Symbiodinium*, *Breviolum*, *Cladocopium*, and *Durusdinium* were sourced from previous publications (Table 1). The binning statistics output from BBSplit (Supplementary Information – Figure 1, Supplementary Data 1) was used to assess which genera of Symbiodiniaceae was dominant

within each sample, referred in the text as the “dominant symbiont.” Coral and dominant symbiont reads were mapped to their respective transcriptome and quantified using the program Salmon v. 1.5.2^{105,106} with default parameters used for corals and a kmer value of 23 for the dominant symbiont.

Differential expression analysis of coral and dominant symbiont transcripts

Coral host and dominant symbiont transcript abundance was imported into R Studio v. 2022.02.2 and length-normalized using the package TXimport v. 1.16.1¹⁰⁷. The remaining transcripts were regularized log (rlog) transformed and tested for differential expression using the package DESeq2 v. 1.30.1¹⁰⁸ with the design $\sim genotype + treatment$ in the host and $\sim host_species + treatment$ in the dominant symbiont (Supplementary Data 5 and 6). Expression profiles within a species or symbiont lineage were filtered for low abundance by removing transcripts with an average rlog expression < 10 . DEGs were identified in each species as those with a statistically significant difference in expression between control and SCTLD-treated corals (Wald test; $padj \leq 0.05$). Principal component analysis (PCA) was performed to identify outliers in both the host and symbiont datasets and to illustrate the spatial relationships of gene expression across samples using the R package PCAtools v. 4.2.0¹⁰⁹ (Supplementary Information – Figure 5). One sample within the host expression dataset (Pstr_d8) was identified as an outlier and removed from the study. One sample within the symbiont dataset (Oann_c2) was identified as an outlier and removed from the symbiont analysis.

Gene Ontology enrichment analysis

Gene Ontology (GO) enrichment analyses were conducted using adaptive clustering of GO categories and Mann-Whitney U tests based on log₂FoldChange values (GO_MWU, https://github.com/z0on/GO_MWU)¹¹⁰. The function “reduce_overlap” from the R package GOplot v. 1.0.2⁷¹ was used to find the top 5 enriched non-redundant Biological Process (BP) and Molecular Function (MF) terms within each species (Supplementary Information – Figure 3)¹¹¹.

To enumerate the number of DEGs in each species involved in immunity, the number of DEGs with GO terms containing at least one of the following words were counted: “immune”, “immunity”, “virus”, and “viral”.

Differential expression analysis of relevant coral homologs

To compare rlog transformed expression of inferred homologs (transcripts with the same annotation) across coral species, species length-normalized counts matrices from Tximport were first merged by Uniprot Entry ID across all five coral species. Rlog normalized expression of all species’ homologs was obtained by running this five-species count matrix through DESeq2 using the design *~species + treatment*, removing homologs with average rlog expression < 10.

Homologs involved in immunity and/or viral infection were isolated by pulling out those with GO terms containing the words “immune”, “immunity”, “virus” and “viral”. Homologs involved in extracellular matrix organization were isolated by pulling out those with GO terms containing the words “extracellular matrix”. A one-way ANOVA followed by TukeyHSD tests were run on these homologs to identify those with significant differential expression between disease states (Supplementary Data 7). Each significant homolog’s protein domains were identified and compared across species to confirm homology by uploading the protein-coding sequence

associated with each transcript to Interpro (<https://www.ebi.ac.uk/interpro/>) (Supplementary Data 8).

Differential expression analysis of relevant coral orthologs

To compare rlog transformed expression of orthologs across coral species, Orthofinder was used to identify groups of orthologous genes across the predicted proteomes of all five coral species, referred to as “orthogroups”^{67,112}. Orthogroup count matrices were generated for each species using Tximport, and then were merged by orthogroup ID across all five coral species. Rlog normalized expression of all species’ orthogroups was obtained by running this five-species count matrix through DESeq2 using the design $\sim species + treatment$, removing orthogroups with average rlog expression < 10 . Each orthogroup was assigned a function using the first *M. cavernosa* transcript in the orthogroup and matching it to the *M. cavernosa* transcriptome annotation. These annotated orthogroups are referred to in the text as “orthologs”. Orthologs involved in immunity were isolated by pulling out those with GO terms containing the words “immune”, “immunity”, “virus” and “viral”. Orthologs involved in extracellular matrix organization were isolated by pulling out those with GO terms containing the word “extracellular matrix”. A one-way ANOVA followed by TukeyHSD tests were run on these orthologs to identify those with significant differential expression between disease states (Supplementary Data 9).

Coral *rab7* correlations to symbiodiniaceae genes

To further investigate the biological processes of the intracellular symbionts that may be triggering symbiophagy, the expression of coral *rab7* was correlated to the expression of three

photosystem genes identified as DEGs in *Breviolum* and *Durusdinium* (*psaA*, *psbB*, and *psbC*). We also correlated the expression of coral *rab7* to four other relevant genes identified from literature searches: two genes known to play a role in stress response (Superoxide dismutase and Heat shock protein 70), one gene involved in maintaining symbiosis with the coral host (Carbonic anhydrase), and a known apoptosis inducer (Apoptosis inducing factor 3)^{87,113,114}. Expression correlations were separated by dominant symbiont genera within the sample and plotted in a correlation matrix (Figure 7, Supplementary Data 14).

Expression variance and evolution model using single-copy orthologs

The expression variance and evolution model was used to identify lineage-specific and highly variable single-copy orthologs across coral species and symbiont genera. Orthofinder was used to identify single-copy orthologs across the five coral species and across the four symbiont genera. The single-copy orthologs were annotated with BlastP v. 2.2.27¹⁰⁴ using the protein sequences from a representative species (*M. cavernosa* for the coral orthologs and *D. trenchii* for the symbiont orthologs). Coral host and dominant symbiont transcript abundance was Imported into R studio and length-normalized using Tximport using single-copy orthogroup IDs as the gene identifier. DESeq2 was run on both sets of single-copy ortholog counts to obtain rlog transformed expression values using the design $\sim \text{species} + \text{treatment}$ in the coral dataset and $\sim \text{genera} + \text{treatment}$ in the symbiont dataset. Single-copy orthologs with average rlog expression < 10 were removed.

The rlog transformed expression of coral and symbiont single-copy orthologs was used in the EVE model⁶⁹ to test gene expression variation both among and within species (Supplementary Data 10 and 12). Genes exhibiting significant ($p \leq 0.05$) expression plasticity or

lineage-specific expression were identified. A one-way ANOVA followed by TukeyHSD tests were used to find significant differences in expression within the plastic orthologs across disease states (control vs. exposed, exposed vs. infected, and control vs. infected) (Supplementary Data 11 and 13). Species average expression of lineage-specific genes was correlated to both species average lesion growth rate and species median relative risk of infection to identify single-copy orthologs contributing to adaptive differences in SCTL D susceptibility.

Histology

Separate tissue samples were taken from each fragment for histology analyses and fixed in zinc-buffered formalin for 24 hours, washed with fresh water for 24 hours, and stored in 70% ethanol for transport to Louisiana State University, Baton Rouge, LA, USA. Samples were decalcified with a 1% HCl EDTA solution and stored in 70% ethanol until processed. Tissues were processed using a Lecia ASP6025, embedded in paraffin wax blocks on a Leica EG1150H embedding machine, and sectioned at five mm thickness on a Leica RM2125RTS microtome. Five serial sections were made 500 mm apart for each sample. Histological slides were stained with hematoxylin and eosin stain on a Leica ST5020, viewed on an Olympus BX41 microscope with an Olympus SC180 camera attachment.

Ten photomicrographs were taken at 40X magnification (60,000 mm² focal area per image) per coral individual across all five serial sections. Photos were analyzed using ImageJ¹¹⁵ software by overlaying a 12-cell grid on the image; each cell had an area of 5000 mm². A random number generator selected one grid-cell per photomicrograph. Within the grid-cell of interest, the areas of all symbiosomes and symbiont cells within symbiosomes were measured.

Twenty-five symbiont and symbiosomes were measured for each coral colony. The condition of symbionts was noted.

Amplicon Sequencing of the Internal Transcribed Spacer 2 (ITS-2) region of Symbiodiniaceae rDNA

DNA was extracted using the ZymoBIOMICS DNA/RNA Miniprep kit (Zymo Research, CA), and the internal transcribed spacer-2 (ITS-2) region of Symbiodiniaceae rDNA was sequenced following Howe-Kerr et al.¹¹⁶ using the primers SYM_VAR_5.8SII (5' GAATTGCAGAACTCCGTGAACC 3') and SYM_VAR_REV (5' CGGGTTCWCTTGTYTGAATTCATGC 3')¹¹⁷ and sequenced on the Illumina MiSeq platform at the Oregon State University Center for Qualitative Life Sciences (CQLS, Corvallis, OR) following details outlined in Howe-Kerr et al.¹¹⁶. The resulting sequencing data were processed using Symportal¹¹⁸.

Acknowledgements

We thank the facilities and diving support staff at the University of the Virgin Islands Center for Marine and Environmental Studies (CMES) and Adam Glahn, Daniel Mele, Danielle Lasseigne, Kathryn Cobleigh, Alex Gutting, Amanda Long, and Bradley Arrington for their assistance with field collections and conducting experiments. Samples were collected under permit #DFW19057U authorized by the Department of Planning and Natural Resources Coastal Zone Management. This is CMES contribution #256. This work was funded by a National Science Foundation (NSF) VI EPSCoR 0814417 and 1946412 and NSF (Biological Oceanography) award numbers 1928753 to MEB and TBS, 1928609 to AMSC, 1928817 to EMM, 1928771 to

LDM, 1927277 to DMH as well as 1928761 and 1938112 to AA, NSF EEID award number 2109622 to MEB, AA, LDM, DMH, and AMSC, and a NOAA OAR Cooperative Institutes award to AA (#NA19OAR4320074).

Data Availability

The raw RNAseq data generated in this study have been deposited in the NCBI database under accession code PRJNA860922 [<https://www.ncbi.nlm.nih.gov/bioproject/PRJNA860922>]. The publicly available data used in this study include the transcriptomes for *Symbiodinium* CassKB8 [transcriptome assembly: <http://medinalab.org/zoox/>, raw reads: <https://www.ncbi.nlm.nih.gov/bioproject/PRJNA80085>], *Breviolum minutum* [transcriptome assembly: <http://zoox.reefgenomics.org/download/>, raw reads: <https://www.ncbi.nlm.nih.gov/bioproject/?term=PRJNA274852>], *Cladocopium goreau* [transcriptome assembly: <http://ssid.reefgenomics.org/download/>, raw reads: <https://www.ncbi.nlm.nih.gov/bioproject/?term=PRJNA307543>] and *Durusdinium trenchii* [transcriptome assembly: <https://datadryad.org/stash/dataset/doi:10.5061/dryad.12j173m>, raw reads: <https://www.ncbi.nlm.nih.gov/bioproject/?term=PRJNA508937>], as well as the genomes for *M. cavernosa* [genome assembly: <https://matzlab.weebly.com/data--code.html>, raw reads: <https://www.ncbi.nlm.nih.gov/bioproject/PRJNA679067>] and *O. faveolata* [genome assembly: https://www.ncbi.nlm.nih.gov/genome/13173?genome_assembly_id=311351, raw reads: <https://www.ncbi.nlm.nih.gov/bioproject/PRJNA381078>]. The Master Coral database used in this study is available in a public Zenodo repository [<https://doi.org/10.5281/zenodo.7838980>]¹¹⁹. Supplementary data are provided as a Supplementary Data file. Source data are provided as a Source Data file.

Code Availability

All shell scripts and R code used in this study are available in a Github repository

[\[https://doi.org/10.5281/zenodo.7839042\]](https://doi.org/10.5281/zenodo.7839042)¹²⁰.

Author Contributions Statement

Conceptualization: TBS, AA, EMM, DMH, AMSC, MEB, LDM. Sample collection: TBS, MEB, SSM, AMSC. Experiment execution: AJV, NJM, BAD, SSM, AMSC, MEB. RNA extraction and processing: KMB, with input from NJM and BAD. Data analysis: KMB and EVB, with input from ME, NJM, and BAD. ITS2 sequencing and analysis: AJV, CEK and AMSC. Histology: AR and DMH. Manuscript writing: KMB and LDM, with editing contributions from all other authors.

Competing Interests Statement

The authors declare no competing interests.

Chapter 2 Figures:

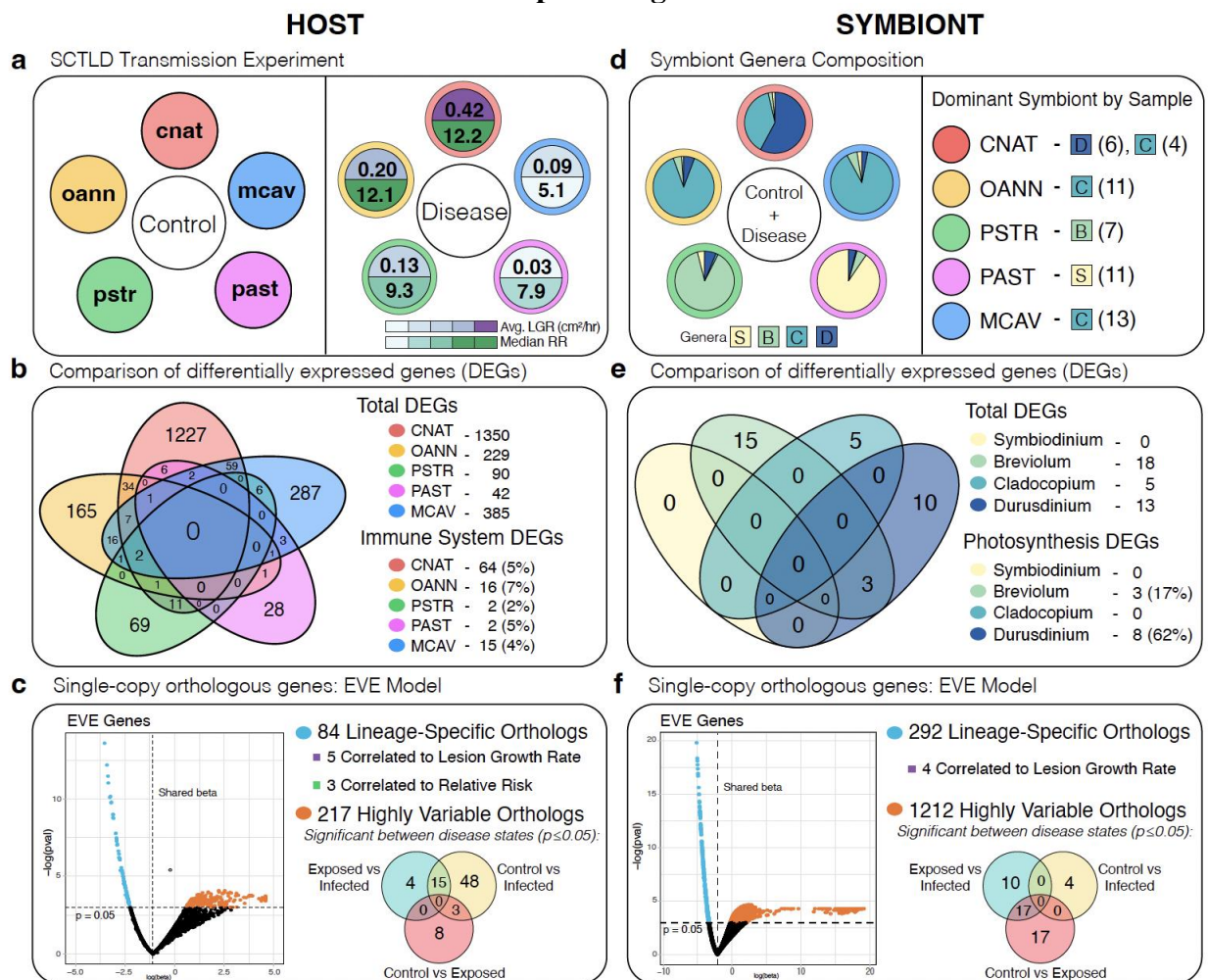
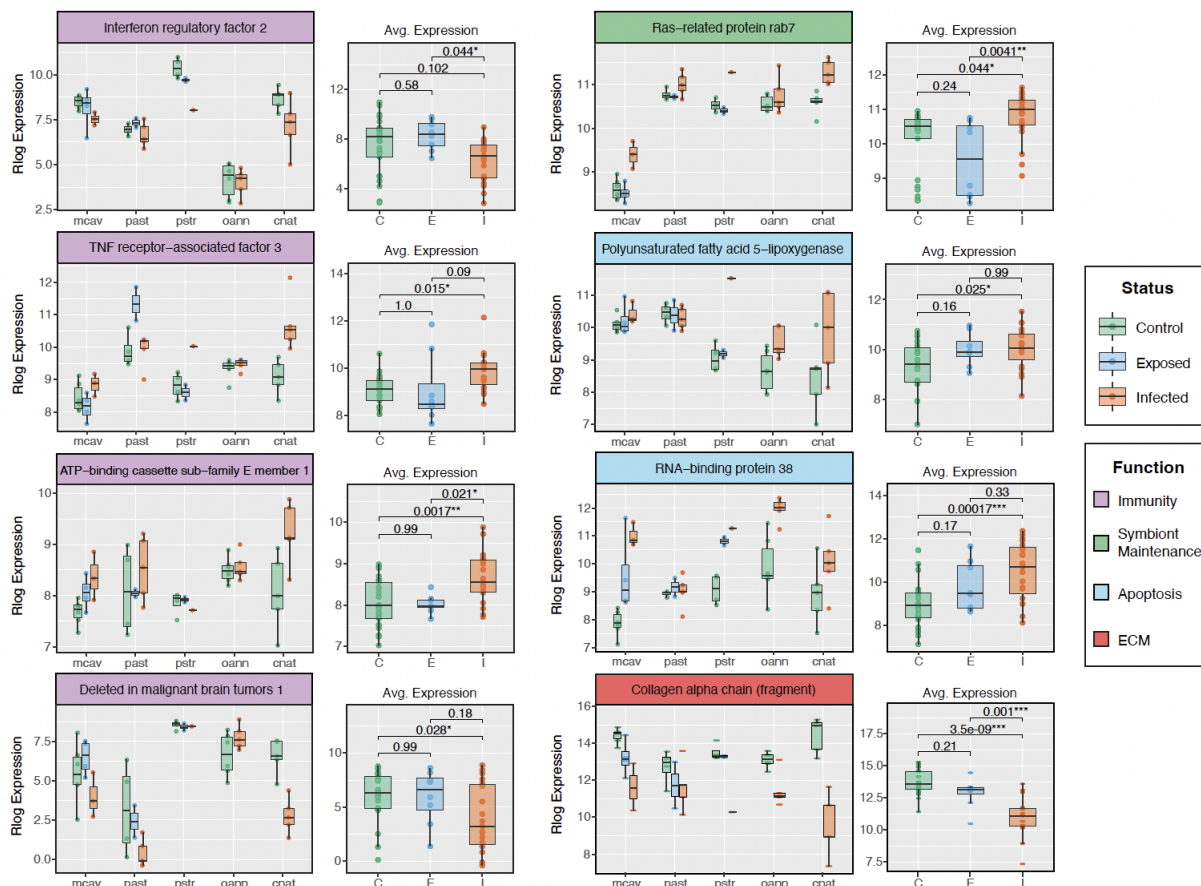


Figure 1: Overview of Experimental Design and Analysis. **a** Summary of the SCTLD transmission experiment in which eight replicates of five susceptible coral species were split in half, with one half exposed to a healthy *D. labyrinthiformis* colony (control) and the other half exposed to a diseased *D. labyrinthiformis* colony (disease). The control panel names the species in the study, and the disease panel shows the resulting species-level disease phenotypes used to inform our statistical analyses. **b** Venn Diagram showing the number of unique and shared DEGs across species between control and disease treatments. The total number of DEGs within each species was enumerated as well as the number and percentage of those involved in immunity and viral response. **c** EVE model summary for host orthologs. 1,766 single-copy orthologs were identified across the five species in our study and their expression was used as inputs for the EVE model used to differentiate genes with lineage-specific and highly variable expression. Pearson correlations were run on lineage-specific orthologs to identify those correlated to disease phenotypes, and one-way ANOVAs followed by TukeyHSD tests were run on highly variable orthologs to identify those with significant differential expression between disease states. **d** Symbiont composition determined by binning RNAseq reads to *Symbiodinium* (S), *Breviolum* (B), *Cladocopium* (C) and *Durusdinium* (D) reference transcriptomes. The first panel shows symbiont genera composition pie charts averaged across samples within each species. The second panel shows the dominant symbiont present within each sample. The expression from these dominant symbionts were used for downstream analyses. **e** Venn Diagram showing the number of unique and shared DEGs across dominant symbionts between control and disease treatments. The total number of DEGs within each was enumerated as well as the number and percentage of those involved in the relevant process of photosynthesis. **f** EVE model summary for dominant symbiont orthologs. 5,125 single-copy orthologs were identified across symbiont genera and their expression was used as input for the EVE model. Pearson correlations were run on lineage-specific orthologs to identify those correlated to disease phenotypes, and one-way ANOVAs followed by TukeyHSD tests were run on highly variable orthologs to identify those with significant differential expression between disease

states. (cnat = *Colpophyllia natans*; oann = *Orbicella annularis*; pstr = *Pseudodiploria strigosa*; past = *Porites astreoides*; mcav = *Montastraea cavernosa*; LGR = Lesion Growth Rate; RR = Relative Risk; ECM = Extracellular Matrix; EVE = Expression Variance and Evolution).



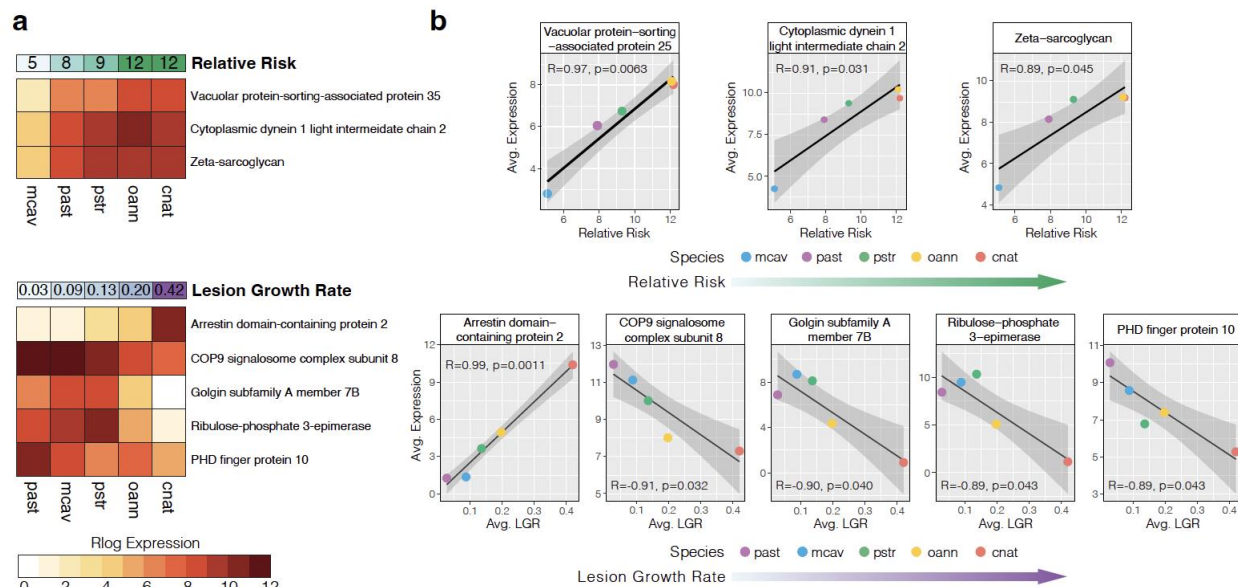


Figure 3: Expression of Single-Copy Coral Orthologs Significantly Correlated to Disease Phenotypes. The eight single-copy orthologs identified by EVE as lineage-specific (exhibiting low expression plasticity within species, but high variation between species) with significant correlation to species-level disease phenotypes (Pearson correlation; $p \leq 0.05$, $R < -0.85$ or $R > 0.85$). **a** Heatmaps plot the rlog transformed expression levels of each ortholog averaged across coral species. **b** Scatterplots plot this expression on the y-axis and the disease phenotype on the x-axis. One-sided Pearson correlation coefficients and P-values are provided for the linear trendline (black), and the grey area represents a 95% confidence interval.

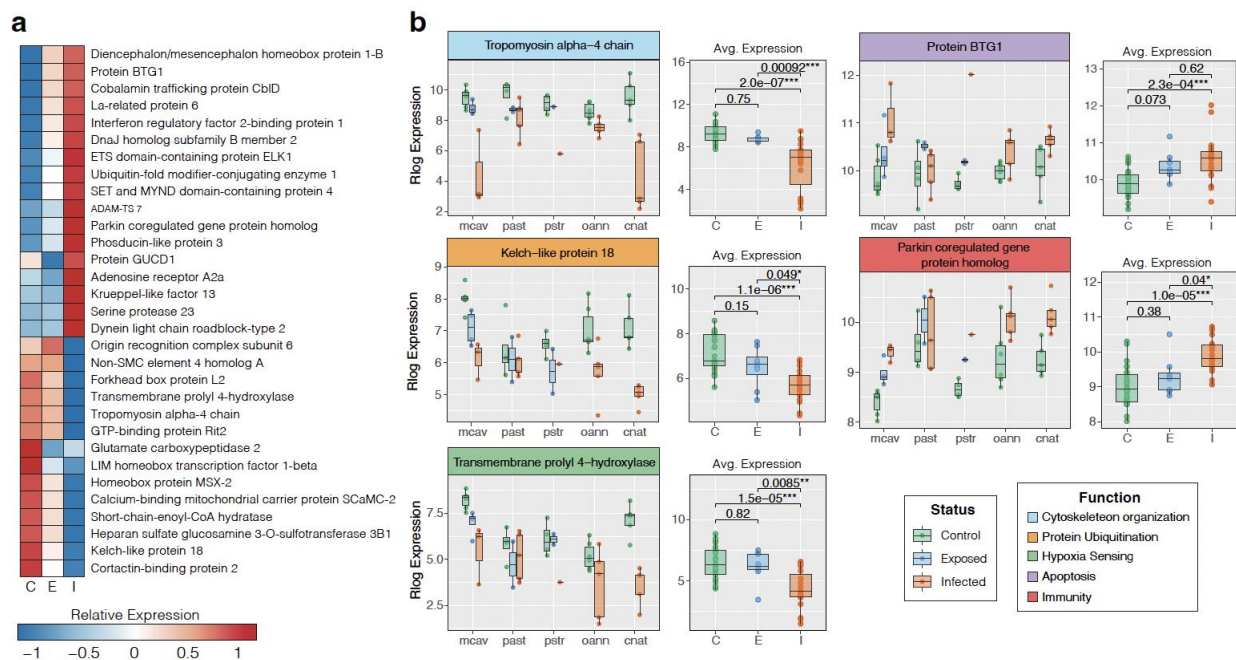


Figure 4: Single-Copy Coral Orthologs with Significant Differences in Expression Between Disease States.

The 31 annotated single-copy orthologs identified by EVE as highly variable (exhibiting expression plasticity across species and samples) that show the most significant differential expression between disease states (TukeyHSD; $p \leq 0.01$). **a** Heatmap plots the relative expression of those 31 highly variable orthologs averaged across disease state: C = Control (n=25), E = Exposed (no lesion, n=8), and I = Infected (with lesion, n=19). **b** Boxplots show the rlog transformed expression of relevant orthologs in each sample, organized by coral species on the left and by disease status on the right. Color of gene headers correspond to biological function obtained from literature searches and Uniprot. Color of boxplots correspond to experimental disease status. P-values represent TukeyHSD results following one-sided ANOVA tests (*) = $p \leq 0.05$; (**) = $p \leq 0.01$, (***) = $p \leq 0.001$. Boxplot elements: center line, median; box limits, upper and lower quartiles; whiskers, 1.5x interquartile range; points beyond whiskers, outliers).

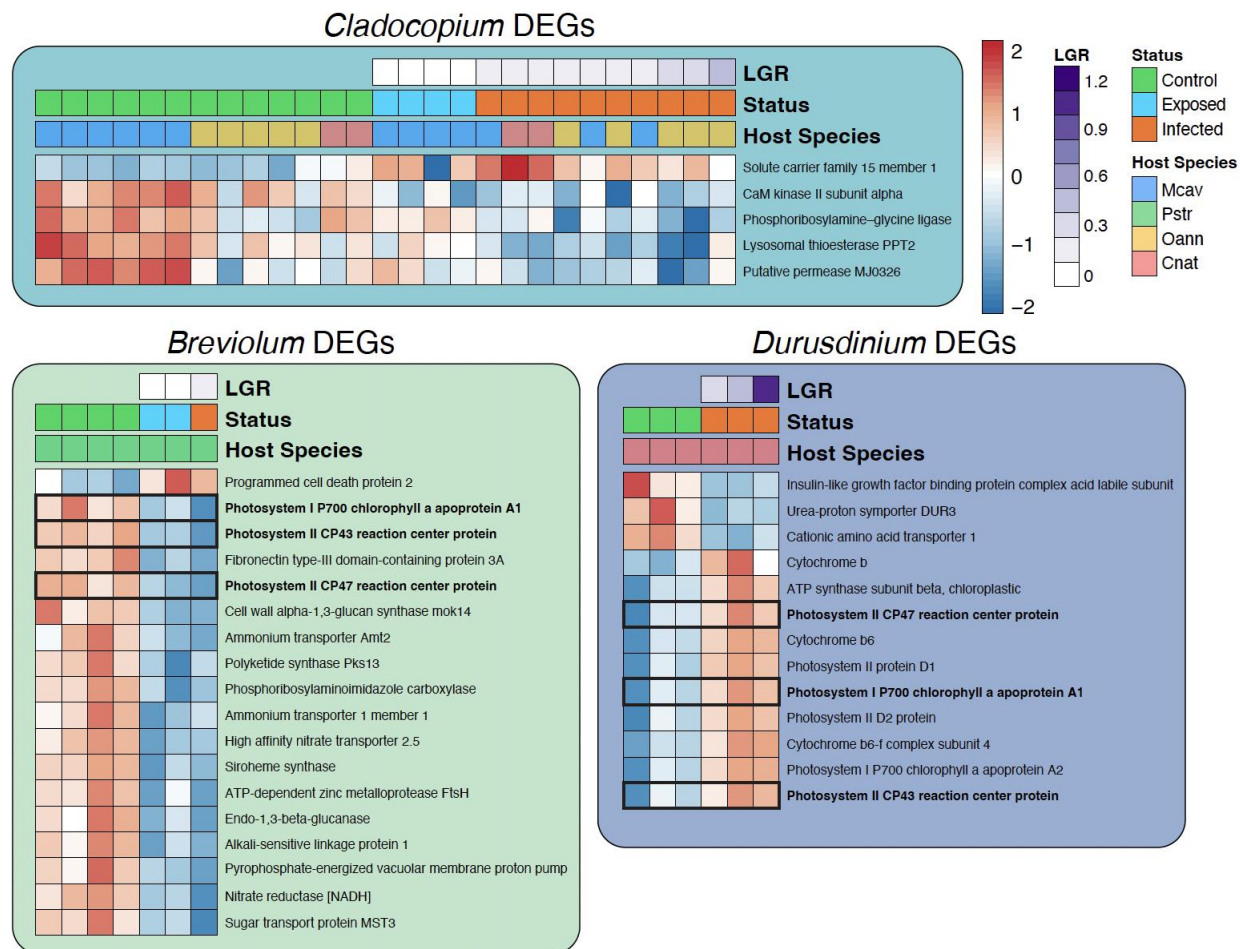


Figure 5: Dominant Symbiont DEGs. Heatmaps showing the relative expression of the significantly differentially expressed genes (control vs. disease treated) from each genus of dominant symbiont. Dominant symbionts belonging to the genera *Breviolum* shared three DEGs with dominant symbionts belonging to the genera *Durusdinium* (boxed rows and bolded gene names). No DEGs were identified in dominant symbionts belonging to the genera *Symbiodinium*. (LGR = Lesion Growth Rate).

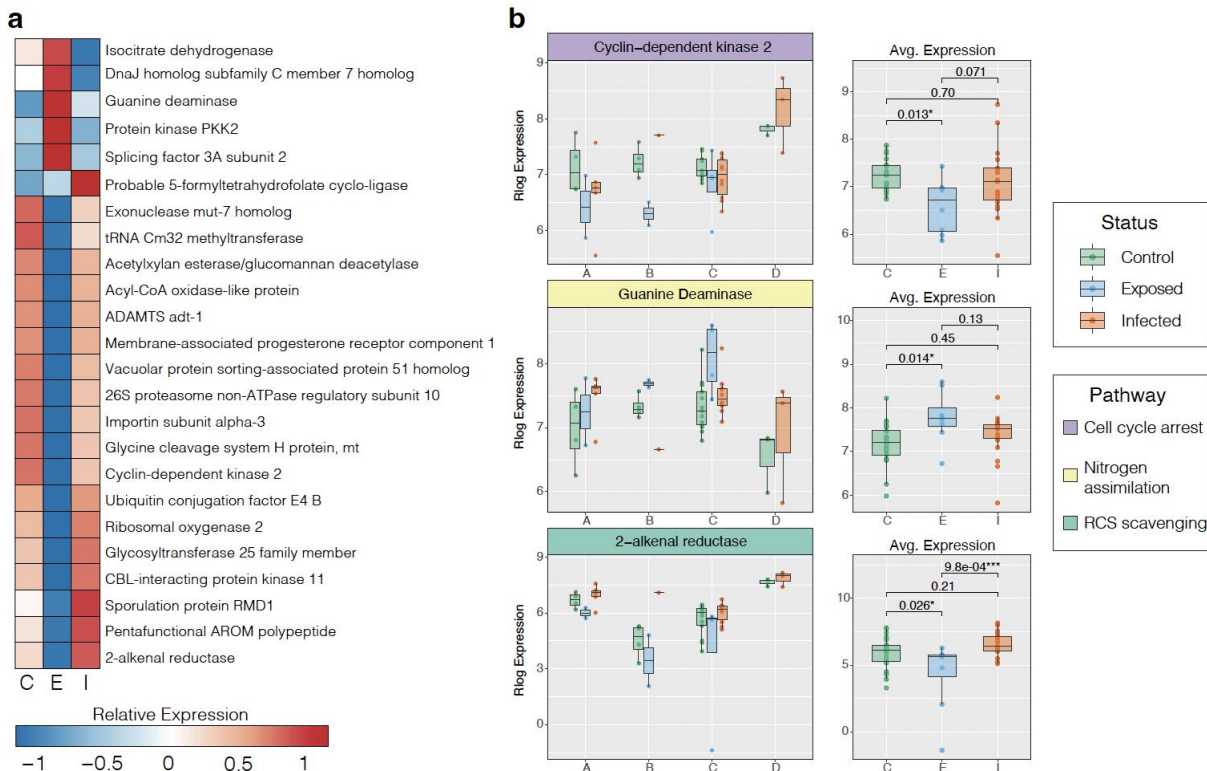


Figure 6: Single-Copy Symbiont Orthologs with Significant Differences in Expression Between Disease States.

The 24 annotated single-copy orthologs identified by EVE as highly variable (exhibiting expression plasticity across genera and samples) that show significant differential expression between disease states (TukeyHSD; $p \leq 0.05$). **a** Heatmap plots the relative expression of those 26 highly variable orthologs averaged across disease state: C = Control ($n=24$), E = Exposed (no lesion, $n=8$), and I = Infected (with lesion, $n=19$). **b** Boxplots show the rlog transformed expression of relevant orthologs in each sample, organized by dominant symbiont genera on the left and by disease status on the right. Color of gene headers correspond to biological function obtained from literature searches and Uniprot. P-values represent TukeyHSD results following one-sided ANOVA tests (*) = $p \leq 0.05$; (**) = $p \leq 0.01$, (***) = $p \leq 0.001$. (A = *Symbiodinium*, B = *Breviolum*, C = *Cladocopium*, D = *Durusdinium*). Boxplot elements: center line, median; box limits, upper and lower quartiles; whiskers, 1.5x interquartile range; points beyond whiskers, outliers).

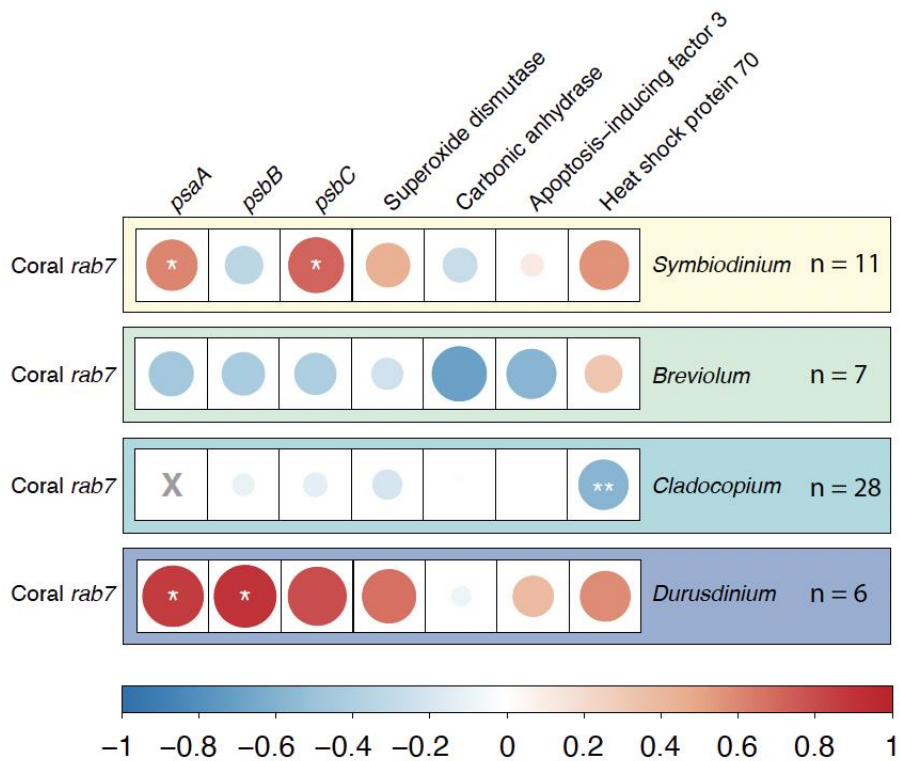


Figure 7: Rab7 Correlations. Correlation matrix showing the pairwise correlation coefficients (R values) between coral *rab7* expression and the expression of nine relevant symbiont genes. The color of the circle corresponds to the R values in the scale and the size of the circle corresponds to the absolute value of that R value. Significant correlations are present with stars (*) = $p \leq 0.05$; (**) = $p \leq 0.01$; (***) = $p \leq 0.001$. Actual p -values can be found in Supplementary Data 14.

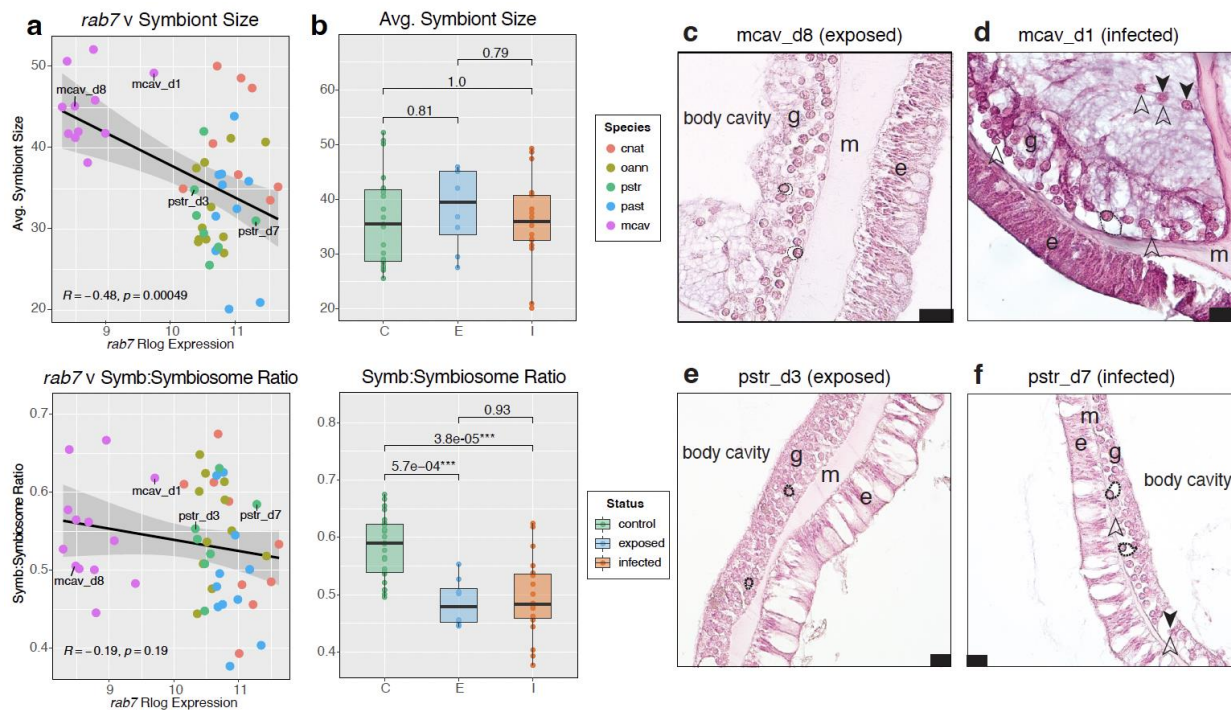


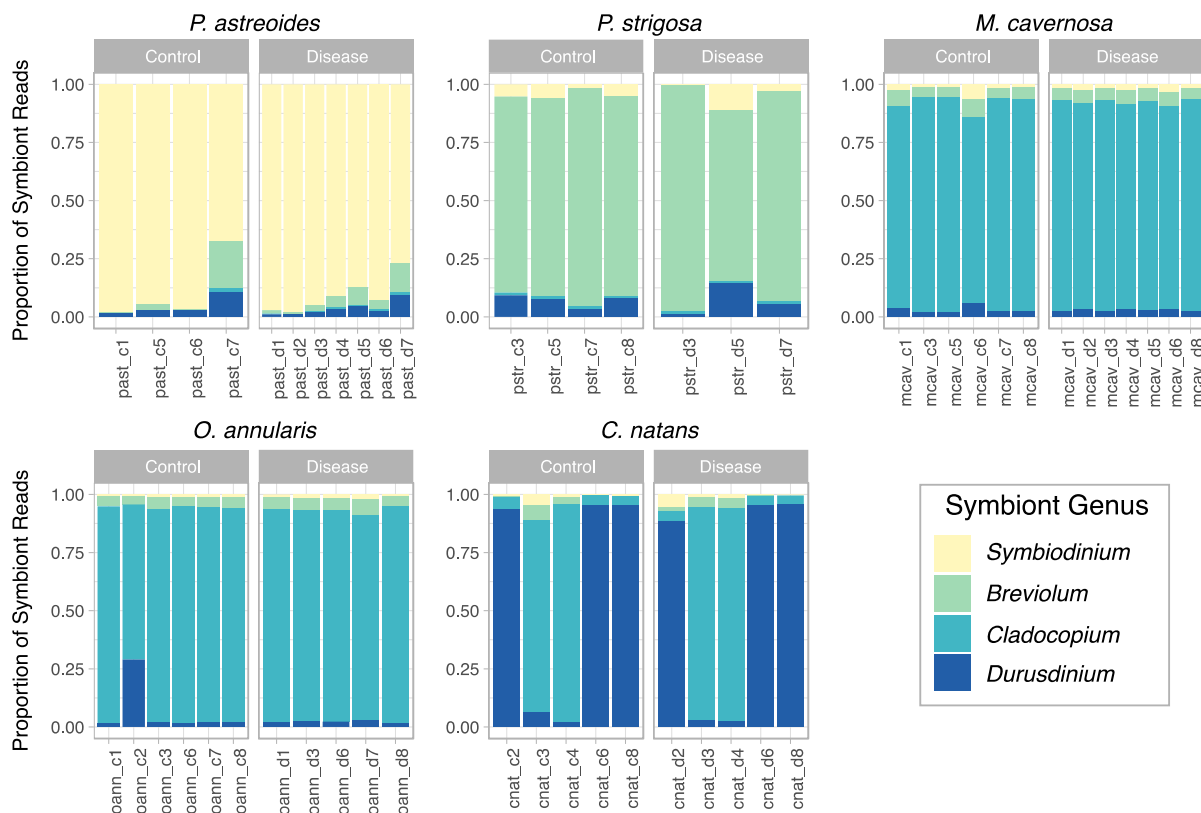
Figure 8: Histology and *rab7* correlation analysis. **a** Scatterplots show *rab7* rlog transformed expression on the x-axis plotted against the histology phenotype on the y-axis. Correlation coefficients and P-values are provided for the linear trendline (black), and the grey area represents a 95% confidence interval. **b** Boxplots show the histology phenotypes plotted by disease status: C = Control (n=25), E = Exposed (no lesion, n=8), and I = Infected (with lesion, n=19). P-values represent TukeyHSD results following one-sided ANOVA tests (*) = $p \leq 0.05$; (**) = $p \leq 0.01$, (***) = $p \leq 0.001$. **c** visually healthy *M. cavernosa* exposed to SCTLD. **d** SCTLD-infected *M. cavernosa* with elevated *rab7* expression **e** visually healthy *P. strigosa* exposed to SCTLD. **f** SCTLD-infected *P. strigosa* with elevated *rab7* expression. e = epidermis; m = mesoglea; g = gastrodermis. Dashed ovals outline symbiosomes, solid ovals outline symbiont cells within symbiosomes; solid arrows = exocytosed symbiont cells; empty arrows = potentially degraded symbiont cells. Scale bar = 20 μm . Boxplot elements: center line, median; box limits, upper and lower quartiles; whiskers, 1.5x interquartile range; points beyond whiskers, outliers.

Chapter 2 Tables:

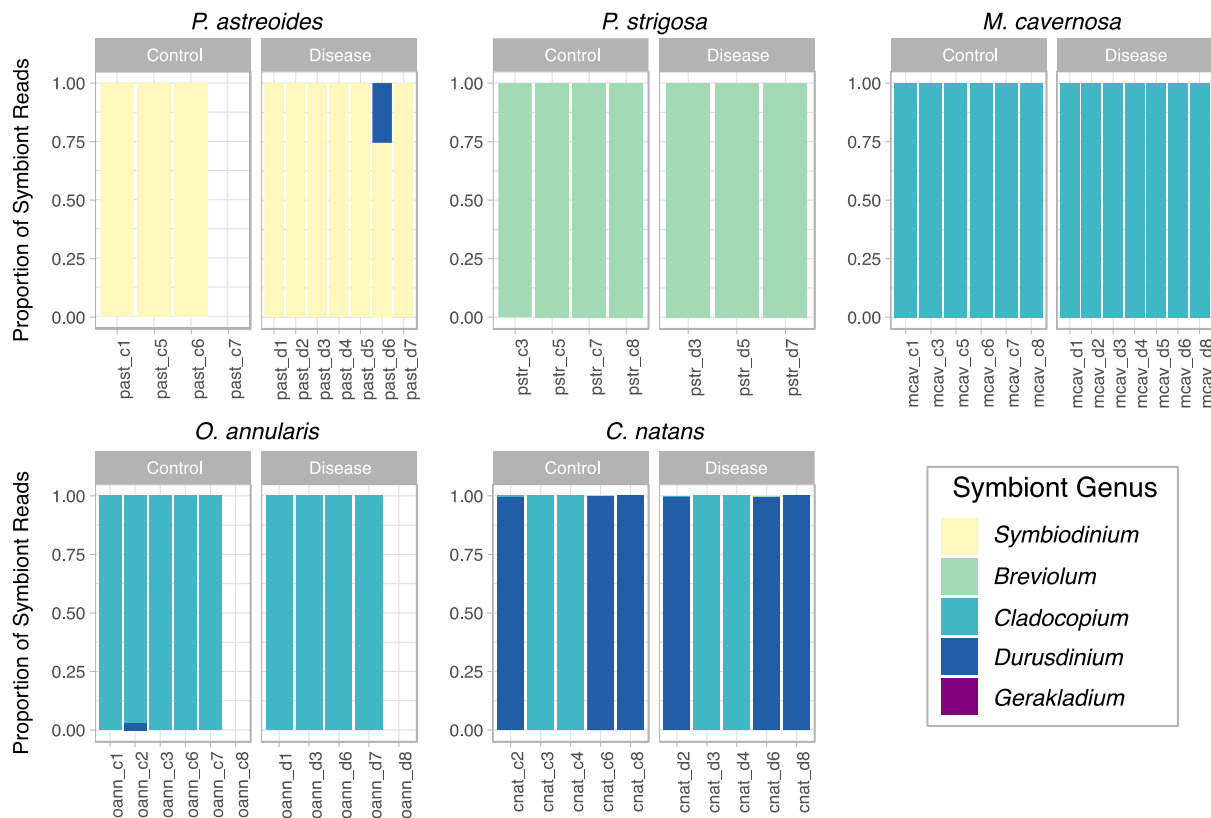
| Species | Type | No. contigs | Complete & single copy | Complete and duplicated | Fragmented | Missing | N50 | Percent annotated |
|---|----------------|-------------|------------------------|-------------------------|------------|---------|--------|-------------------|
| Coral host transcriptome assembly metrics based on metazoan reference | | | | | | | | |
| <i>C. natans</i> | <i>de novo</i> | 50,582 | 631 | 86 | 115 | 146 | 12,255 | 27% |
| <i>M. cavernosa</i> | genome-guided | 38,865 | 709 | 75 | 91 | 103 | 8,027 | 30% |
| <i>O. annularis</i> | genome-guided | 34,741 | 719 | 99 | 95 | 65 | 7,601 | 38% |
| <i>P. astreoides</i> | <i>de novo</i> | 37,167 | 806 | 44 | 60 | 68 | 6,457 | 36% |
| <i>P. strigosa</i> | <i>de novo</i> | 23,116 | 603 | 104 | 79 | 192 | 4,970 | 42% |
| Symbiodiniaceae transcriptome assembly metrics based on eukaryote reference | | | | | | | | |
| <i>S. CassKB8</i> | <i>de novo</i> | 72,152 | 123 | 6 | 39 | 87 | 17,845 | 15% |
| <i>B. minutum</i> | <i>de novo</i> | 51,199 | 172 | 6 | 19 | 58 | 11,053 | 20% |
| <i>C. goreau</i> | <i>de novo</i> | 65,838 | 110 | 66 | 18 | 61 | 18,032 | 18% |
| <i>D. trenchii</i> | <i>de novo</i> | 82,273 | 173 | 13 | 15 | 54 | 17,347 | 13% |

Table 1: Reference transcriptome sources and assembly metrics. Reference transcriptomes for *M. cavernosa*, *C. natans*, and *P. astreoides* were sourced from Dimos et al. (2022)⁶⁸. Reference transcriptomes for *S. CassKB8*, *B. minutum*, *C. goreau* and *D. trenchii* were sourced from Bayer et al. (2012)¹²¹, Parkinson et al. (2016)¹²², Davies et al. (2018)¹²³, and Bellantuono et al. (2019)¹²⁴, respectively. The “Percent annotated” column shows the percentage of protein-coding transcripts that were annotated with an evalue cutoff of $1.0e^{-6}$.

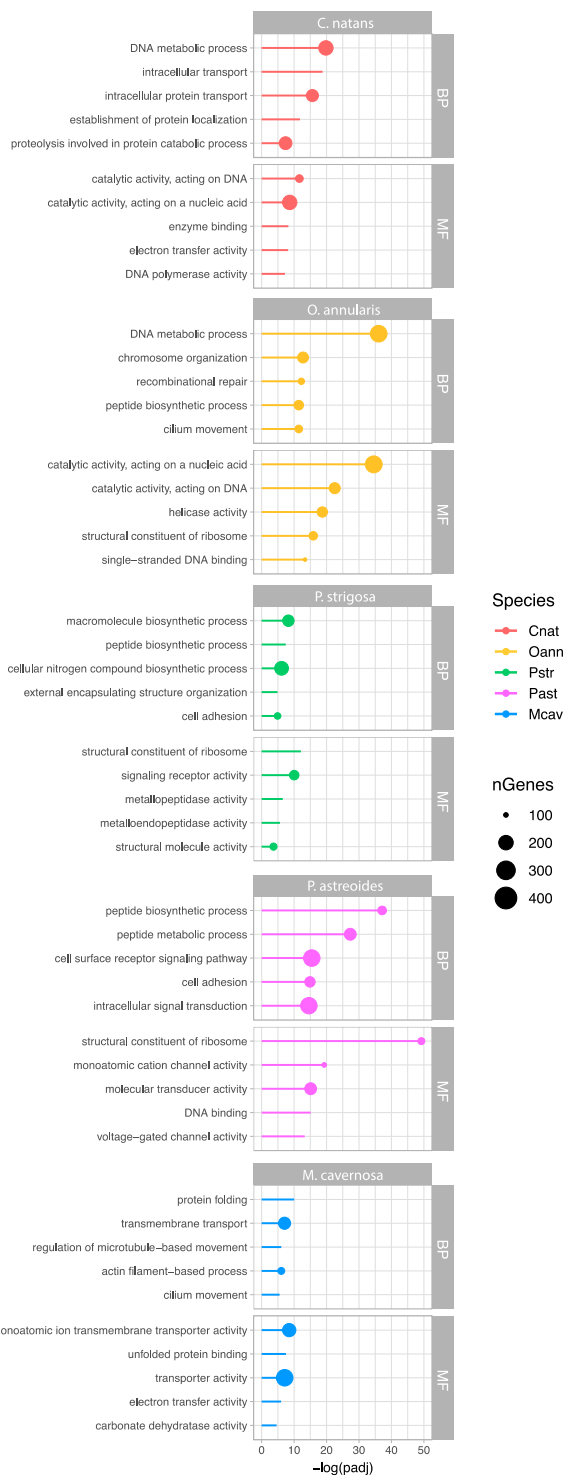
Chapter 2 Supplementary Information:



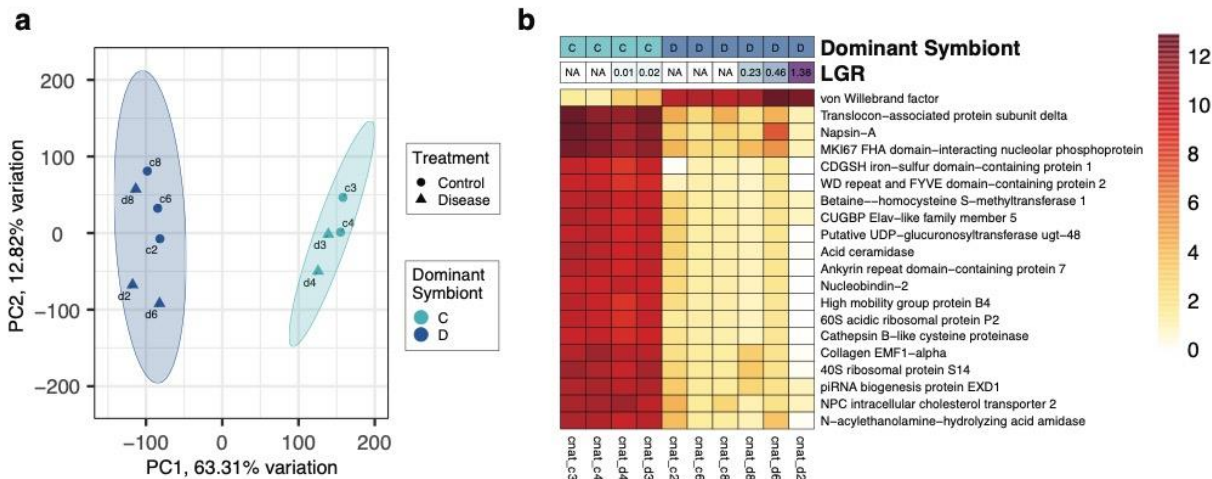
Supplementary Figure 1: Symbiont composition within each sample determined by BBSplit. Barplots show the proportion of total symbiont reads that mapped to each Symbiodiniaceae reference transcriptome provided. Plots are organized by host species and divided by control and disease (SCTLD exposure) samples. The dominant symbiont in each sample was determined by selecting the genus with the highest proportion of symbiont reads in that sample.



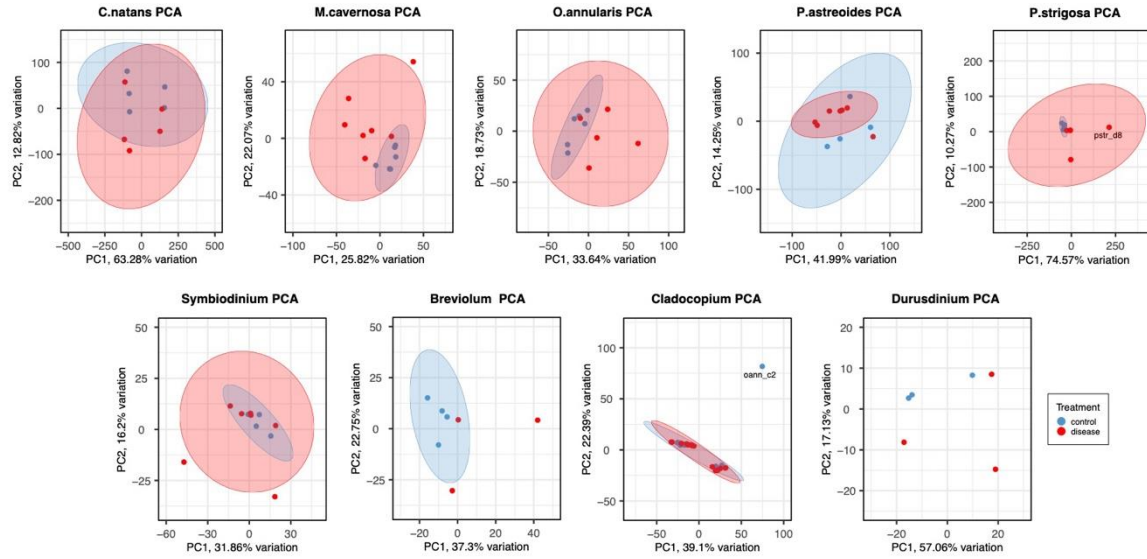
Supplementary Figure 2: Symbiont composition within each sample based on Illumina MiSeq of the internal transcribed space-2 (ITS-2) region of Symbiodiniaceae rDNA. Barplots show the relative abundance of hits to a given Symbiodiniaceae genus based on Symportal DIVs. Plots are organized by host species and divided by control and disease (SCTLD exposure) samples.



Supplementary Figure 3: GO Enrichment of Coral Species DEGs. The top 5 nonredundant Biological Process (BP) and Molecular Function (MF) GO terms enriched within each species' gene expression using adaptive clustering of GO categories and Mann-Whitney U tests based on \log_2 FoldChange values. Length of the bar represents the $-\log$ transformed P-value for the enrichment annotated with that GO term. Size of bubble represents the number of genes within each GO category.



Supplementary Figure 4: Principal Component Analysis (PCA) of *C. natans* expression. **a** PCA of *C. natans* rlog transformed gene expression data from all samples. Note that Principal Component 1 (PC1) explains 63.31% of variance between the two groups of samples and is driven by the dominant symbiont genera within the sample and not by disease treatment. **b** Heatmap plotting the rlog transformed expression of the top 20 PC1 loadings from each sample in **a**. These are the *C. natans* genes that are driving the variance within PC1 and have different expression levels based on the dominant symbiont genera within the coral sample. Note that corals hosting *Durusdinium* symbionts had much larger lesion growth rates than corals hosting *Cladocopium*. (C = *Cladocopium*; D = *Durusdinium*; c = control (treatment); d = disease (treatment)).



Supplementary Figure 5: Principal Component Analysis (PCA) to detect outliers. PCAs plot the rlog normalized expression of all transcripts with measurable expression within each coral species and dominant symbiont. One sample (pstr_d8) was removed from the coral expression dataset, and one sample (oann_c2) was removed from the symbiont expression dataset.

Chapter 3: Investigating stony coral tissue loss disease susceptibility and progression: insights
from gene expression, histology, and physiology

Authors: Kelsey M. Beavers^{1*}, Ashley M. Rossin², Madison A. Emery¹, Emily W. Van Buren¹,
Daniel M. Holstein², Amy Apprill³, Marilyn E. Brandt⁴, Erinn M. Muller⁵, Adrienne M.S.
Correa⁶, Laura D. Mydlarz¹

¹Department of Biology, University of Texas at Arlington, Arlington, TX, USA

²Department of Oceanography and Coastal Sciences, Louisiana State University, Baton Rouge,
LA, USA

³Marine Chemistry and Geochemistry Department, Woods Hole Oceanographic Institution,
Woods Hole, MA, USA

⁴Center for Marine and Environmental Studies, University of the Virgin Islands, St. Thomas,
USVI, USA

⁵Mote Marine Laboratory, Sarasota, FL, USA

⁶Department of Environmental Science, Policy and Management, University of California,
Berkeley, CA, USA

SYNOPSIS

Stony coral tissue loss disease (SCTLD) poses a significant threat to Caribbean reef ecosystems, yet our understanding of the factors that influence susceptibility to this disease remains incomplete. By integrating histology, immune and antioxidant assays, and gene expression analyses from a multi-species SCTLD transmission experiment, this study takes a comprehensive approach to investigate the cellular processes that distinguish highly susceptible species from their less vulnerable counterparts. We find that high susceptibility is characterized by elevated constitutive expression of genes involved in reactive oxygen species (ROS) metabolism and responding to endoplasmic reticulum (ER) stress, alongside low baseline immune activity and high oxidative stress. Alternatively, we find that low susceptibility is characterized by elevated constitutive expression of genes involved in immune regulation and DNA damage responses, as well as high baseline immune activity and low oxidative stress. Furthermore, we provide evidence that these constitutive differences in coral gene expression and physiology may be influenced by the dominant algal endosymbiont (family Symbiodiniaceae) hosted by a coral. Finally, we identify common cellular features associated with SCTLD; namely the downregulation of actin cytoskeleton genes accompanied by changes in symbiosome morphology. This comprehensive analysis provides a deeper understanding of the mechanisms underlying SCTLD susceptibility and emphasizes the importance of considering both host physiology and Symbiodiniaceae community in coral reef conservation efforts.

INTRODUCTION

Climate change has led to a significant increase in the prevalence and severity of infectious diseases¹²⁵, especially in marine organisms¹²⁶. Coral reef ecosystems are particularly

at risk in this changing environment, as an increase in the number and geographic distribution of coral epizootics has led to significant population declines of reef-building (scleractinian) species across the globe²³. The long evolutionary history of scleractinian corals has resulted in differential investment in immune mechanisms^{54,68}, which contribute to differences in disease incidence and severity at the species- and family-level^{52,53}. As climate pressures intensify, a holistic understanding of the cellular and molecular processes contributing to disease susceptibility is necessary for the implementation of effective disease prevention and mitigation efforts.

Stony corals, like all invertebrates, possess an innate immune system and antioxidant enzymes responsible for maintaining cellular homeostasis⁵⁵. One key aspect of innate immunity in corals involves the phenoloxidase (PO) cascade, synonymous with the melanin synthesis pathway, wherein PO enzymes are activated in response to microbial stimuli or tissue damage, ultimately leading to melanin deposition^{127,128}. The resulting melanin product plays a multifaceted role in immune defense, forming physical barriers that aid in pathogen encapsulation and wound healing^{129,130}. In addition, reactive oxygen species (ROS), such as superoxide anion (O_2^-) and hydrogen peroxide (H_2O_2), formed as by-products of aerobic cellular metabolism, act as second messengers required for the maintenance of cell signaling, proliferation, growth, apoptosis, and cytoskeletal organization¹³¹. Elevated levels of ROS can have direct toxic effects on cells due to their ability to damage DNA and organelle structures¹³². Stony corals possess antioxidant enzymes that mitigate oxidative damage by neutralizing harmful reactive oxygen species (ROS), thus playing an important role in redox homeostasis¹³³⁻¹³⁵. These enzymes include superoxide dismutase (SOD), which converts superoxide anion radicals to hydrogen peroxide, and catalase, which detoxifies hydrogen peroxide^{136,137}.

Understanding the dynamics of innate immunity and antioxidant mechanisms is central to coral disease research.

Caribbean coral reefs are currently experiencing one of the most destructive infectious disease outbreaks in recorded history – stony coral tissue loss disease (SCTLD). SCTLD affects at least half of all scleractinian coral species in the Western Atlantic and Caribbean²⁶ and is characterized by rapid tissue loss that can result in whole colony mortality in months^{28,29,46,47,138}. Since its emergence off the coast of Florida in 2014, SCTLD has spread throughout the Caribbean, resulting in significant losses of coral cover and the extirpation of species in some regions²⁵. To date, the etiologic agent(s) of SCTLD remains unknown, although research has implicated bacterial^{33–35,37,65,139} and/or viral^{42,43} pathogen involvement.

The use of histopathology, metabolomics, and transcriptomics have advanced our understanding of SCTLD pathogenesis¹⁴⁰. Within the coral tissue, SCTLD presents as tissue necrosis originating in the gastrodermis where the coral's Symbiodiniaceae are housed in host-derived vacuoles (symbiosomes)⁴⁴. Histopathology has also identified common cellular phenotypes of SCTLD, including increased symbiosome vacuolization, symbiont exocytosis, gastrodermal separation from the mesoglea, and virus-like particles exclusively localized within Symbiodiniaceae cells^{42,44,66,141}, implicating coral-Symbiodiniaceae dysbiosis in the pathology of this disease. Metabolomic profiling has revealed a high degree of variation in the production of Symbiodiniaceae-derived metabolites in SCTLD-affected corals¹⁴², supporting this hypothesis. In addition, gene expression analyses have shown that SCTLD-affected corals exhibit signatures of *in situ* degradation of dysfunctional Symbiodiniaceae¹⁴³ as well as genes involved in innate immune signaling, apoptosis, and extracellular matrix rearrangement^{67,143,144}.

Despite significant progress in SCTLD research, the precise factors underlying SCTLD susceptibility remain unknown. Here, we contextualize the gene expression from a multi-species SCTLD transmission experiment⁶⁶ with histology, immune and antioxidant protein assays, and dominant Symbiodiniaceae genus to holistically investigate the factors that distinguish high susceptibility species from their less vulnerable counterparts. First, we identify the histological, immune, and antioxidant traits that exhibit significant interspecies variation, as well as those that change in response to SCTLD. Then, we isolate gene co-expression networks significantly correlated to species relative risk of SCTLD and health state. Finally, we correlate the expression of these networks to our measured histology and biochemical traits as well as to the dominant Symbiodiniaceae genus in each sample. By relating expression profiles with cellular phenotypes, we show that adaptive variations in baseline immune regulation and DNA damage responses influence cellular stress levels within corals, influencing their ability to fight off SCTLD and other diseases. Additionally, we identify common processes involved in SCTLD progression across multiple species of coral, such as elevated oxidative stress, symbiosome vacuolization, and the downregulation of genes responsible for maintaining cell structure integrity.

METHODS

SCTLD transmission experiment

A full description of the experimental design and results of the SCTLD transmission experiment has been published⁶⁶. To summarize, a SCTLD transmission experiment was carried out in April of 2019 on the St. Thomas campus of the University of the Virgin Islands (UVI) wherein one fragment from each of five species of stony coral (*Colpophyllia natans*, *Montastraea cavernosa*, *Orbicella annularis*, *Porites astreoides*, and *Pseudodiploria strigosa*)

was placed into a control mesocosm equidistant from a healthy *Diploria labyrinthiformis* donor colony, and a corresponding genet fragment was placed into an experimental mesocosm equidistant from a *D. labyrinthiformis* donor colony exhibiting signs of SCTL D. Eight replicates per species (in a total of 16 mesocosms) were used. Coral fragments in the experimental mesocosms were monitored for lesion appearance for eight days, and fragments that developed lesions were removed when 30% tissue loss was achieved. Corresponding control genet fragments were removed at the same time. No control fragments developed lesions. Immediately upon removal, portions of each fragment were retained for histological analysis and the rest of the fragment was flash frozen and then stored at -80°C until processing for RNA and protein extraction. In this study, only control fragments and the fragments showing signs of expanding SCTL D lesions (SCTL D-affected corals) were used for histopathology, gene expression analysis, and biochemical protein assays. At the end of the transmission experiment, disease prevalence results were used to calculate median relative risk of SCTL D for each species of coral. Full relative risk calculations can be found in the Supplementary Material.

Protein extraction

To perform protein activity assays, tissue was first removed from the coral skeleton with a Paansche airbrush filled with extraction buffer (50 mM TRIS with 0.05 mM dithiothreitol (DTT), pH 7.8) following protocols outlined previously¹⁴⁵. The tissue extracts were homogenized and cells were lysed using a PowerGen 125 tissue homogenizer (Fisher Scientific). From the resulting homogenate, 1 mL was flash frozen and reserved for melanin analysis. The remainder of the homogenate was centrifuged for 10 min at 4°C, 1500 RPM. The resulting

supernatant (protein-enriched cell-free extract) was split into two 2 mL aliquots and flash frozen in liquid nitrogen before storage at -80°C .

Biochemical protein assays

Biochemical protein assays were conducted following established protocols for scleractinian corals, with minor modifications when necessary^{127,145–147}. Immune protein activity was measured using assays estimating PO cascade activity (PO activity and melanin concentration) and antioxidant activity (catalase and SOD). All assays were standardized by either protein concentration or dry tissue weight, as appropriate. All colorimetric assays were run in duplicate 96 well plates using a Synergy two multi-detection microplate reader and Gen 5 software (Biotek Instruments, Winooski, VT, USA). Full details on each protein assay can be found in the Supplementary Material.

Histopathology measurements

The fragments retained for histology were processed following the procedure outlined previously⁶⁶. Full details on histological processing can be found in the Supplementary Material. Ten pictographs were taken at 40X magnification ($60,000\ \mu\text{m}^2$ focal area per image) per coral fragment across all five serial sections. Using ImageJ, a 12-cell grid was overlaid on each image with each grid-cell having an area of $5,000\ \mu\text{m}^2$. A random number generator was used to select one grid-cell per pictograph for analysis in each coral sample. Within each selected grid-cell, the areas of all symbiont cells and symbiont-hosting vacuoles (symbiosomes) were measured. Twenty-five symbiont and symbiosome areas were measured within each coral sample, requiring a variable number of pictographs to achieve the desired number of measurements to calculate the

average ratio of symbiont to symbiosome size in each sample. In addition, the percent of symbiont cells exocytosed from the coral gastrodermis were measured for all symbionts within the grid-cell. All ten pictographs per coral fragment were used to calculate the average percent of exocytosed symbionts in each sample. All symbionts within proper focal distance were counted.

Statistical analyses

Kruskal-Wallis tests were conducted to identify immune, antioxidant, and histology traits significantly different across health states, coral species, and dominant symbiont genera using the R package ‘stats’ v. 4.2.2¹⁴⁸. Samples with missing trait data were removed from the analyses. Pairwise post-hoc comparisons were performed on all significant results using the Dunn test with the R package ‘FSA’ v. 0.9.5¹⁴⁹. Multiple comparison *p*-values were adjusted using the Holm-Bonferroni method. A *p*-value ≤ 0.05 was considered significant. All statistical analyses were performed in R v. 4.2.2¹⁴⁸.

Gene expression data collection and quantification

The raw RNA-seq data generated from our previous study¹⁴³ were sourced from NCBI (BioProject PRJNA860922). *P. strigosa* was removed from the study due to small sample size in the species, leaving 21 control corals and 18 SCTL D-affected corals from four species (*M. cavernosa*, *P. astreoides*, *O. annularis*, and *C. natans*). Reads were processed following the protocol outlined previously¹⁴³. First, raw reads were quality-filtered using FastP v. 0.20.1⁹⁴ under default parameters. Reference transcriptomes and their annotations for each species of coral were sourced from Beavers et al. (2023)¹⁴³. Reference transcriptomes representing the Symbiodiniaceae genera *Symbiodinium*, *Breviolum*, *Cladocopium*, and *Durusdinium* were

sourced from previous studies^{121–124}. Coral and Symbiodiniaceae reads were isolated using the above transcriptomes as references with BBSplit v. 38.90¹⁰⁶, and the binning statistics output was used to determine the percent of *Symbiodinium*, *Cladocopium*, and *Durusdinium* reads in each sample. This information was used to identify the dominant genus of Symbiodiniaceae present within each sample, referred to throughout the text as the “dominant symbiont”. Coral reads were mapped to their respective transcriptomes and quantified using Salmon v. 1.5.2¹⁰⁵.

Identifying gene expression networks correlated to experiment outcome and trait data

To compare gene expression levels across species, predicted proteomes associated with each coral species were first sourced from Beavers et al. (2023)¹⁴³ and run through Orthofinder v. 2.5.2¹¹². The output from Orthofinder was used to identify groups of orthologous genes (orthogroups) across the predicted proteomes. Orthogroup count matrices were generated for each species using Tximport v. 1.26.1¹⁰⁷ and were then merged across the four coral species by orthogroup ID. The resulting four-species orthogroup count matrix was run through DESeq2 1.38.3¹⁰⁸ using the design $\sim \textit{species} + \textit{health_state}$ to obtain orthogroup regularized log (rlog) expression. Orthogroups with an average rlog expression < 10 were removed.

Weighted Gene Co-Expression Network Analysis (WGCNA) was run on the shared coral orthogroups using the WGCNA R package v.1.72.5¹⁵⁰. WGCNA attempts to identify clusters (modules) of highly correlated genes that can then be related to external trait data. First, samples were hierarchically clustered by orthogroup expression to identify outliers, and none were detected (Supp. Figure 1). Next, automatic network construction was performed (parameters: soft threshold power = 18, network type = signed, correlation = bidweight midcorrelation, max percent outliers = 10%, minimum module size = 75) (Supp. Figure 2). Then, the expression of all

orthogroups within each module was summarized by eigengene value and correlated to health state, relative risk of SCTLD, antioxidant and immune activity, histology measurements, and the dominant symbiont genus within each sample using Pearson correlations (Supp. Figure 3). The four modules with the most significant correlation to relative risk and the one module significantly correlated to health state were selected for further analysis.

Functional enrichment of selected gene co-expression networks

To perform functional enrichment on each selected gene co-expression network (module), first the predicted proteome for *M. cavernosa* was uploaded to STRING v. 12.0¹⁵¹ using the ‘Add organism’ tool (*M. cavernosa* STRING ID: STRG0A22FEF). Then, orthogroups within each co-expression network were annotated with one representative protein sequence ID from *M. cavernosa*. These annotated orthogroups are referred to throughout the text as genes. Then, these lists of genes were uploaded to STRING to perform functional enrichment on each co-expression network. Strength of the enrichment was calculated as $\text{Log}_{10}(\text{number of proteins annotated with the term} / \text{number of proteins expected to be annotated with the term in a random network of the same size})$. Gene Ontology (GO): Biological Process terms with an enrichment False Discovery Rate (FDR) ≤ 0.05 and strength > 0.5 were saved for each co-expression network, and a curated list of the five most relevant terms were plotted. The response of specific groups of genes within each module was examined by calculating the eigengene expression of orthogroups belonging to a selected GO: Biological Process term as described previously¹⁵².

RESULTS

Transmission experiment

Full transmission experiment results have been published previously⁶⁶. To summarize, 100% of the *C. natans* and *O. annularis* fragments developed lesions consistent with SCTLD gross morphology, followed by 62.5% of *P. astreoides* fragments and 37.5% of *M. cavernosa* fragments⁶⁶. Relative risk assessment revealed that *C. natans* and *O. annularis* had the highest median relative risk (12.19 and 12.09, respectively), followed by intermediate risk in *P. astreoides* (7.91) and the lowest risk in *M. cavernosa* (5.10), which exhibited significantly lower risk compared to the other species⁶⁶.

Statistical analysis

Average symbiont:symbiosome size and average percent exocytosis of symbionts (exopercent) were the only two traits that showed significant differences between control and SCTLD-affected corals (Figure 1, Table S1a). Catalase activity, PO activity, and melanin concentration exhibited significant constitutive differences between coral species and dominant symbiont genera (Figure 1, Tables S1b and S1d). Catalase activity was significantly higher in *C. natans* compared to *P. astreoides* (Figure 1, Table S1c) and in *Durisdinium*-dominant corals relative to the other symbiont genera (Figure 1, Table S1e). PO activity was significantly higher in *M. cavernosa* compared to both *C. natans* and *P. astreoides* (Figure 1, Table S1c) and in *Cladocopium*-dominant corals relative to *Durisdinium*-dominant corals (Figure 1, Table S1e). Melanin concentration was significantly higher in *P. astreoides* compared to *O. annularis* (Figure 1, Table S1c) and in *Symbiodinium*-dominant corals relative to *Cladocopium*-dominant corals (Figure 1, Table S1e).

Gene expression data collection and quantification

Raw RNA-seq reads from 21 control samples (*M. cavernosa*: $n = 6$; *P. astreoides*: $n = 4$, *O. annularis*: $n = 6$; *C. natans*: $n = 5$) and 18 SCTLD-affected samples (*M. cavernosa*: $n = 3$; *P. astreoides*: $n = 5$; *O. annularis*: $n = 5$; *C. natans*: $n = 5$) were downloaded from NCBI, resulting in a total of 2.1 billion raw reads with an average of 54.3 million raw reads per sample. Running the adapter-trimmed and quality-filtered reads through BBSplit resulted in a total of 18.3 million reads binned to the coral host and 18.7 million reads binned to the samples' dominant symbiont. Mapping the coral reads to their respective transcriptomes resulted in an average mapping rate of 86% (Table S2).

Identifying gene expression networks correlated to experiment outcome and trait data

Orthogroup count matrix generation resulted in 18,397 orthogroups expressed in *M. cavernosa*, 18,255 in *P. astreoides*, 18,459 in *O. annularis*, and 20,966 in *C. natans*. Merging count matrices across coral species resulted in a four-species count matrix with 8,327 shared orthogroups. After DESeq2 rlog normalization and removal of orthogroups with a rlog expression < 10 , a total of 8,179 orthogroups with measurable expression levels across all species remained (Table S3).

WGCNA automatic network construction of 8,179 orthogroups resulted in 17 modules ranging in size from 1,022 to 112 orthogroups. In addition, an eighteenth module (grey module) contained 237 orthogroups that could not be placed in a co-expression network. Correlating module eigengene values to the transmission experiment outcome data resulted in 11 modules significantly correlated (p -value ≤ 0.05) to relative risk and one module significantly correlated to disease status (Supp. Figure 3, Table S4). The magenta module and black module eigengenes had the strongest positive correlation to relative risk ($R = 0.97$, $p = 2e-25$; $R = 0.81$, $p = 3e-10$,

respectively). The blue module and tan module eigengenes had the strongest negative correlation to relative risk (blue: $R = -0.86$, $p = 1e-12$; tan: $R = -0.74$, $p = 9e-08$). The grey module was the only module with a significant correlation to disease status ($R = -0.72$, $p = 2e-07$). These five modules were selected for further analysis, and their relationships to each trait is shown in Figure 2A.

Functional enrichment of selected gene co-expression networks

Positively correlated to relative risk

Functional enrichment of the magenta module identified 18 significantly enriched (FDR ≤ 0.05 ; strength > 0.5) GO: Biological Process terms, including ‘Ubiquitin-dependent protein catabolic process’, ‘Regulation of MAPK cascade’, and ‘Reactive oxygen species (ROS) metabolic process’ (Figure 2b, Table S5). The expression within the magenta module was positively correlated with SOD activity ($R = 0.47$) and predominantly hosting *Durusdinium* ($R = 0.39$) and was negatively correlated with PO activity ($R = -0.49$), melanin concentration ($R = -0.46$), and predominantly hosting *Symbiodinium* ($R = -0.48$) (Figure 2a).

Functional enrichment of the black module identified 40 significantly enriched (FDR ≤ 0.05 ; strength > 0.5) GO: Biological Process terms, including ‘Response to endoplasmic reticulum (ER) stress’, ‘Regulation of apoptotic process’, and ‘Cellular respiration’ (Figure 2b, Table S5). Like the magenta module, the black module was positively correlated with SOD activity ($R = 0.41$) and predominantly hosting *Durusdinium* ($R = 0.37$) and was negatively correlated with PO activity ($R = -0.74$). Unlike the magenta module, this module was negatively correlated with predominantly hosting *Cladocopium* ($R = -0.51$) (Figure 2a).

Overall expression within the magenta module was lower in *M. cavernosa* and *P. astreoides* compared to *O. annularis* and *C. natans* (Figure 3a), whereas overall expression within the black module was lower in only *M. cavernosa* compared to the three other species (Figure 3b). Genes annotated with the enrichment term ‘ROS metabolic process’ from the magenta module and genes annotated with the enrichment term ‘Response to ER stress’ from the black module were selected for further analysis by calculating their eigengene expression within each sample and correlating this to PO activity and SOD activity. Lists of genes associated with these GO terms can be found in Table S6. Both groups of genes exhibited a significant negative correlation with PO activity (‘ROS metabolic process’: $R = -0.36$, $p = 0.026$; ‘Response to ER stress’: $R = -0.63$, $p < 0.001$) (Figure 3c,d) and a significant positive correlation with SOD activity (‘ROS metabolic process’: $R = 0.43$, $p = 0.0066$; ‘Response to ER stress’: $R = 0.51$, $p < 0.001$) (Figure 3e,f). Genes involved in ROS metabolism from the magenta module included Catalase (*CAT*) and Peroxiredoxin 4 (*PRDX4*), and genes involved in responding to ER stress within the black module included Activating transcription factor 6 beta (*ATF6B*) and Synoviolin 1 (*SYVNI*) (Figure 5).

Negatively correlated to relative risk

Functional enrichment of the blue module identified 24 significantly enriched ($FDR \leq 0.05$; strength > 0.5) GO: Biological Process terms, including ‘Regulation of immune response’, ‘Regulation of autophagy’, and ‘Import into cell’ (Figure 2b, Table S5). This module was positively correlated with PO activity ($R = 0.32$), melanin concentration ($R = 0.41$), and predominantly hosting *Symbiodinium* ($R = 0.5$) and was negatively correlated with SOD activity ($R = -0.38$) (Figure 2a).

Functional enrichment of the tan module identified 13 significantly enriched ($FDR \leq 0.05$; strength > 0.5) GO: Biological Process terms, including ‘response to radiation’, ‘signal transduction in response to DNA damage’, and ‘ncRNA processing’ (Figure 2b, Table S5). Like the blue module, the tan module was positively correlated with PO activity ($R = 0.57$) and negatively correlated with SOD activity ($R = -0.37$). Unlike the blue module, this module was positively correlated with predominantly hosting *Cladocopium* ($R = 0.46$) and negatively correlated with predominantly hosting *Durusdinium* ($R = -0.71$).

Overall expression within the blue module was higher in *M. cavernosa* and *P. astreoides* compared to *O. annularis* and *C. natans* (Figure 4a), whereas overall expression within the tan module was highest in *M. cavernosa*, intermediate in *P. astreoides* and *O. annularis*, and lowest in *C. natans* (Figure 4b). Genes annotated with the enrichment term ‘Regulation of immune response’ from the blue module and genes annotated with the enrichment term ‘Signal transduction in response to DNA damage’ from the tan module were selected for further analysis by calculating their eigengene expression within each sample and correlating this to relevant trait data (Melanin concentration and SOD activity for the blue module and PO activity and SOD activity for the tan module). Lists of genes associated with these GO terms can be found in Table S6. The expression of genes involved in regulating immune responses showed a positive correlation with melanin concentration ($R = 0.41$, $p = 0.0091$) (Figure 4c) and a marginally significant negative correlation with SOD activity ($R = -0.3$, $p = 0.061$) (Figure 4e). Similarly, the expression of genes involved in signal transduction in response to DNA damage was positively correlated with PO activity ($R = 0.44$, $p = 0.0051$) (Figure 4d), and negatively correlated with SOD activity ($R = -0.35$, $p = 0.028$) (Figure 4f). Genes involved in immune regulation from the blue module included Phosphoinositide-3-Kinase Adaptor Protein 1

(*PIK3AP1*) and OUT Deubiquitinase With Linear Linkage Specificity (*OTULIN*), and genes involved in responding to DNA damage from the tan module included ATM Serine/Threonine Kinase (*ATM*) and Eukaryotic Translation Initiation Factor 2 Alpha Kinase 4 (*EIF2AK4*) (Figure 5).

Negatively correlated to SCTL D

Functional enrichment of the grey module identified only two significantly enriched ($FDR \leq 0.05$; strength > 0.5) GO: Biological Process terms: ‘Ribonucleoprotein complex biogenesis’ and ‘Extracellular matrix organization’ (Figure 2b, Table S5). This module was not correlated with dominant symbiont genus, but was negatively correlated with catalase activity ($R = -0.4$) and was positively correlated with average symbiont:symbiosome size ($R = 0.45$) (Figure 2a).

The eigengene expression patterns within the grey module associated with health status revealed that expression within this module was lower in all species exhibiting active SCTL D lesion morphology relative to controls (Supp. Figure 4a,b). Genes annotated with the two GO: Biological Process terms enriched in this module, ‘Extracellular matrix organization’ and ‘Ribonucleoprotein complex biogenesis’ were selected for further analysis by calculating their eigengene expression within each sample and correlating this to catalase activity and average symbiont:symbiosome size. Lists of genes associated with these GO terms can be found in Table S6. These two groups of genes exhibited opposite correlations to catalase activity (‘Extracellular matrix organization’: $R = 0.49$, $p = 0.0014$; ‘Ribonucleoprotein complex biogenesis’: $R = -0.52$, $p < 0.001$) (Supp. Figure c,d), and neither group of genes were correlated with average

symbiont:symbiosome size (Supp. Figure 4e,f). Additionally, neither group of genes showed a relationship to health status (Supp. Figure 4c-f).

Because the grey module contains genes outside of a detectable co-expression network, we posit that individual genes, rather than groups of co-expressed genes, are collectively driving the observed module eigengene correlations to health status, catalase activity, and symbiosome vacuolization. Therefore, the top ten grey module genes with the most significant eigengene correlation to disease status were isolated (Table S3). These included two genes involved in cytoskeletal organization: Tropomyosin beta chain (*TPM2*) and Myosin regulatory light polypeptide 9 (*MYL9*). Both genes were significantly downregulated in SCTLD-affected corals relative to controls (Figure 6). In addition, the expression of both genes was negatively correlated with catalase activity (*TPM2*: $R = -0.43$, $p = 0.0062$; *MYL9*: $R = -0.37$, $p = 0.024$) and positively correlated with average symbiont:symbiosome size (*TPM2*: $R = 0.47$, $p = 0.0026$; *MYL9*: $R = 0.51$, $p = 0.0012$) (Figure 6).

DISCUSSION

SCTLD has had a devastating impact on Caribbean coral reefs, resulting in extreme losses of coral cover since its emergence in 2014^{138,153,154}. A comprehensive understanding of the cellular mechanisms driving SCTLD susceptibility and pathogenesis is beneficial to conservation, intervention, and restoration efforts aimed at identifying factors contributing to disease resistance. Here, we leverage the results from a SCTLD transmission experiment to investigate the immune, antioxidant, and histological phenotypes, as well as the gene expression profiles and Symbiodiniaceae genera associated with relative risk of SCTLD and disease progression. We find that highly susceptible species exhibit constitutively higher expression of

genes involved in mitigating ROS and ER stress at the expense of maintaining optimal immune function. Additionally, we show that constitutively higher expression of genes involved in immune regulation and DNA damage responses is protective against SCTLD and is correlated with increased baseline melanin cascade activity and decreased oxidative stress. Finally, we identify common processes involved in SCTLD progression across multiple species of coral, namely the downregulation of genes responsible for maintaining cytoskeletal structure, elevated levels of oxidative stress, and increased symbiosome vacuolization.

Phenotype patterns

Coral species and dominant symbiont genera, but not health status, had the largest effect on the measured antioxidant and immune traits. Variations in immune activity (PO activity and melanin concentration) were predominantly influenced by coral species. Notably, *M. cavernosa*, the species with the lowest median relative risk of SCTLD in this study, had significantly higher levels of PO activity compared to the other species, supporting evidence that constitutively higher levels of melanin synthesis confers resistance to disease¹⁵⁵. Conversely, catalase activity was primarily influenced by the dominant symbiont genus hosted by a coral. Specifically, *Durisdinium*-dominant corals exhibited significantly higher levels of catalase activity, suggesting that the presence of *Durisdinium* spp. may elevate baseline hydrogen peroxide levels in corals, necessitating heightened scavenging activity. This observation aligns with our previous findings, where corals dominant in *Durisdinium* spp. exhibited the fastest lesion growth rates of all coral fragments following exposure to SCTLD¹⁴³. The same *Durisdinium* symbionts displayed gene expression signatures of photosynthetic overexcitation and metabolic dysfunction compared to the other symbiont genera, likely producing elevated levels of ROS that can leak

into and damage coral cells¹⁴³. Taken together, these results support evidence that predominantly hosting *Durusdinium* spp. may increase susceptibility to SCTL^{143,156} and emphasize the importance of considering both coral species and symbiont community in disease management strategies.

The average symbiont to symbiosome size ratio and average percent exocytosis of symbionts were the only measured traits that showed a significant difference between control and SCTL^{143,156}-affected corals, further implicating Symbiodiniaceae in the pathology of this disease. Our histopathology results align with previous studies that found increased vacuolization around Symbiodiniaceae cells in SCTL^{143,156}-affected samples^{44,141}, which may indicate disrupted nutrient transfer from the symbiont to the coral animal¹⁵⁷. This potential disruption of symbiotic homeostasis has significant implications for coral health and could contribute to the severity of SCTL.

Expression patterns and phenotypes associated with SCTL susceptibility

To connect cellular phenotypes and Symbiodiniaceae community composition to gene expression, we identified shared gene co-expression networks across four phylogenetically distinct coral species and correlated network expression to our SCTL outcome data. We found that nearly two thirds (11/17) of the identified co-expression networks were significantly correlated to species relative risk of getting SCTL, and that the expression within these networks seemed to be influenced by the dominant symbiont within a coral sample. Our findings indicate the presence of species-specific differences in gene expression networks and shed light on how these differences may contribute to coral susceptibility to SCTL. Moreover, the influence of Symbiodiniaceae community content on gene expression suggests a complex

interplay between host gene expression and symbiont dynamics in shaping disease susceptibility in corals.

High SCTLD susceptibility is associated with low PO activity, high SOD activity, and elevated constitutive expression of genes involved in cellular stress responses

Through WGCNA, we identified two networks of co-expressed genes with strong positive correlations to relative risk of SCTLD. Constitutively higher expression of genes within these networks was associated with low PO (immune) activity, high SOD activity (oxidative stress), and predominantly hosting *Durusdinium* spp. Within these networks, we found enrichment of terms involved in coral general stress response pathways, including ROS metabolism¹⁵⁸, MAPK signaling⁸⁹, ER stress responses¹⁵⁹, and apoptosis¹⁶⁰. Although *Durusdinium* is considered a thermotolerant symbiont¹⁶¹, these findings point at a potential trade-off, where increased thermotolerance conferred by hosting *Durusdinium* spp. comes at the cost of elevated cellular stress levels and reduced immune activity in its hosts.

Our analysis of genes involved in ROS metabolism and ER stress responses revealed insights into the relationship between cellular stress, immune activity, and SCTLD susceptibility. ROS metabolism genes exhibited heightened expression levels in the most vulnerable species, and included *CAT* and *PRDX4*, known antioxidants crucial for the mitigation of hydrogen peroxide toxicity¹⁶². This heightened expression suggests a baseline state of elevated oxidative stress in these corals, potentially influenced by the presence of *Durusdinium* spp. Similarly, *ATF6B* and *SYVNI*, regulators of the ER stress response¹⁶², were also upregulated, indicative of cellular stress caused by the accumulation of unfolded or misfolded proteins¹⁶³. Prolonged ER stress can lead to cytotoxicity due to the disruption of protein folding and calcium homeostasis,

ultimately triggering apoptotic pathways¹⁶³. Interestingly, these heightened stress responses were negatively correlated with immune function, as evidenced by the low PO activity observed in these high-risk corals. Taken together, these findings suggest that corals with elevated ROS and ER stress levels are prone to initiating cell death pathways rather than a robust immune response upon pathogen exposure, making them more susceptible to diseases such as SCTL D.

Low SCTL D susceptibility is associated with high PO activity, low SOD activity, and elevated constitutive expression of genes involved in immune regulation and DNA damage responses

We also identified two networks of co-expressed genes with strong negative correlations to relative risk of SCTL D. Constitutively higher expression of genes within these networks was associated with high PO activity and low SOD protein activity, indicative of higher baseline levels of immune function and reduced oxidative stress in these less susceptible corals. Additionally, expression within these networks was lower in corals dominant in *Durusdinium* spp., further implicating a link between Symbiodiniaceae community composition, host immune activity, and cellular stress levels. Within these networks, we found enrichment of terms involved in immunity, import across plasma membranes, autophagy, and signaling in response to DNA damage, suggesting that these pathways are constitutively expressed at higher levels in the species with lower SCTL D susceptibility.

Our analysis of genes involved in immune regulation and DNA damage responses revealed insights into the mechanisms conferring resistance to SCTL D. Genes involved in immune regulation exhibited heightened expression levels in the less susceptible species, and included *PIK3API* and *OTULIN*, genes involved in preventing excessive inflammatory

responses and maintaining immune homeostasis¹⁶². The heightened expression of these genes likely represents a proactive immune system that is primed to respond swiftly and effectively against pathogens while also limiting excessive inflammation that can damage cells. Similarly, genes involved in responding to DNA damage showed elevated expression in these species. For example, *ATM*, which plays a crucial role in coordinating DNA damage repair processes and cell cycle checkpoints to prevent the replication of damaged DNA¹⁶², and *EIF2AK4*, a gene that downregulates protein synthesis in response to stressors like UV irradiation¹⁶², exhibited constitutively higher expression in the lower risk species. These expression patterns are indicative of a robust DNA damage response system that can maintain genome stability during cellular stress. Interestingly, these immune and DNA damage response genes were positively correlated with immune function, as evidenced by the high PO activity and melanin concentration observed in the lower risk corals. This positive correlation suggests a link between these defense mechanisms and the ability to fend off disease. Therefore, stronger baseline immune regulation and DNA damage responses likely plays a key role in protecting corals against SCTLD, highlighting the importance of these pathways in coral health and resilience.

SCTLD triggers oxidative stress, symbiosome vacuolization and downregulation of actin cytoskeletal genes

Only one module was correlated to health status: the grey module containing genes outside of an identifiable co-expression network. Unlike the modules correlated to relative risk, the expression within this module showed no significant relationship to host species or the dominant symbiont in the coral sample. However, the expression within this module did show significant correlations to both catalase activity and symbiosome vacuolization

(symbiont:symbiosome size). This is supported by our results showing that catalase activity trended higher in the SCTL D-affected corals relative to controls, and that significant symbiosome vacuolization was observed in the diseased corals relative to controls, regardless of the dominant Symbiodiniaceae genus in a sample.

Two genes involved in cytoskeletal organization, *TPM2* and *MYL9*, exhibited significant downregulation in diseased corals. *TPM2* encodes beta-tropomyosin, a member of the actin filament binding protein family involved in regulating actin cytoskeleton organization and dynamics¹⁶². Tropomyosin isoforms are known to localize predominantly within alga-hosting cells in stony corals⁸⁸, and their expression signatures decrease at night when coral endosymbionts transition from photosynthesis to respiration⁸⁹. These results support the hypothesis that alga-hosting cells experience major cytoskeletal rearrangement in response to the metabolic functions of their Symbiodiniaceae⁸⁹. In addition, *MYL9* is involved in regulating actin-myosin interactions and cytoskeletal dynamics¹⁶². Decreased expression of *TPM2* and *MYL9* was associated with higher levels of both symbiosome vacuolization and catalase activity, indicating a relationship between cytoskeletal dynamics, ROS levels, and symbiosome morphology. These shared gene expression patterns and phenotypes across species corroborate evidence that SCTL D causes metabolic dysbiosis between the coral host and its Symbiodiniaceae, resulting in the inability to mount an effective response against pathogens and maintain cellular homeostasis.

CONCLUSION

By integrating immune and antioxidant measures, histopathology, and gene expression analyses across multiple species of coral, we have identified key processes contributing to

interspecies variation in SCTL D susceptibility. First, we find that our measured protein phenotypes predominantly varied with coral species and dominant symbiont genera, rather than with health state. Furthermore, we show that high SCTL D susceptibility is characterized by reduced immune activity, higher oxidative stress levels, and elevated constitutive expression of genes involved in responding to ROS and ER stress. Conversely, low susceptibility is characterized by higher immune activity, reduced oxidative stress, and elevated constitutive expression of genes involved in immune regulation and DNA damage responses. We also provide evidence that the expression of genes associated with interspecies variation in SCTL D susceptibility is influenced by the Symbiodiniaceae community within a coral. Finally, we identify elevated oxidative stress, significant symbiosome vacuolization, and the downregulation of actin cytoskeleton genes as common cellular processes involved in SCTL D progression. Taken together, our study disentangles the complex dynamics between host physiology, symbiont community, and SCTL D susceptibility.

ACKNOWLEDGEMENTS

The authors would like to thank the facilities and staff at the University of the Virgin Islands Center for Marine and Environmental Studies (CMES) and Sonora Meiling, Nicholas MacKnight, Bradford Dimos, Alex Veglia, Adam Glahn, Daniel Mele, Danielle Lasseigne, Kathryn Cobleigh, Alex Gutting, Amanda Long, and Bradley Arrington for their assistance with field collections and conducting experiments. We also acknowledge the work of Morgan and Gillian Coleman and Annie Lamke in the collection of histology data. This work was funded by National Science Foundation (NSF) Biological Oceanography award numbers 1928753 to MEB, 1928609 to AMSC, 192817 to EMM, 1928771 to LDM, 1927277 to DMH, and 1928761 to AA,

as well as NSF EEID award number 2109622 to MEB, AA, LDM, and AMSC, and a NOAA OAR Cooperative Institutes award to AA (#NA19OAR4320074).

DATA AVAILABILITY

The raw RNAseq data used in this study was accessed via the NCBI database under accession code PRJNA860922. Publicly available data used in this study include the reference transcriptomes and proteomes for *M. cavernosa*, *P. astreoides*, *O. annularis*, and *C. natans* that can be found in a public GitHub repository (<https://github.com/kbeavz/SCTLD-Transmission-Experiment-USVI>), as well as the reference transcriptomes for *Symbiodinium* CassKB8 (BioProject PRJNA80085), *Breviolum minutum* (BioProject PRJNA274852), *Cladocopium goreau* (BioProject PRJNA307543), and *Durusdinium trenchii* (BioProject PRJNA508937). All R code used in this study is publicly available on GitHub (<https://github.com/Mydlarz-Lab/SCTLD-Susceptibility-and-Pathogenesis>).

AUTHOR CONTRIBUTIONS

Conceptualization: A.A., E.M.M., D.M.H., A.M.S.C., M.E.B., L.D.M. Sample collection: M.E.B., A.M.S.C. Experiment execution: A.M.R., A.M.S.C., M.E.B. Relative risk calculation: E.M.M. Histology: A.M.R. and D.M.H. Protein assays: K.M.B. and L.D.M. Data analysis: K.M.B., with input from M.A.E., E.W.VB., L.D.M., E.M.M., and A.M.S.C. Manuscript writing: K.M.B. and L.D.M., with editing contributions from all other authors.

CONFLICT OF INTEREST DISCLOSURE

The authors declare no competing interests.

Chapter 3 Figures:

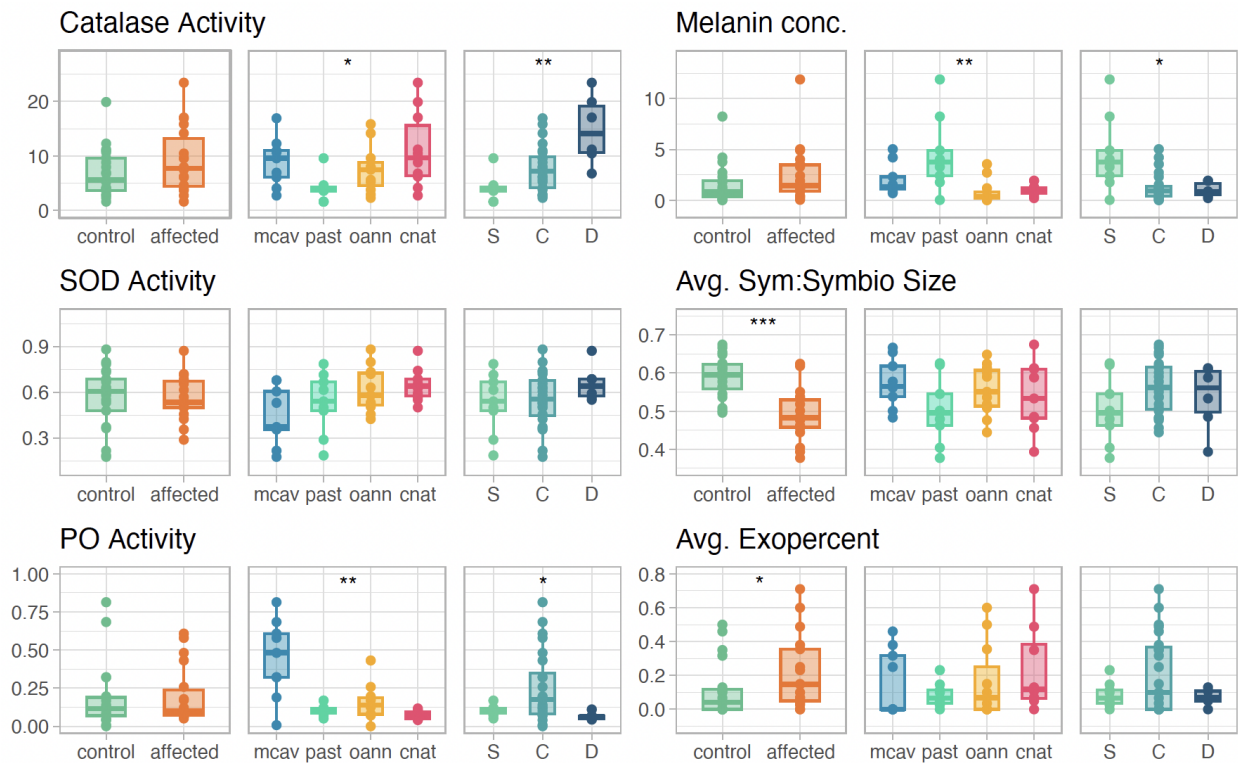


Figure 1: Measured phenotype traits for all samples from two health states (control, SCTLD-affected) from the SCTLD transmission experiment, grouped by disease status (left-most plots), coral species (middle plots), and dominant symbiont genera (right-most plots). Coral species are listed in order from lowest to highest median relative risk. Significant Kruskal-Wallis test results are denoted with asterisks: ‘*’ $p < 0.05$, ‘**’ $p < 0.01$, ‘***’ $p < 0.001$. (SOD = superoxide dismutase, PO = phenoloxidase, Sym:Symbio = symbiont:symbiosome, Exopercent = percent exocytosis of symbionts, mcav = *M. cavernosa*, past = *P. astreoides*, oann = *O. annularis*, cnat = *C. natans*, S = *Symbiodinium*, C = *Cladocopium*, D = *Durudinium*).

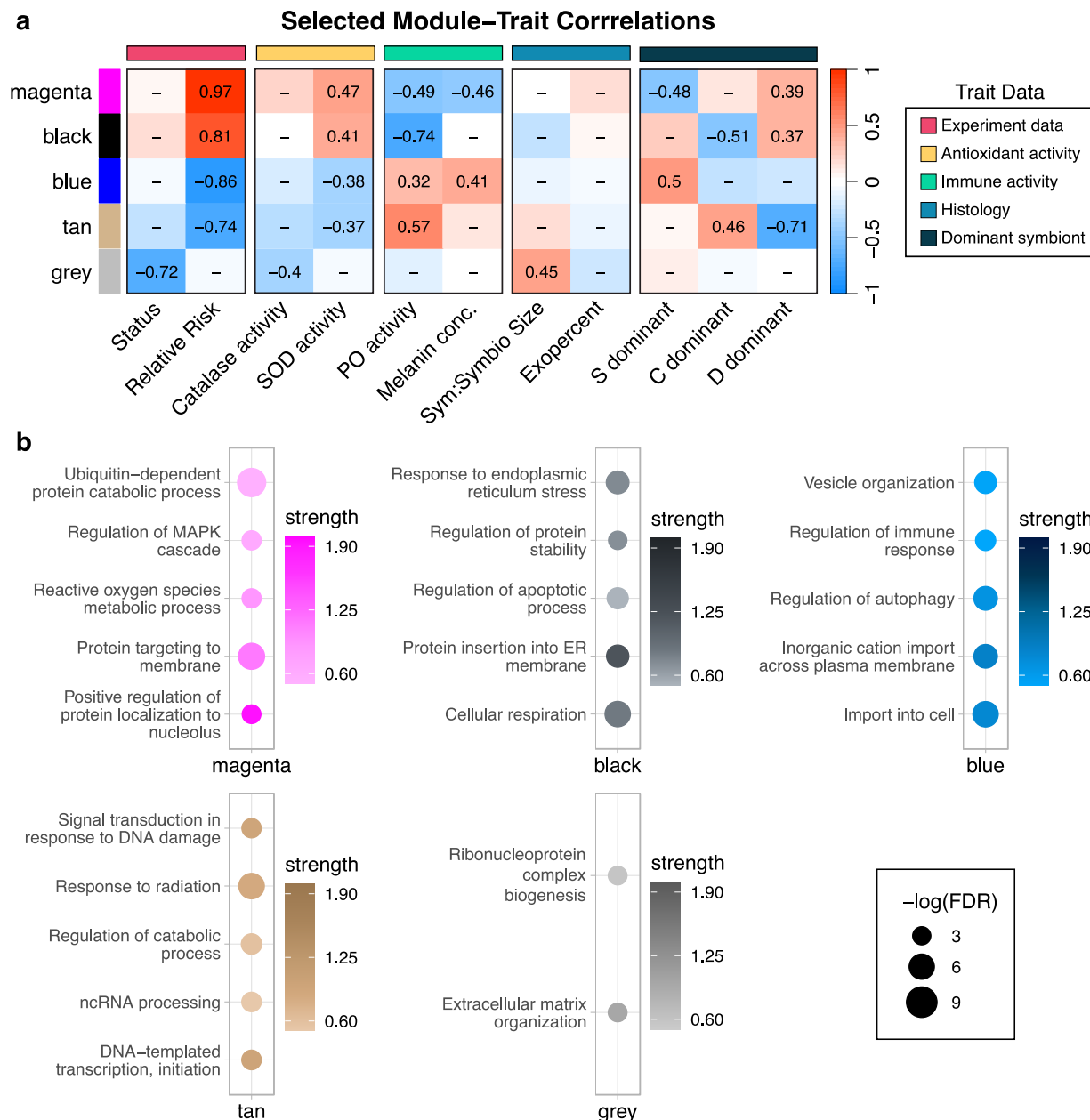


Figure 2: Weighted Gene Co-Expression Network Analysis (WGCNA) Results. **a** Shortened module-trait relationship heatmap showing the top two modules significantly positively and negatively correlated with relative risk and the one module significantly correlated with health status. The heatmap shows the significant correlations (Pearson's R , p -value ≤ 0.05) between the module eigengenes and the trait data. 'Status', 'S dominant', 'C dominant' and 'D dominant' are categorical traits indicating health status (control = 0, affected=1) and whether the coral was dominant in *Symbiodinium*, *Cladocopium*, or *Durusdinium* (no = 0, yes = 1). **b** Functional enrichment (Gene Ontology: Biological Process) of the modules shown in **a**. Size of circle represents the $-\log$ transformed false discovery rate (FDR) for the enrichment, corrected for multiple testing using Benjamini-Hochberg procedure. Color intensity represents the strength of the enrichment: \log_{10} (number of genes in the network annotated with the term / number of genes expected to be annotated with the same term in a random network of the same size).

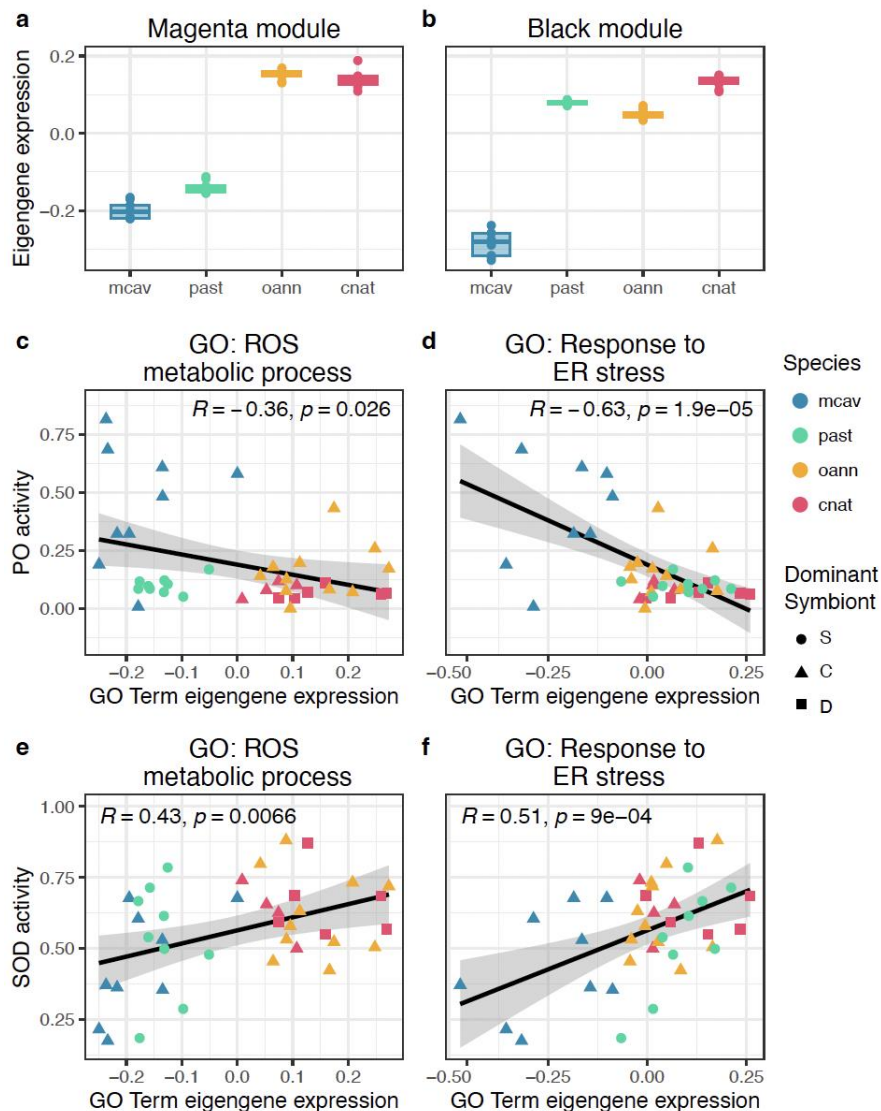


Figure 3: Eigengene analysis of modules associated with high relative risk of SCTL D. **a,b** Boxplots show the median and interquartile range of the **a** magenta and **b** black module eigengenes (the first principal component of the expression within each module) with respect to coral species. Coral species are listed in order from lowest to highest median relative risk. **c,d** The correlation (Pearson's R) between PO activity and the eigengene expression by sample for the significantly enriched gene ontology terms within the **c** magenta module ('Reactive oxygen species metabolic process'; $n = 5$ genes) and the **d** black module ('Response to endoplasmic reticulum stress'; $n = 8$ genes). **e,f** The correlation between SOD activity and the eigengene expression by sample for the same gene ontology terms in **c** and **d**, respectively. Shading around regression lines indicates the 95% confidence interval.

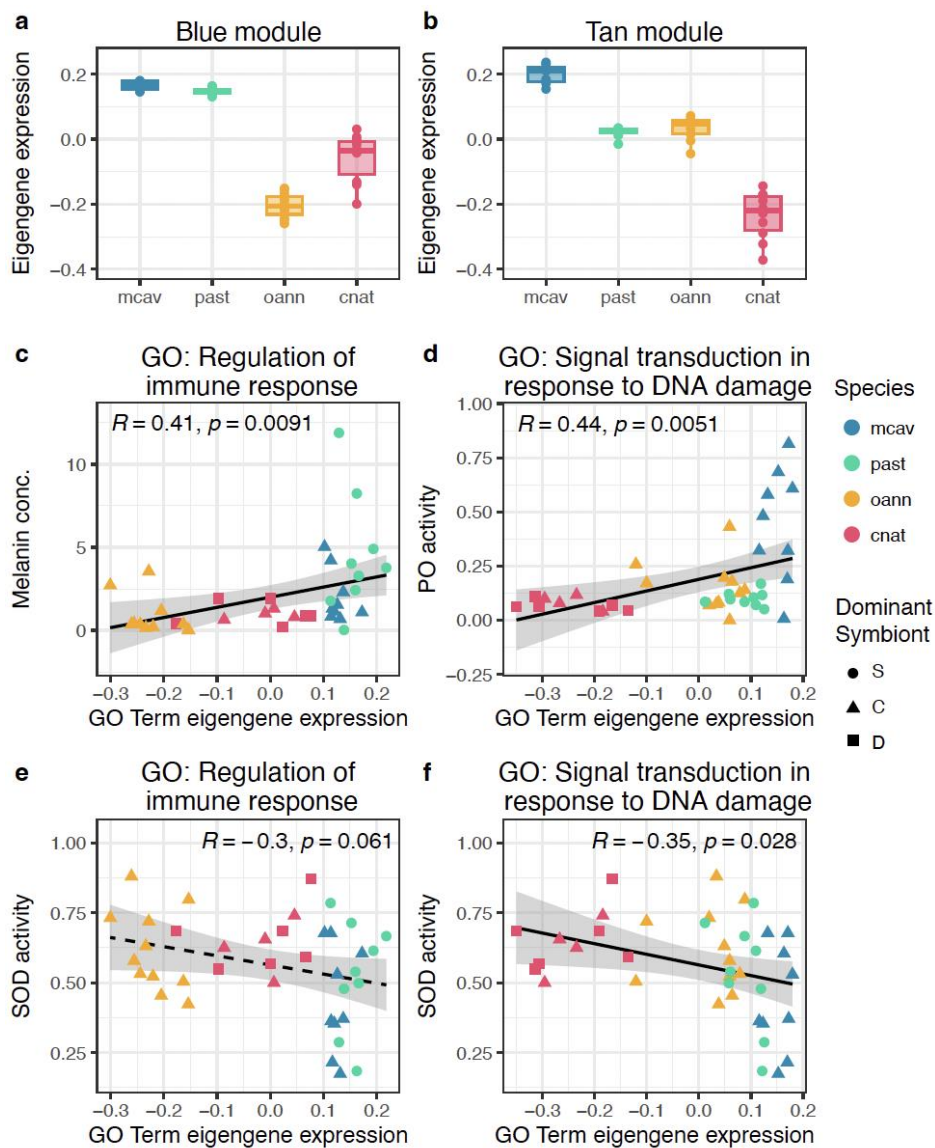


Figure 4: Eigengene analysis of modules associated with low relative risk of SCTL D. **a,b** Boxplots show the median and interquartile range of the **a** blue and **b** tan module eigengenes (the first principal component of the expression within each module) with respect to coral species. Coral species are listed in order from lowest to highest median relative risk. **c,d** The correlation (Pearson's R) between **c** melanin concentration and **d** PO activity and the eigengene expression by sample for the significantly enriched gene ontology terms within the **c** blue module ('Regulation of immune response'; $n = 13$ genes) and the **d** tan module ('Signal transduction in response to DNA damage'; $n = 5$ genes). **e,f** The correlation between SOD activity and the eigengene expression by sample for the same gene ontology terms in **c** and **d**, respectively. Shading around regression lines indicates the 95% confidence interval. Solid lines indicate significant correlations (p -value ≤ 0.05) and dashed lines indicate marginally significant correlations (p -value ≤ 0.1).

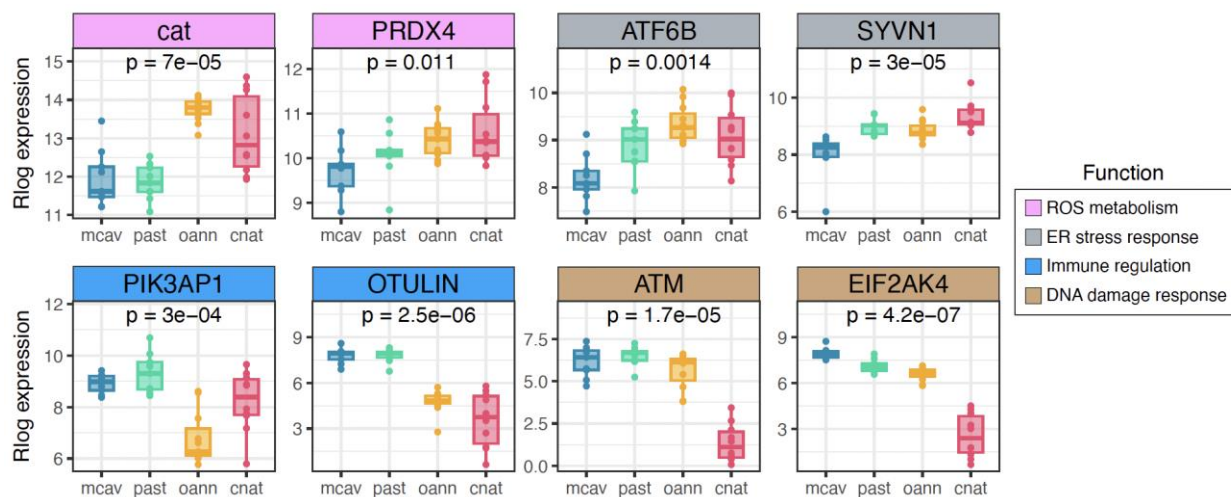


Figure 5: Eight selected genes with high significance to relative risk of SCTL D. Boxplots show the expression of each gene across species, with Kruskal-Wallis p -values. Coral species are listed in order from lowest to highest median relative risk. Colored labels indicate which Gene Ontology (GO): Biological Process enrichment term the gene belongs to. (mcav = *M. cavernosa*, past = *P. astreoides*, oann = *O. annularis*, cnat = *C. natans*).

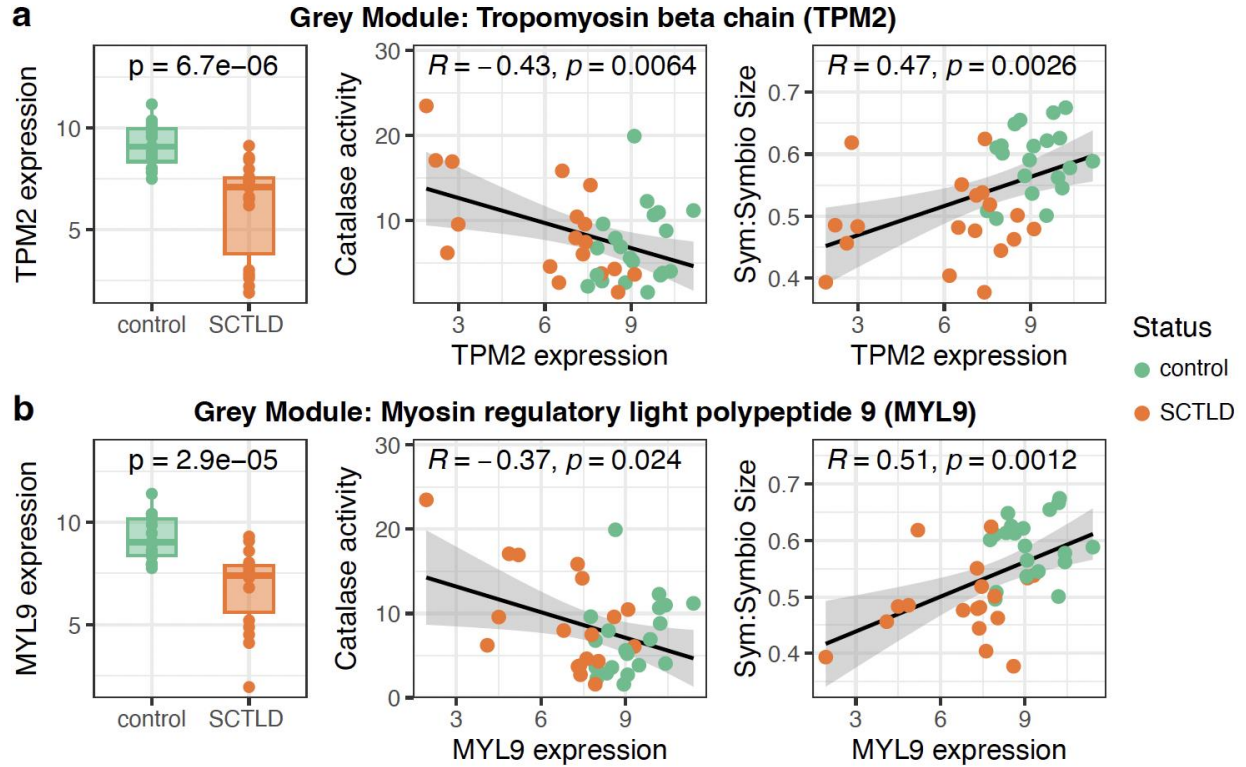


Figure 6: Two grey module genes with high significance to health status. Boxplots showing the expression of each gene in the control and SCTLD-affected corals is shown in the left-most plots, with Kruskal-Wallis p -values. The individual expression of each gene and its correlation (Pearson's R) to its two most significant phenotypic traits is shown in the middle and right-most plots.

Chapter 3 Supplementary Information:

METHODS

Relative Risk Calculation

At the end of the transmission experiment, disease prevalence results were used to calculate relative risk of SCTLD for each species of coral with the following equation:

$$\text{Relative Risk} = [(A / (A + B)) / (C / (C + D))]$$

where A was the number of fragments showing signs of SCTLD after exposure to a diseased colony, B was the number of fragments showing no signs of SCTLD after being exposed to a diseased colony, C was the number of fragments showing signs of SCTLD after being exposed to an apparently healthy control colony, and D was the number of fragments showing no signs of SCTLD after being exposed to an apparently healthy control colony⁶⁶. Relative risk was calculated using a Bayesian approach that was estimated using a binomial likelihood distribution and a uniform-Beta prior distribution⁶⁶. The median relative risk was calculated for each species to qualitatively compare the risk of being affected by SCTLD⁶⁶.

Protein concentration assay

The amount of total protein in each sample was determined using the Bicinchoninic (BCA) Protein Assay kit (G-Biosciences 786-750) standardized to bovine serum albumin (BSA) following the manufacturer's instructions. These concentrations were used to standardize all biochemical assays conducted, excluding melanin concentration.

Immune assays

All immune assays were conducted following established protocols for scleractinian corals^{127,145–147}. Phenoloxidase (PO) activity was measured by first diluting 20 μL of protein-enriched cell-free extract in 20 μL of buffer solution (100 mM TRIS with 0.05 mM DTT, pH 7.0). These samples were then incubated with 20 μL trypsin (0.1 mg/mL) for 15 minutes at room temperature to activate PO, and the enzymatic reaction was initiated by adding 30 μL of 10 mM dopamine to each well. Absorbance was read every minute for 10 minutes at 490 nm. PO activity is presented as $\Delta\text{Abs}_{490\text{ nm}} \text{ mg protein}^{-1} \text{ min}^{-1}$.

The reserved homogenate for melanin concentration analysis was vacuum dried using a Savant AES 1000 Automatic Environmental SpeedVac for 24 hours. Following water evaporation, total dry tissue weight was measured. The tissue was then disrupted by vortexing with a spatula of glass beads ($\sim 200 \mu\text{L}$ in volume) for 10 seconds. Finally, 300 μL of sodium hydroxide (NaOH; 10 M) was added to the samples and vortexed again for 30 seconds. To extract the melanin, samples were incubated for 48 hours at room temperature in the dark. Following incubation, the tubes were centrifuged for 12 minutes at room temperature, 1500 RPM. Then, 40 μL of the supernatant was transferred to two replicate half-area flat-bottom UV-transparent plates (Corning Life Sciences 3679) and absorbance was recorded at 410 nm. A standard curve of melanin dissolved in NaOH (10 M) was used to convert absorbance to mg melanin. Melanin concentration is presented as $\text{mg melanin mg tissue}^{-1}$.

Antioxidant assays

All antioxidant assays were conducted following established protocols for scleractinian corals^{127,145–147}. Catalase activity was measured by adding 10 μL of protein-enriched cell-free

extract and 40 μL of buffer (100 mM TRIS with 0.05 DTT, pH 6.0) to two replicate standard flat-bottom UV-transparent plates (Corning Life Sciences 3635). Then, 40 μL of hydrogen peroxide (H_2O_2) (25 mM) was added to each well to initiate the reaction with catalase. Absorbance was measured at 240 nm every 30 seconds for 3.5 minutes. Scavenged H_2O_2 was measured as the change in absorbance (initial-final) during the linear portion of the curve and was converted to $\mu\text{mol H}_2\text{O}_2$ using a standard curve of H_2O_2 . Catalase activity is presented as $\mu\text{mol H}_2\text{O}_2$ scavenged $\text{mg protein}^{-1} \text{ min}^{-1}$.

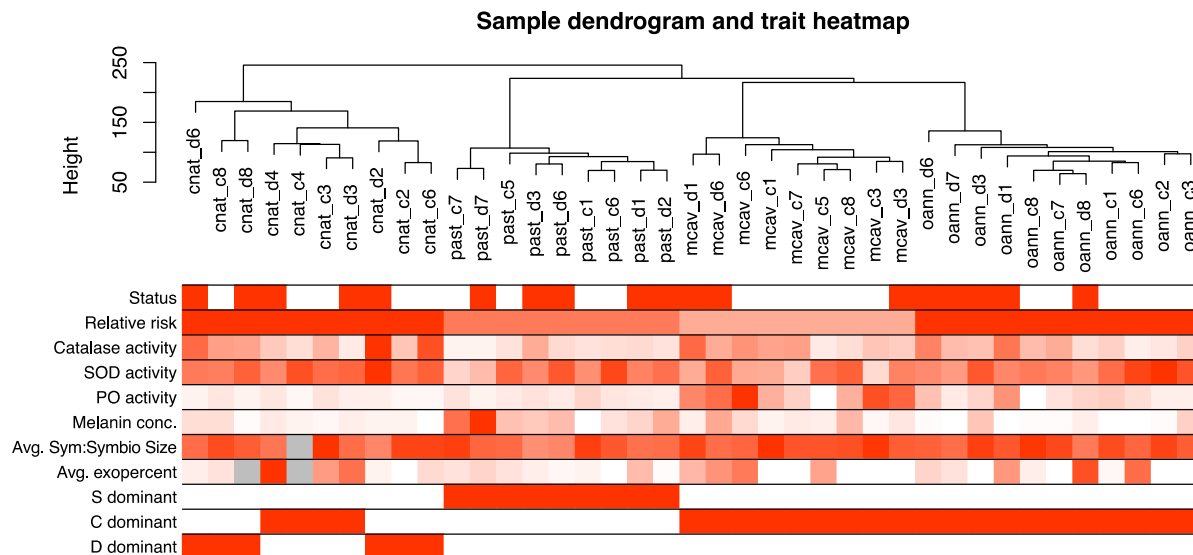
Superoxide dismutase (SOD) activity was measured using the SOD Determination Kit from MilliporeSigma (Sigma-Aldrich CS009). Following protocol instructions, 20 μL of protein-enriched cell-free extract was added to two replicate 96-well flat-bottom plates. Next, 20 μL Dilution Buffer was added to two ‘No SOD’ control wells on each plate, and 40 μL Dilution Buffer was added to two ‘Blank’ wells on each plate. Then, 160 WST working solution was added to each sample, control, and blank well. To initiate the reaction, 20 μL of xanthine oxidase working solution was added to each sample well, and to the ‘No SOD’ control wells. The plates were incubated at room temperature for 30 minutes and then absorbance was read at 450 nm. SOD activity was calculated for each sample using the following equation:

$$\text{SOD inhibition rate \%} = \frac{(A - B) - (C - B)}{(A - B)} \times 10$$

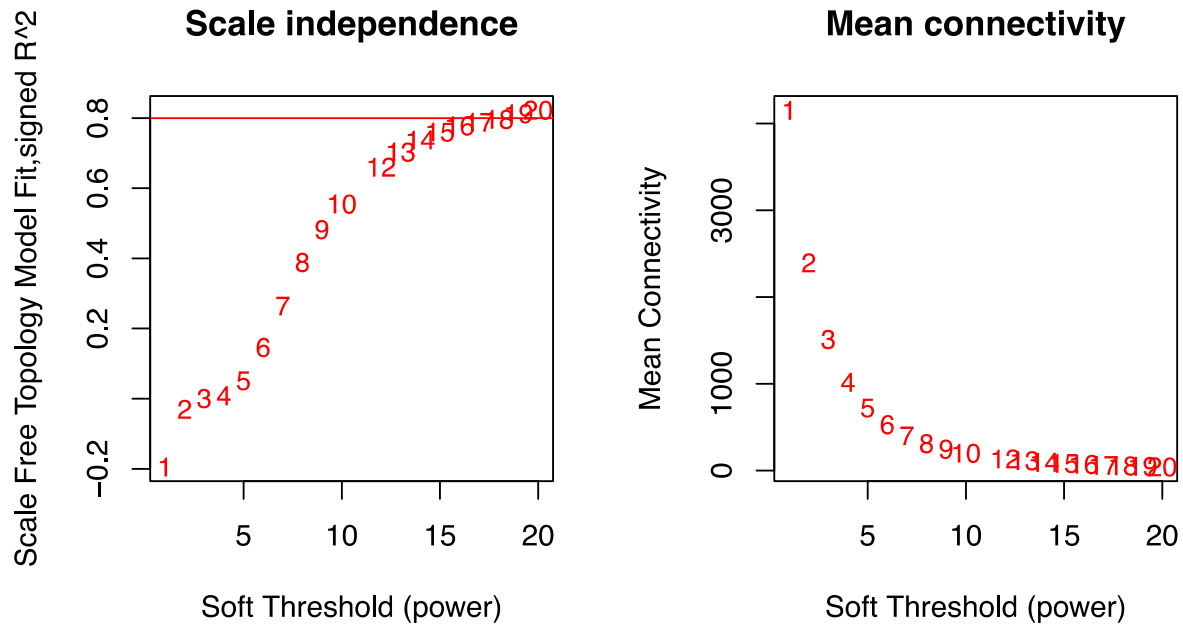
where A = the average absorbance of ‘No SOD’ control wells, B = the average absorbance of the ‘Blank’ wells and C = the absorbance of the sample. SOD activity is presented as SOD inhibition rate mg protein^{-1} .

Histopathology measurements

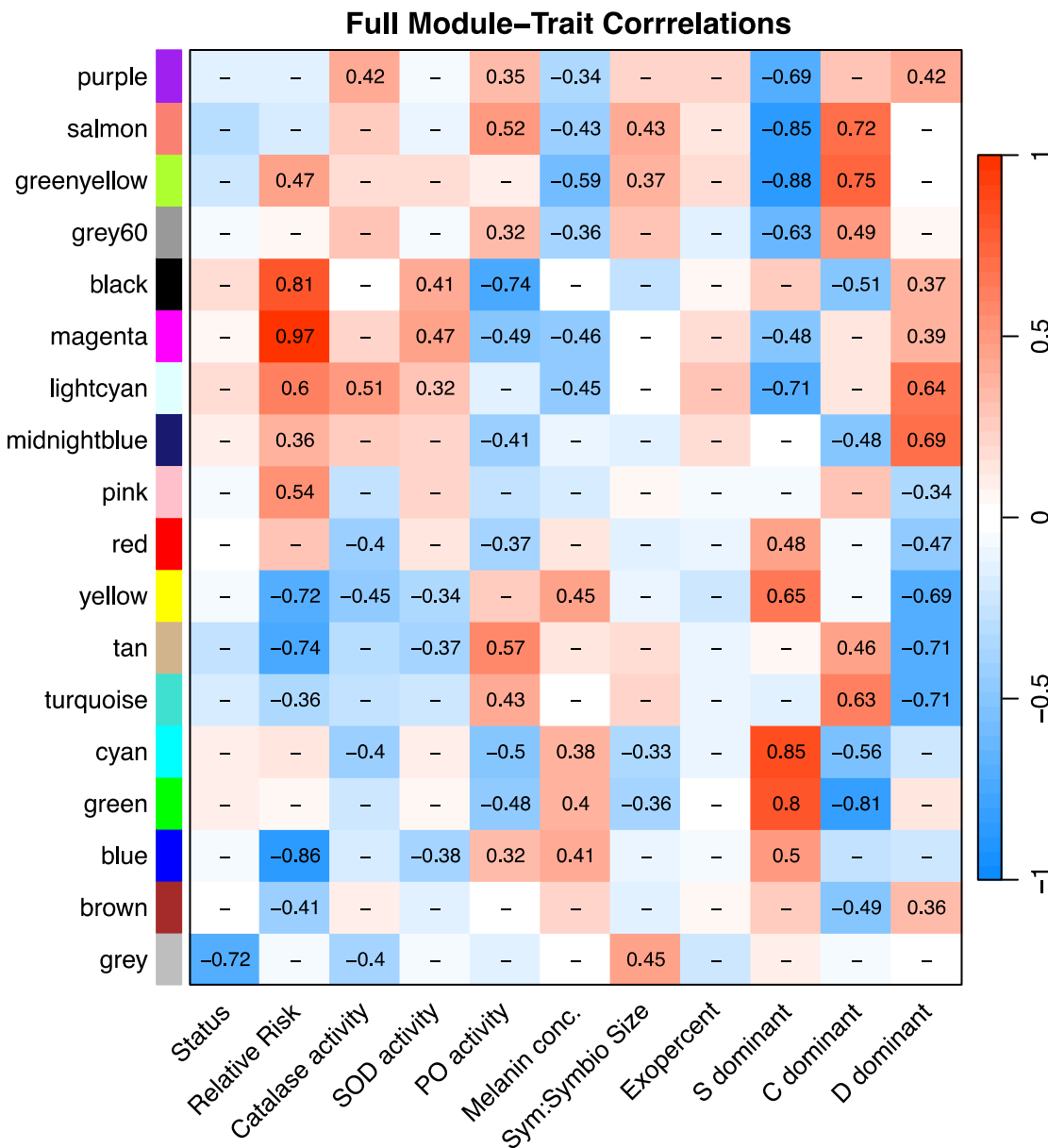
Fragments were fixed in zinc-buffered formalin for 24 hours, washed with seawater for 24 hours, and stored in 70% ethanol. Samples were then decalcified for a 1% HCl EDTA solution and stored in 70% ethanol until ready for processing. Samples were then processed using a Lecia ASP6025, embedded in paraffin wax blocks on a Leica EG1150H embedding machine, and sectioned at five μm thickness on a Leica RM2125RTS microtome. For each sample, five serial sections were made $\sim 500 \mu\text{m}$ apart. Resulting histological slides were stained with hematoxylin and eosin stain on a Leica ST5020, viewed on an Olympus BX41 microscope with an Olympus SC180 camera attachment, and analyzed using ImageJ software¹⁶⁴.



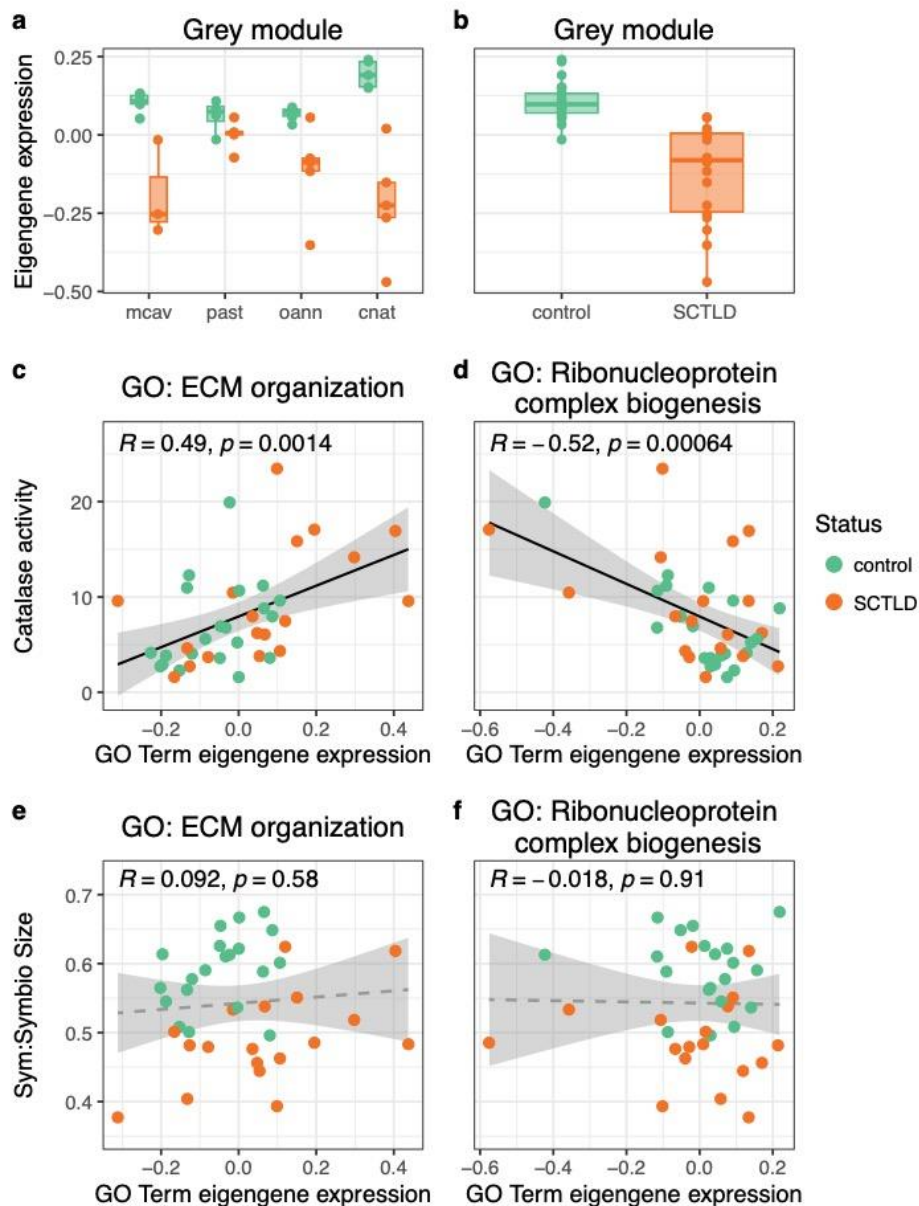
Supplemental Figure 1: Sample dendrogram and trait heatmap from WGCNA showing how the samples cluster by orthogroup expression and their relationships to all the traits measured in this study.



Supplemental Figure 2: WGCNA soft thresholding power selection. The left panel shows the Scale-Free Topology Index as a function of the Soft Thresholding Power reaching a saturation point at a Soft Thresholding Power value = 17. The right panel shows the Mean Connectivity as a function of the Soft Thresholding Power.



Supplemental Figure 3: Full Weighted Gene Co-Expression Network Analysis (WGCNA) Results. The heatmap shows the significant correlations (Pearson's R , p -value ≤ 0.05) between the module eigengenes and the trait data. 'Status', 'S dominant', 'C dominant', and 'D dominant' are categorical traits indicating the health status (control = 0, affected = 1) and whether the coral was dominant in *Symbiodinium*, *Cladocopium*, or *Durussdinium* (no = 0, yes = 1).



Supplemental Figure 4: Eigengene analysis of the grey module associated with health status. **a,b** Boxplots show the median and interquartile range of grey module eigengenes (the first principal component of the expression within the module) with respect to **a** coral species and health state and **b** species-combined health state. **c,d** The correlation (Pearson's R) between catalase activity and the eigengene expression by sample for the significantly enriched gene ontology terms **c** 'Extracellular matrix (ECM) organization' ($n = 7$ genes) and **d** 'Ribonucleoprotein complex biogenesis' ($n = 11$ genes) within the grey module. **e,f** The correlation between average symbiont:symbiosome size and the eigengene expression by sample for the same gene ontology terms in **c** and **d**, respectively. Shading around regression lines indicates the 95% confidence interval. Solid lines indicate significant correlations (p -value ≤ 0.05) and grey dashed lines indicate insignificant correlations.

Chapter 4: Classifying gene expression profiles of various tissue states in stony coral tissue loss
disease

Authors: Kelsey M. Beavers¹, Daniela Guterrez-Andrade¹, Emily W. Van Buren¹, Madison A. Emery¹, Marilyn E. Brandt², Amy Apprill³, Laura D. Mydlarz¹

¹Department of Biology, University of Texas at Arlington, Arlington, TX, USA

²Center for Marine and Environmental Studies, University of the Virgin Islands, St. Thomas, USVI, USA

⁵Marine Chemistry and Geochemistry Department, Woods Hole Oceanographic Institution, Woods Hole, MA, USA

ABSTRACT

Stony coral tissue loss disease (SCTLD) remains a substantial threat to coral reef diversity already threatened by global climate change. Restoration efforts and effective treatment of SCTLD requires an in-depth understanding of its pathogenesis in the coral holobiont as well as mechanisms of disease resistance. Here, we present a supervised machine learning framework to describe SCTLD progression in a major reef-building coral, *Montastraea cavernosa*, and its dominant algal endosymbiont, *Cladocopium goreaui*. Through the combined use of support vector machine recursive feature elimination (SVM-RFE) and differential expression analysis, we identify a subset of biologically relevant genes with the highest classification performance on three types of coral tissue collected from a natural reef environment: healthy tissue on a healthy colony, healthy tissue on a SCTLD-infected colony, and lesion tissue on a SCLTD-infected colony. By characterizing the gene expression signatures associated with these tissue health states in both the coral host and its algal endosymbiont (family Symbiodiniaceae), we describe the key processes involved in SCTLD resistance and disease progression within the coral holobiont. Broadly, our results indicate that SCTLD infection causes dysbiosis between the coral host and its Symbiodiniaceae and describes the metabolic and immune shifts that occur as the holobiont transitions from a healthy state to a diseased state. Our disease classification framework provides a novel method to accurately describe various health states of endangered coral species and brings us closer to developing effective solutions for disease monitoring and intervention.

INTRODUCTION

Coral reefs are among the most threatened ecosystems on the planet. Anthropogenic ocean warming among other stressors has triggered mass bleaching and disease outbreaks, resulting in substantial coral cover and reef biodiversity loss on nearly all the world's tropical coral reefs^{15,18,22,23,165,166}. Recovery windows between stress events have narrowed at an unprecedented rate, limiting the ability of reefs to recover without intervention, and highlighting the importance of coral reef preservation and restoration efforts as well as meaningful action on climate change^{167,168}. Recent efforts have focused on the identification of coral species, individuals, genes, and symbionts that can withstand multiple types of stressors^{169–172}. The rapid expansion of high-throughput (omics) datasets such as genomics, transcriptomics, and metabolomics and the advancement of novel statistical methods such as machine learning hold promise for the accurate identification and characterization of emerging and persistent threats to coral reef ecosystems.

One disease event that has significantly altered coral reef assemblages and functionality is stony coral tissue loss disease (SCTLD)^{48,153}. First observed off the coast of Miami, Florida in 2014, SCTLD has led to significant losses of coral throughout the Florida Coral Reef Tract and the wider Caribbean^{27,64,154,173–175} and is the most pervasive and virulent coral disease on record. Despite research efforts, the etiology of SCTLD, like many coral diseases, remains unknown, likely due to the complexity of microbial and eukaryotic assembles that associate with coral^{23,59,62,176}. However, shifts in the bacterial^{33–35,37,65,66,139,141} and viral^{42,43} consortium have been implicated in SCTLD infection, and antibiotic treatment has proven effective at halting active lesion progression^{38–41}. Furthermore, histopathology has identified SCTLD tissue necrosis originating in the coral gastrodermis where the coral's algal endosymbionts (Symbiodiniaceae)

reside⁴⁴ as well as morphologic changes consistent with Symbiodiniaceae pathology in apparently healthy and SCTLD-affected corals⁴², leading to the hypothesis that SCTLD may be caused by an infection of Symbiodiniaceae rather than the coral host itself.

Recent omics analyses have provided further insight into the cellular mechanisms underpinning SCTLD infection and pathogenesis. Metabolomics on healthy and SCTLD-infected corals has revealed variations in Symbiodiniaceae-derived lipid and tocopherol production in response to disease¹⁴², supporting the case for Symbiodiniaceae involvement. Transcriptomic analyses have identified signatures of *in situ* degradation of photosynthetically dysfunctional Symbiodiniaceae¹⁴³ as well as commonly differentially expressed genes involved in innate immunity, apoptosis and extracellular matrix (ECM) structure in SCTLD-infected corals^{67,144}. Interestingly, paired *ex situ* transmission and *in situ* intervention experiments showed that amoxicillin treatment led to a ‘reversal’ of many of these signaling pathways, suggesting that disease intervention provides benefits to the coral beyond removal of pathogens and opportunistic microbes¹⁴⁴. Despite these advances in our understanding of SCTLD, there is still a need to identify the central processes involved in SCTLD progression to assist coral preservation and restoration projects.

Next-generation gene expression technologies have revolutionized infectious disease research, allowing scientists to measure expression-level changes of thousands of genes in response to experimental or natural infection¹⁷⁷. However, gene expression datasets are high-dimensional in nature, and the differentially expressed genes (DEGs) produced often contain redundant and biologically irrelevant data¹⁷⁸. Integrating supervised machine learning (ML), defined as the process of learning from labelled examples to predict or classify an outcome of interest¹⁷⁹, into DEG analyses offers a promising solution to address the ‘curse of

dimensionality¹⁸⁰ within large omics datasets. Support vector machine recursive feature elimination (SVM-RFE) is a popular supervised ML algorithm that attempts to find the features (genes) in a dataset that best define the class (phenotype) data¹⁸¹, and has many applications in gene expression research. For example, SVM-RFE has been used to predict drought-resistant genes in *Arabidopsis thaliana*¹⁸² and to identify genes for accurate cancer classification¹⁸¹ and Alzheimer's disease diagnosis in humans¹⁸³. Broadly, feature selection using SVM-RFE has been shown to be successful at isolating a subset of nonredundant and biologically relevant genes from a larger dataset to then build a model that can accurately assign data points to a predefined set of classes.

Here, we implement a novel supervised ML approach to classify the gene expression associated with various tissue health states in a major reef-building coral *M. cavernosa* and its dominant algal endosymbiont, *C. goreau*. By utilizing a simultaneous combination of SVM-RFE and differential expression analysis, we identify genes that are both biologically relevant and have the highest discriminatory power within three types of coral tissue collected from a natural reef environment: healthy tissue on a healthy colony, healthy tissue on a SCTL D-infected colony, and lesion tissue on a SCTL D-infected colony. Identifying the most relevant genes associated with different states of SCTL D disease progression brings us closer to understanding the pathogenesis of this disease and developing effective solutions to treat and prevent its spread.

METHODS

Sample collection and design

All samples were collected under permit #DFW19057U authorized by the Department of Planning and Natural Resources Coastal Zone Management. Coral fragments were collected by

divers on SCUBA with hammers and chisels from two reefs in St. Thomas, United States Virgin Islands (USVI) showing signs of active SCTL D (acute multi-focal lesions) in February of 2020: Buck Island (18.27883°, -64.89833°) and Black Point (18.3445°, -64.98595°). At both sites, one coral fragment was collected from each apparently healthy colony (Buck Island, $n=3$; Black Point, $n=3$), termed healthy tissue on a healthy colony (HH). Two fragments were collected from each diseased colony: one immediately adjacent to the SCTL D lesion line (Buck Island, $n=3$; Black Point, $n=5$), termed lesion tissue on a diseased colony (LD), and one approximately 10 cm from the lesion line (Buck Island, $n=3$; Black Point, $n=5$), termed healthy tissue on a diseased colony (HD). The sampling scheme is shown in Figure 1A-C. Coral fragments were placed in individual bags that were sealed and transported to land on ice before being flash frozen at -80°C.

RNA extraction and sequencing

Total RNA was extracted following the protocol outlined previously¹⁴³ following the RNAqueous-4PCR Total RNA Isolation Kit from Invitrogen (Life Technologies AM1914). A pea-sized amount of frozen coral tissue was scraped off each fragment into a 2 mL microcentrifuge tube using a sterilized bone cutter. Lysis buffer was added to each microcentrifuge tube followed by mechanical disruption using a refrigerated Qiagen TissueLyser II at 30 oscillations/s for 60 s. Elution was performed in two 30 μ L steps at a time. After combining elutions, contaminating DNA and chromatin were removed using the Ambion DNase I kit from Invitrogen (Life Technologies AM 2222). Resulting total RNA samples were sent to Novogene Co., LTD (Beijing, China) for quality assessment using an Agilent Bioanalyzer 2100. All samples passed quality assessment with RNA integrity (RIN) values ≥ 7 and were

preprocessed for mRNA enrichment using polyA tail capture. cDNA libraries were prepared using the NEBNext Ultra II RNA Library Prep Kit from Illumina and sequenced on the Illumina NovaSeq 6000 for 150 bp, paired-end sequencing.

***M. cavernosa* transcriptome assembly and annotation**

All bioinformatic analyses were carried out on the Frontera system of the Texas Advanced Computing Center¹⁸⁴. Raw reads from Novogene were adapter-trimmed and quality-filtered in one step using FastP v. 0.20.1⁹⁴ using the -c flag for base correction and the -x flag for polyA tail trimming. Then, six samples (two from each health state) were used to generate a *de novo* metatranscriptome using Trinity v. 2.14.0⁹⁸. Non-coral transcripts were filtered out of this metatranscriptome using the *in-silico* filtration method outlined previously⁹⁷. First, the longest transcript isoform was obtained using the `get_longest_isoform_seq_pr_trinity_gene.pl` script within the Trinity v. 2.14.0 package⁹⁸. This assembly was then Blasted against a Master Coral database¹¹⁹ comprised of both genome-derived predicted gene models and transcriptomes spanning a wide diversity of coral families using BlastX v. 2.2.27¹⁸⁵. Transcripts with less than 95% identity of this Master Coral database and shorter than 150 bp in length were filtered out of the assembly. TransDecoder v. 5.5.0¹⁸⁶ was used to generate a predicted protein-coding sequence from the longest open reading frame from each transcript, resulting in a predicted proteome for *M. cavernosa*. Sequences with high similarity were then collapsed using `cd-hit` v. 4.8.1¹⁰² under default parameters. The resulting sequences were then extracted from the initial assembly to generate the *M. cavernosa* reference transcriptome. Assembly metrics can be found in Table 1. Finally, the transcriptome was annotated with reviewed UniprotKB/Swiss-Prot Entry IDs using BlastX v. 2.2.27¹⁸⁵.

Isolation and quantification of holobiont reads

To separate *M. cavernosa* and Symbiodiniaceae reads, BBSplit v. 38.90¹⁰⁶ was used with the *M. cavernosa* reference transcriptome generated above and Symbiodiniaceae transcriptomes of similar assembly quality representing the genera *Symbiodinium*, *Breviolum*, *Cladocopium*, and *Durusdinium* sourced from previous publications as binning references^{121–124}. The binning statistics output was used to identify *Cladocopium* as the dominant Symbiodiniaceae genera present in each sample (Table S1). A predicted proteome was generated from the *C. goreau* reference transcriptome used above with TransDecoder v. 5.5.0¹⁸⁶. Similar sequences in the proteome were collapsed using cd-hit v. 4.8.1¹⁰². The resulting sequences were then extracted from their initial assembly to generate the final *C. goreau* reference transcriptome. Assembly metrics for this transcriptome can be found in Table 1. The resulting *C. goreau* assembly was then annotated with reviewed UniprotKB/Swiss-Prot Entry IDs using BlastX v. 2.2.27¹⁸⁵. Finally, *M. cavernosa* and *C. goreau* reads were mapped to their respective transcriptome and quantified using Salmon v. 1.5.2¹⁰⁵ under default parameters for *M. cavernosa* reads and a kmer value of 23 for *C. goreau* reads.

Supervised machine learning classification of holobiont reads

All data analysis was performed using R v. 4.2.2¹⁴⁸. Gene count matrices were generated for the quantified *M. cavernosa* and *C. goreau* transcripts using Tximport v. 1.16.1¹⁰⁷. Annotated *M. cavernosa* and *C. goreau* genes with an $evalue < 1.0e^{-6}$ were kept for differential expression analyses. Regularized log (rlog) normalized expression was obtained in each dataset using DESeq2 v. 1.38.3¹⁰⁸ with the design $\sim Site + Disease_state$, removing genes with an

average rlog expression < 10 . Genes (features) were ranked by their classification accuracy and biological relevance in the HH, HD, and LD tissue from the *M. cavernosa* and *C. goreau* gene expression using a combination of support vector machine recursive feature elimination (SVM-RFE) and differential expression analysis (*t*-statistic) using sigFeature v. 1.16.0¹⁷⁸ (Figure 1D) (Tables S2-7). To test the classification efficacy of each model's features, external stratified *k*-fold cross-validation was performed on the top 400 features from each dataset also using sigFeature v. 1.16.0¹⁷⁸ (Figure 1D-F).

Functional enrichment of top features in *M. cavernosa*

Functional enrichment was performed on both the up- and down-regulated genes within the top 500 features from each tissue health state in *M. cavernosa* and *C. goreau*. To find the upregulated features in each tissue health state, \log_2 FoldChange values from DESeq2 relative to the other two other tissue health states were obtained for the top 500 features. Features with a \log_2 FoldChange > 0 relative to the two other tissue health states were classified as “upregulated”, while those with a \log_2 FoldChange < 0 were classified as “downregulated” (Tables S8-13). For example, to identify upregulated HH features, \log_2 FoldChange was obtained for the comparisons between HH and HD corals as well as between HH and LD corals, and those features out of the top 500 HH features that had higher expression in HH corals relative to both HD and LD corals were deemed “upregulated”. To perform functional enrichment of those up- and down-regulated features, first the predicted proteomes of *M. cavernosa* and *C. goreau* generated above were uploaded to STRING v. 12.0¹⁵¹ using the ‘Add organism’ tool (*M. cavernosa* STRING ID: STRG0A38MOJ, *C. goreau* STRING ID: STRG0A06ZQW). Then, lists of the up-regulated and down-regulated features were uploaded to STRING separately. All Gene Ontology, Reactome,

and KEGG terms were saved, and a curated list of the 5 most relevant and non-redundant up- and downregulated terms were plotted (Figures 2 and 3).

Expression analysis of potential tissue health state biomarkers

The top 15 features from each tissue health state in both *M. cavernosa* and *C. goreau* were selected for further analysis due to their high classification potential. Rlog values were obtained for each list of the top 15 features in *M. cavernosa* and plotted in relative expression heatmaps (Figures 4A, 5A, and 6A). To confirm gene function, protein domain architecture was obtained and analyzed for each feature by uploading their protein sequence to InterPro¹⁸⁷ (Tables S14-19). From each tissue health state's top 15 features, the top feature as well as four other highly relevant features were plotted in boxplots (Figures 4B, 5B, and 6B). Additionally, three features from each tissue health state in *C. goreau* were selected based on their differential expression significance and functional relevance and were plotted in boxplots (Figure 7).

RESULTS

Transcriptome assembly and annotation

Sequencing of 22 coral tissue samples resulted in a total of 1.035 billion raw reads with an average of 47 million raw reads per sample. *De novo* transcriptome assembly of the *M. cavernosa* cleaned, quality-filtered, coral-only reads resulted in an assembly of 73,047 contigs with a N50 size of 16,467 bp and filtering of the *C. goreau de novo* transcriptome from Davies et al.¹²³ resulted in an assembly of 48,013 contigs with a N50 size of 13,469 bp (Table 1). Of those, 33,614 *M. cavernosa* and 26,245 *C. goreau* contigs were annotated with an annotation $evalue < 1.0e^{-6}$.

Isolation and quantification of holobiont reads

A total of 692 million reads were assigned to *M. cavernosa* and 139 million to *C. goreau*. An average of 31.5 million reads and 6.34 million reads were assigned to *M. cavernosa* and *C. goreau* per sample, respectively. Mapping of *M. cavernosa* and *C. goreau* reads to their respective reference transcriptome resulted in average mapping rates of 92.2% and 91.5%, respectively (Table S1). Following transcript quantification, a total of 19,039 and 11,289 length-normalized transcripts with an annotation evalue $< 1.0e^{-6}$ were expressed in *M. cavernosa* and *C. goreau*, respectively. Filtering out genes with an average rlog expression < 10 resulted in 17,229 and 2,224 genes with significant levels of expression in *M. cavernosa* and *C. goreau*, respectively.

Supervised machine learning classification of holobiont reads

The 17,229 annotated genes with significant expression in *M. cavernosa* were used to produce the feature ranked lists from the HH, HD and LD coral gene expression datasets (Tables S2-7). Of the *M. cavernosa* features, 1,562 HH, 5,286 HD, and 5,329 LD had significant differential expression relative to the other two tissue health states (t -statistic P -value < 0.05). External stratified k -fold cross-validation showed high classification performance of each tissue health state's top 400 coral features: within the HH dataset and LD datasets, 0% average misclassification was achieved with the top 390 and 130 features, respectively, and within the HD dataset, 12% average misclassification was achieved with the top 370 features (Figure 1E). The 2,158 annotated genes with significant expression in *C. goreau* were used to produce the feature ranked lists from the HH, HD and LD symbiont gene expression datasets. Of the *C.*

goreau features, 152 HH, 114 HD, and 291 LD had a significant differential expression relative to the other two tissue health states (t -statistic P -value < 0.05). External stratified k -fold cross-validation showed high classification performance of each tissue health state's top 400 symbiont features: within the HH and HD datasets, 0% average misclassification was achieved with the top 160 and 210 features respectively, and within the LD dataset, 5% average misclassification was achieved with the top 360 features (Figure 1F).

Functional enrichment of top features in *M. cavernosa*

Of the top 500 *M. cavernosa* HH features, 369 were upregulated and 130 were downregulated relative to both HD and LD tissue. Functional enrichment of those genes showed that completely healthy tissue on *M. cavernosa* is characterized by increased unsaturated fatty acid biosynthesis, collagen formation, and actin binding as well as decreased nitric oxide biosynthesis, glycogen biosynthesis, and amino acid catabolism (Figure 2). Of the top 500 *M. cavernosa* HD features, 202 were upregulated and 297 were downregulated relative to both HH and LD tissue. Functional enrichment of those genes showed that healthy tissue on a SCTLD-infected *M. cavernosa* colony is characterized by increased translation, amide biosynthesis, and aminoacyl-tRNA biosynthesis as well as decreased cilium movement and assembly and mitochondrion organization (Figure 2). Of the top 500 *M. cavernosa* LD features, 229 were upregulated and 271 were downregulated relative to both HH and HD tissue. Functional enrichment of those genes showed that lesion tissue on a SCTLD-infected *M. cavernosa* colony is characterized by increased innate immunity through C-type lectin receptor pattern recognition, NF-kappaB (NF- κ B) signaling, and autophagosome maturation as well as decreased collagen

chain trimerization, chloride transmembrane transport, and unsaturated fatty acid biosynthesis (Figure 2).

Of the top 500 *C. goreau* HH features 259 were upregulated and 225 were downregulated relative to both HD and LD tissue. Functional enrichment of those genes showed that *C. goreau* from completely healthy tissue is characterized by increased long-chain fatty acid biosynthesis, heat shock responses, and sphingolipid metabolism as well as decreased pyruvate metabolism and phenylpropanoid biosynthesis (Figure 3). Of the top 500 *C. goreau* HD features, 224 were upregulated and 221 were downregulated relative to both HH and LD tissue. Functional enrichment of those genes showed that *C. goreau* from healthy tissue on a SCTLD-infected colony is characterized by increased organonitrogen and organophosphate biosynthesis as well as decreased regulation of the mitotic cell cycle and iron uptake and transport (Figure 3). Of the top 500 *C. goreau* LD features, 224 were upregulated and 276 were downregulated relative to both HH and HD tissue. Functional enrichment of those genes showed that *C. goreau* from lesion tissue on a SCTLD-infected colony is characterized by increased thiamine metabolism and proteasomal protein catabolism as well as decreased inorganic anion transmembrane transport, chloride channel activity, and signaling by nuclear receptors (Figure 3).

Expression analysis of potential tissue health state biomarkers

Of the top 15 HH features in *M. cavernosa*, 13 (86.7%) were upregulated and two (13.3%) were downregulated relative to both HD and LD tissue (Figure 4A). The top feature in HH corals was the upregulated Transmembrane protein 145 (*Tmem145*), an integral membrane component associated with transforming growth factor beta (TGF β) signaling (Table S14)¹⁸⁷.

Other notable genes within the top 15 HH features include: Prokineticin receptor 1 (*PROKR1*), Inhibin beta B chain (*INHBB*), Baculoviral IAP repeat-containing protein 1 (*NAIP*) and Deleted in malignant brain tumors 1 protein (*Dmbt1*) (Figure 4). Of the top 15 HD features in *M. cavernosa*, five (33.3%) were upregulated and ten (66.7%) were downregulated relative to both HH and LD tissue (Figure 5A). The top feature in HD corals was the upregulated Dicarboxylate carrier SLC25A8 (*Ucp2*), a mitochondrial uncoupling protein that primarily functions in decreasing mitochondrial membrane potential and reactive oxygen species (ROS) production (Table S15)¹⁸⁷. Other notable genes within the top 15 HD features include: Ras-related protein Rab-5A (*Rab5a*), Cilia- and flagella-associated protein 298 (*cfap298*), Ciliary microtubule inner protein 2B (*fam166b*), and Chaperone protein DnaJ (*dnaJ*) (Figure 5). Of the top 15 LD features in *M. cavernosa*, 14 (93.3%) were upregulated and one (6.7%) was downregulated relative to both HH and HD tissue (Figure 6A). The top feature in LD corals was the downregulated Tropomyosin-1 (*TPM1*), a non-muscle tropomyosin isoform involved in the control and regulation of the cell's cytoskeleton (Table S16)¹⁸⁷. Other notable genes within the top 15 LD features include: two Collagen alpha-1(II) chain homologs (*col2a1 [a]* and *col2a1 [b]*), two Collagen alpha-2(I) chain homologs (*colla2 [a]* and *colla2 [b]*), GFP-like fluorescent chromoprotein cFP484 (*GFPL*), and Superoxide dismutase [Cu-Zn] 1 (*sodA*) (Figure 6).

Of the top 15 HH features in *C. goreau*, six (40%) were upregulated and nine (60%) were downregulated relative to both HD and LD tissue (Figure S1). The top feature in HH *C. goreau* symbionts was the upregulated Protein NO VEIN, which contains a histidine kinase/HSP90-like ATPase superfamily domain found in several ATP-binding proteins (Table S17)¹⁸⁷. Other notable genes within the top 15 HH features include Inner membrane ALBINO3-like protein 2, chloroplastic (*ALB3.2*) and Cytochrome b5 (*Cyt-b5*) (Figure 7). Of the top 15 HD

features in *C. goreau*, seven (46.7%) were upregulated and eight (53.3%) were downregulated relative to both HH and LD tissue (Figure S2). The top feature in HD *C. goreau* symbionts was the upregulated Aspartate ammonia-lyase (*aspA*), which converts L-aspartate to fumarate and ammonia during the tricarboxylic acid cycle (Table S18)¹⁸⁷. Other notable genes within the top 15 HD features include Serine/threonine-protein kinase STY17 (*STY17*) and Soluble starch synthase 1, chloroplastic/amyloplastic (*SSI*) (Figure 7). Of the top 15 LD features in *C. goreau*, 13 (86.7%) were upregulated and two (13.3%) were downregulated relative to both HH and HD tissue (Figure S3). The top feature in LD *C. goreau* symbionts was the downregulated High affinity nitrate transporter 2.5 (*NRT2.5*), which is involved in the transmembrane transport of nitrogen (Table S19)¹⁸⁷. Other notable genes within the top 15 LD features include Fucoxanthin-chlorophyll a-c binding protein E, chloroplastic (*FCPE*) and glycosyltransferase-like KOBITO 1 (*ELDI*) (Figure 7).

DISCUSSION

Supervised machine learning (ML) is a powerful tool that uses known characteristics to detect meaningful patterns within large, unstructured, and complex datasets¹⁸⁸. Here, we use a supervised ML approach to classify the expression patterns associated with three different SCTLD health states in a principal reef building coral, *M. cavernosa*, and its dominant algal endosymbiont, *C. goreau*. By combining differential expression analysis with SVM-RFE, we produce a ranked list of *M. cavernosa* and *C. goreau* genes that are associated with healthy tissue on a healthy colony (HH), healthy tissue on a diseased colony (HD), and lesion tissue on a diseased colony (LD) to investigate the processes involved in SCTLD pathogenesis. We find that

all three health states have distinct coral and endosymbiont gene expression profiles, as evidenced by the high classification power of each dataset's top features (Figure 8).

HH Tissue is Characterized by High Fatty Acid Biosynthesis and Symbiotic Homeostasis

Metabolism within healthy tissue is broadly characterized by high levels of fatty acid biosynthesis in both *M. cavernosa* and *C. goreaui*. Fatty acid biosynthesis is critically important for various biological processes, such as maintaining membrane structure and function, energy storage and metabolism, and cell signaling¹⁸⁹. Symbiodiniaceae have been shown to supply their coral hosts with diverse saturated and polyunsaturated fatty acids¹⁹⁰, and previous work has found that Symbiodiniaceae-derived lipid content is higher in healthy *M. cavernosa* corals as opposed to SCTLD-infected corals¹⁴². The enrichment of fatty acid biosynthesis in both the coral host and its algal symbiont in healthy tissue further emphasizes the importance of this metabolic pathway in maintaining overall health and symbiotic homeostasis.

Within the top *M. cavernosa* HH features, we found high expression of genes involved in TGF β signaling (*Tmem145* and *INHBB*). The TGF β signaling pathway is conserved throughout metazoan evolution and functions in a variety of processes such as development, cellular homeostasis, and immune regulation¹⁹¹. In symbiotic cnidarians, TGF β signaling is known to suppress host immunity to establish and maintain symbiosis with Symbiodiniaceae¹⁹²⁻¹⁹⁴. Notably, all transcriptomic studies of SCTLD to date have identified higher expression of TGF β signaling genes in healthy corals compared to their SCTLD-infected counterparts^{67,143,144}. High constitutive levels of TGF β signaling, therefore, may constitute an important mechanism of SCTLD resistance through the maintenance of symbiosis and prevention of a detrimental inflammatory response.

Indeed, another upregulated gene within the top *M. cavernosa* HH features includes *Dmbt1*, known to be involved in maintaining intestinal epithelia mucosal homeostasis by preventing bacterial invasion and suppressing inflammation in humans¹⁹⁵. Previous transcriptomic studies in marine invertebrates have shown differential regulation of *Dmbt1* expression in response to both bacterial challenge and symbiont acquisition^{73,145,196,197}, supporting the hypothesis that this gene contributes to maintaining healthy associations with commensal microbes⁷³. Downregulation of this gene in SCTLD-infected corals was accompanied by shifts in mucus microbial community structure^{37,143}. The higher expression of *Dmbt1* in healthy coral colonies suggests a role in disease resistance through the establishment and maintenance of mucosal microbial homeostasis and the prevention of opportunistic infection.

The top feature in HH *C. goreau* annotated to Protein NO VEIN (*NOV*), a plant-specific nuclear factor required for cell-fate decisions in *Arabidopsis thaliana*¹⁹⁸. Interpro protein domain analysis found a Histidine kinase/Heat Shock Protein 90 (HSP90)-like ATPase superfamily domain within this gene's protein-coding sequence. This conserved domain is found in proteins involved in both cellular signaling and protein folding through the histidine kinase domain and the HSP90-like ATPase domain, respectively¹⁸⁷. Histidine kinases are responsible for triggering signal transduction in response to environmental stimulus, such as nutrient availability, pH, osmolarity and light, while HSP90-like ATPases are molecular chaperones that play an essential role in protein folding and stabilization¹⁸⁷. High expression of this gene in *C. goreau* from healthy coral tissue may therefore suggest heightened sensitivity to environmental cues and prevent the accumulation of misfolded proteins. Additional coral disease research may benefit from elucidating the precise function of this gene in *C. goreau*, given its putative ability to provide natural resilience against SCTLD and its role in cellular homeostasis.

HD Tissue Is Responding to SCTLD by Promoting Symbiont Acquisition and Retention

Visibly healthy tissue on a SCTLD-infected colony has been shown to exhibit cellular morphological changes associated with pathology, such as anisometric viral-like particle (AVLP) accumulation and cavity formation within Symbiodiniaceae⁴². While the healthy tissue on a diseased colony can have intermediate levels of expression of many genes (Figures 4 and 6), our supervised ML approach identified features strongly up- or downregulated by both *M. cavernosa* and *C. goreau* in this tissue. Our results provide further evidence that visibly healthy tissue on a diseased colony exhibits a unique gene expression profile indicative of a preemptive response to infection.

In contrast to the high levels of fatty acid metabolism seen in the HH tissue enrichments, functional enrichment of the HD features showed significant upregulation of amide biosynthesis in both *M. cavernosa* and *C. goreau*. These results are indicative of a shift in metabolic functioning between symbiotic partners during the onset of colony infection with SCTLD. Amides serve as components of proteins, enzymes, and signaling molecules and are involved in many biological processes. In response to stress or infection, the cell may increase amide biosynthesis to ensure an adequate supply of amino acids for the synthesis of stress-response proteins or for repairing damaged proteins¹⁹⁹. This upregulation of amide biosynthesis by both the coral host and its algal endosymbiont provides evidence that the visually healthy tissue on a SCTLD-infected colony exhibits unique metabolic signatures, perhaps in preparation to mount an immune response.

Analysis of the top features from HD *M. cavernosa* provides further evidence of a unique response to SCTLD infection in the visually healthy tissue of a diseased coral colony. Within those features, we found upregulation of *Rab5a*, a gene whose protein product is a prototypical

marker of early endosomal and phagocytic vesicles²⁰⁰. In cnidarians, Rab proteins play a crucial role in mediating endosymbiosis through the maturation or arrest of Symbiodiniaceae-hosting phagocytic vesicles called symbiosomes²⁰¹. In the sea anemone *Aiptasia pulchella*, Rab5 localizes to symbiosomes containing newly ingested or established Symbiodiniaceae, but not in symbiosomes containing dead or dysfunctional Symbiodiniaceae²⁰², highlighting its role in arresting phagosome maturation and subsequent endosymbiont digestion. Interestingly, some intracellular pathogens have been shown to modulate host *Rab5* expression, allowing them to persist and replicate within arrested phagosomes^{203–205}. The upregulation of *Rab5a* by *M. cavernosa* in the HD tissue may therefore indicate an effort, either mediated by the coral host or its Symbiodiniaceae, to promote and maintain algal endosymbiont retention within the healthy tissue of a colony infected with SCTL D.

In addition, HD *M. cavernosa* exhibited a downregulation of two genes (*cfap298* and *fam166b*) involved in cilia movement and assembly. In corals, cilia are directly involved in heterotrophic feeding and nutrient acquisition²⁰⁶, and the downregulation of *cfap298* and *fam166b* may indicate a reduction in host nutrient acquisition from the surrounding seawater. Interestingly, within the top HD features from *C. goreau*, we saw upregulation of *STY17*, a serine/threonine protein kinase that phosphorylates chloroplast-destined precursor proteins. In the plant *Arabidopsis thaliana*, *STY17* knockout resulted in delayed assimilation of chlorophyll and a reduction in photosynthetic capacity, highlighting the vital role of this gene in chloroplast biogenesis and differentiation²⁰⁷. A shift in the metabolic exchange between corals and their algal endosymbionts in the visually healthy tissue on a SCTL D-infected colony likely indicates an increased reliance on Symbiodiniaceae for energy and nutrient acquisition.

LD Tissue is characterized by immune activity, loss of extracellular matrix structure, and host-endosymbiont dysbiosis

Functional enrichment of features in LD *M. cavernosa* shows upregulation of genes involved in innate immunity, including C-type lectin (CTL) receptor binding and NF- κ B signaling. CTLs can recognize exogenous ligands to activate innate immunity through the NF- κ B and lectin complement pathways²⁰⁸, and have been identified in many cnidarian species²⁰⁹. When activated, NF- κ B launches a wide array of host responses, including phagocytosis, inflammation, antimicrobial killing mechanisms and host cell apoptosis or autophagy²¹⁰. Interestingly, previous studies have shown that Symbiodiniaceae are able to suppress host NF- κ B signaling to maintain symbiosis within their cnidarian hosts^{211–214}. It is possible that the upregulation of NF- κ B activation in lesioned tissue could be due to direct pathogen exposure, a breakdown in host immune suppression caused by algal endosymbiont dysbiosis, or a combination of the two. Importantly, corals exposed to SCTLD *ex situ* also displayed increased expression of genes involved in NF- κ B expression, but this response was absent following amoxicillin treatment that effectively slowed or halted lesion progression¹⁴⁴. It therefore appears that the ability to suppress inflammation and maintain symbiotic homeostasis via NF- κ B regulation is central to halting lesion progression.

Additionally, we saw enrichment of the term ‘autophagosome maturation’ within the LD *M. cavernosa* features, suggesting a heightened activation of autophagy at the lesion tissue in corals infected with SCTLD. One of the most ancient forms of innate immunity, autophagy in animal cells is the process by which cytoplasmic contents, including intracellular bacteria and viruses, are engulfed within a double-membrane autophagosome which is then delivered to lysosomes for degradation and recycling²¹⁵. Autophagy of Symbiodiniaceae is called

symbiophagy, the process by which the host-derived symbiosome is transformed from an arrested state of phagocytosis into a digestive organelle⁸⁵. Rab7, an established marker of symbiophagy, was upregulated in multiple species in response to SCTL D infection, implicating symbiophagy in the pathology of SCTL D¹⁴³. While we did not find *Rab7* in our top LD *M. cavernosa* features, the enrichment of autophagosome maturation is further evidence of either an activation of an autophagic immune response against a pathogen, an activation of symbiophagy in response to dead or dysfunctional Symbiodiniaceae, or both concomitantly. The significance of autophagosome maturation in SCTL D-infected corals further highlights the intricate relationship between innate immunity and symbiosis maintenance during the pathogenesis of SCTL D and represents a promising target for further research in disease prevention and intervention efforts.

Analysis of the top LD features in *M. cavernosa* shows that SCTL D lesion tissue is predominantly characterized by a dramatic downregulation of genes involved in maintaining extracellular matrix (ECM) and actin cytoskeletal structure. The top feature in LD *M. cavernosa* was the downregulated *Tpm1*, a gene implicated in stabilizing cytoskeletal actin filaments in non-muscle cells. Interestingly, Beavers et al.¹⁴³ showed that a similar gene, Tropomyosin 4 (*Tpm4*), exhibited significant downregulation in five species of coral after experimental exposure to SCTL D¹⁴³. Furthermore, tropomyosin is also downregulated in a closely related Scleractinian coral, *Orbicella faveolata*, during thermal stress and bleaching²¹⁶. It is therefore likely that actin cytoskeletal structure in SCTL D lesion tissue is experiencing disruption due to oxidative stress and dysregulated nutrient transfer caused by symbiosis breakdown.

In addition, five collagen genes (two Collagen alpha-1(II) chain homologs (*col2a1 [a]* and *col2a1 [b]*), two Collagen alpha-2(I) chain homologs (*col1a2 [a]* and *col1a2 [b]*), and one

collagen alpha-2(XI) chain (*coll1a1*) were downregulated within the top LD *M. cavernosa* features. These results contrast those seen in a SCTL D transmission experiment by Traylor-Knowles et al.⁶⁷, who saw differential up- and downregulation of collagen genes in response to early infection, leading to their hypothesis that corals infected with SCTL D are activating wound healing mechanisms in response tissue degradation⁶⁷. In our field-collected samples, however, the drastic downregulation of ECM components represents a compromised ability of the coral tissue to maintain its structural integrity, impeding its ability to effectively heal lesions and rendering them more vulnerable to secondary infections. Additional investigation of the ECM and cytoskeletal dynamics involved in SCTL D progression may therefore be critical in developing effective treatment and conservation measures to combat this deadly disease.

Examining host and endosymbiont features together, we find evidence of photosystem dysfunction, ROS production, and dysbiosis in the SCTL D lesion tissue. *EDLI*, a glycosyltransferase-like protein that acts as a negative regulator of photomorphogenesis, was upregulated in *C. goreau* within the lesion tissue, signifying a redirection of cellular resources away from growth-related processes. In addition, *FCPE*, a component of the light-harvesting complex embedded in the thylakoid membrane, was also upregulated in *C. goreau* from the lesion tissue, which could represent a strategy to enhance the efficiency of photosynthesis under stress conditions. However, within the top features in LD *M. cavernosa*, we found downregulation of *GFPL*, a green fluorescent protein-like pigment that is implicated in photoprotection of Symbiodiniaceae²¹⁷ as well as a drastic increase in expression of *sodA*, an established coral antioxidant involved in reducing harmful superoxide radicals^{77,218}. A compromise in *M. cavernosa*'s ability to protect its algal endosymbiont from excess light in the lesion tissue could explain the observed shifts in chloroplast function by *C. goreau*, leading to

photosystem stress, leakage of ROS into host tissue, and a subsequent antioxidant response by the coral host. These gene expression signatures resemble those seen during bleaching¹⁶ and represents further evidence of host-endosymbiont dysbiosis within the SCTL D lesion tissue.

CONCLUSION

In summary, our characterization of gene expression profiles associated with various tissue health states in *M. cavernosa* and its dominant algal endosymbiont, *C. goreau*, supports evidence that SCTL D infection causes dysbiosis between the coral host and its Symbiodiniaceae. While this study does not confirm the etiologic agent of SCTL D, it does highlight the unique shifts in host-endosymbiont functioning both during the onset of colony infection and during the progression of SCTL D lesions. Visually healthy tissue on a SCTL D-infected colony appears to be mounting a response to colony infection by promoting Symbiodiniaceae uptake and retention, perhaps as a mechanism to increase autotrophic nutrient acquisition to prepare an immune response. If SCTL D is indeed caused by a pathogen of Symbiodiniaceae, this strategy could be detrimental to the coral host as it promotes increased acquisition of potentially infected endosymbionts. SCTL D lesion tissue, alternatively, provides insight into the cellular mechanisms involved in tissue loss. This tissue health state exhibited strong signals of runaway inflammation, loss of cellular integrity, and an inability to maintain symbiotic homeostasis. Some of the gene expression signatures in the lesion tissue exhibit similarity to a bleaching response, such as disruption of actin cytoskeleton structure and oxidative stress in the coral and photosystem dysregulation in the algal endosymbiont. The compounded stress of mounting an inflammatory response in addition to a breakdown in host-endosymbiont physiology could therefore explain the rapid tissue loss observed in SCTL D progression.

Our bioinformatic pipeline utilizing supervised machine learning provides a novel method to characterize disease pathogenesis in both the coral and their algal endosymbionts that fine-tunes traditional gene expression analyses by isolating the most biologically relevant genes with the highest classification power. With the growing availability of high-throughput data, these methods can be widely integrated into omics analyses to accurately characterize various coral physiological states, such as white plague disease, bleaching, and emerging disease outbreaks. With this classification framework, we can better understand the health states of endangered coral species to develop effective and long-lasting restoration efforts.

ACKNOWLEDGEMENTS

The authors would like to thank the facilities and staff at the University of the Virgin Islands Center for Marine and Environmental Studies (CMES), and especially Dr. Cynthia Becker, for their assistance with field collections. Samples were collected under permit #DFW19057U authorized by the Department of Planning and Natural Resources Coastal Zone Management. This is CMES contribution #256. Bioinformatic analyses were performed on the Frontera supercomputer at the Texas Advanced Computing Center. This work was funded by National Science Foundation (NSF) VI EPSCoR 0814417 and 1946412 and NSF (Biological Oceanography) award numbers 1928753 to M.E.B., 1928771 to L.D.M., as well as 1928761 and 1938112 to A.A., NSF EEID award number 2109622 to M.E.B., A.A., L.D.M., and a NOAA OAR Cooperative Institutes award to A.A. (#NA19OAR4320074).

DATA ACCESSIBILITY STATEMENT

Raw sequence data and associated sample metadata are deposited in the NCBI SRA database (BioProject PRJNA1062758). Publicly available data used in this study include the reference transcriptomes for *Symbiodinium* CassKB8 (BioProject PRJNA80085), *Breviolum minutum* (BioProject PRJNA274852), *Cladocopium goreau* (BioProject PRJNA307543), and *Durusdinium trenchii* (BioProject PRJNA508937). The Master Coral database used is available in a public Zenodo repository (<https://doi.org/10.5281/zenodo.7838980>) (Beavers 2023). All shell scripts and R code used will be made available in an archived Github repository on Zenodo upon publication.

BENEFIT-SHARING STATEMENT

Benefits Generation: Benefits from this research accrue from the sharing of our data, methods, and results on public databases as described above.

AUTHOR CONTRIBUTIONS

Conceptualization: K.M.B., E.V.B., A.A., L.D.M. Sample collection: K.M.B., M.E.B., A.A. RNA extraction and processing: K.M.B. Data analysis: K.M.B, D.G.A., with input from M.E. and E.V.B. Manuscript writing: K.M.B and L.D.M., with editing contributions from all authors.

CONFLICT OF INTEREST DISCLOSURE

The authors declare no competing interests.

Chapter 4 Figures:

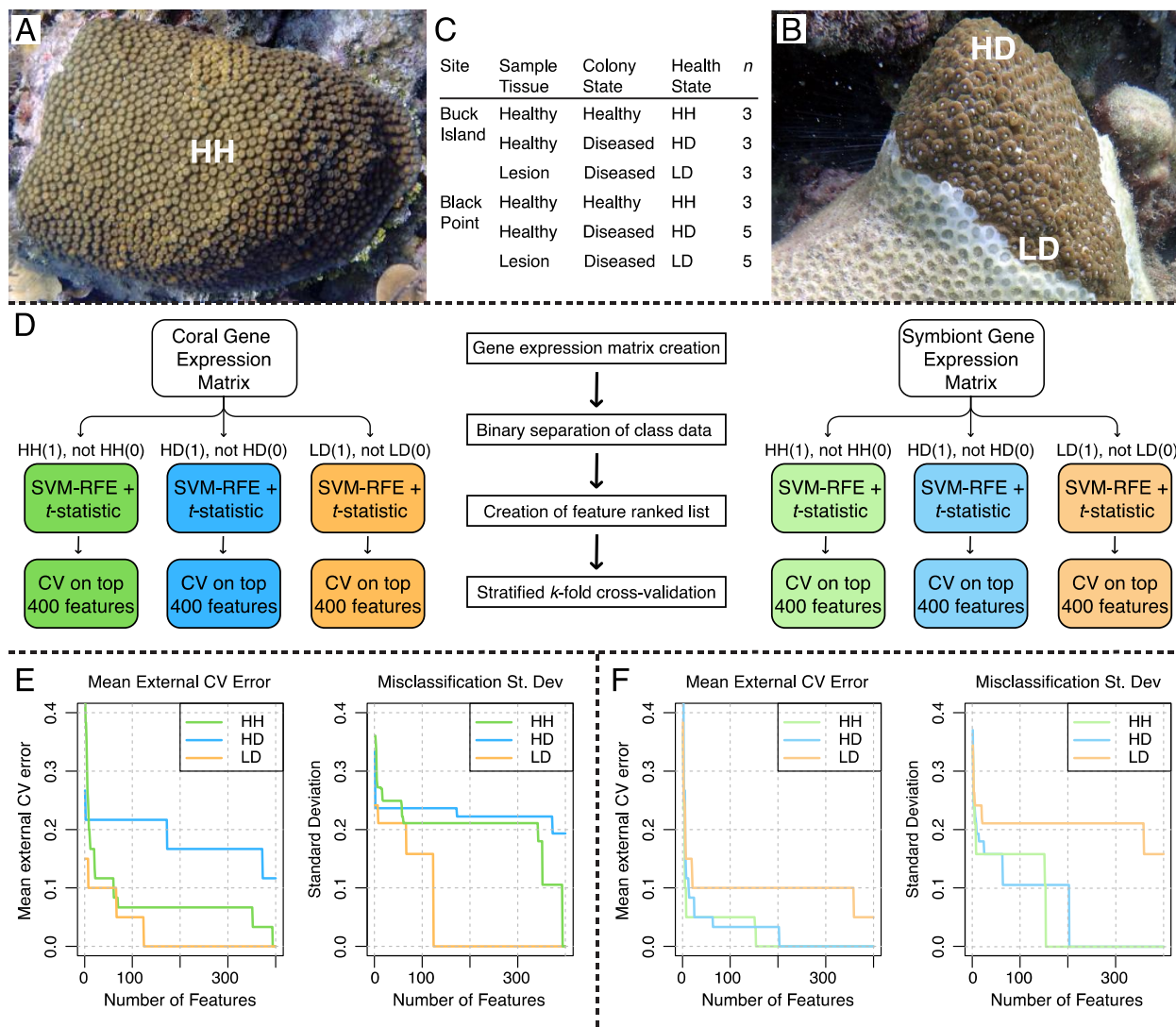


Figure 1: Experimental design and analysis workflow. **A-B** Photographs showing the three tissue health states collected: healthy tissue on a healthy colony (HH), healthy tissue on a diseased colony (HD), and lesion tissue on a diseased colony (LD). **C** Sampling data. **D** Supervised machine learning (ML) pipeline using a combination of SVM-RFE and differential expression *t*-statistic using the sigFeature R package¹⁷⁸. **E** External stratified *k*-fold cross-validation results on the top 400 *M. cavernosa* features from each tissue health state. **F** External stratified *k*-fold cross-validation results on the top 400 *C. goreaui* features from each tissue health state (SVM-RFE support vector machine recursive feature elimination, CV cross-validation). **A,B** Amy Apprill

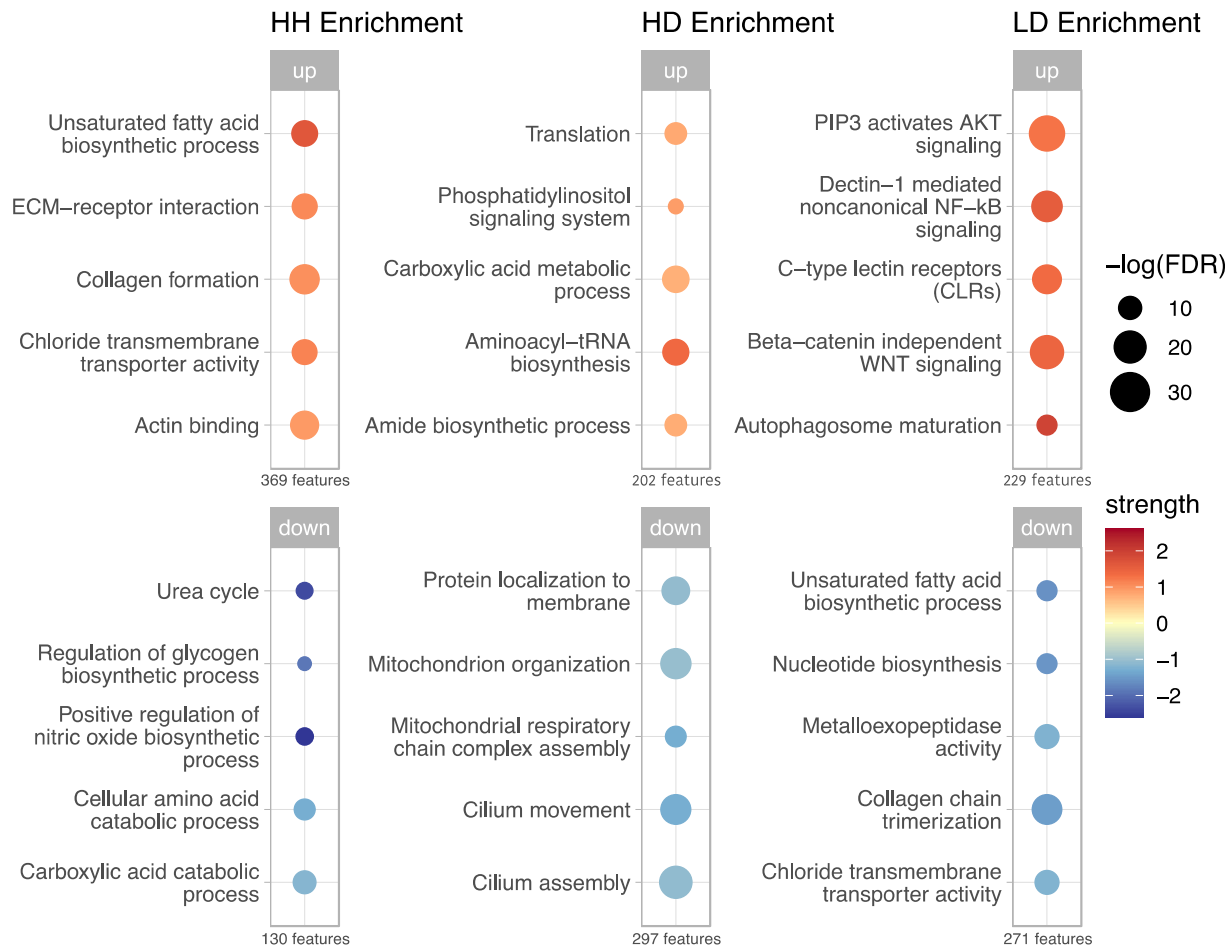


Figure 2: Functional enrichment of up- and downregulated genes within the top 500 *M. cavernosa* features from each tissue health state. The lists of up- and downregulated genes from each tissue health state were uploaded individually to STRING v. 12.0 using the uploaded proteome of *M. cavernosa* as the reference organism (STRING ID: STRG0A38MOJ). The number of genes in each list are shown beneath each bubble plot. Upregulated enrichments are shown on the top panel and downregulated enrichments are shown on the bottom panel. Size of bubble represents the $-\log$ transformed false discovery rate for the enrichment, corrected for multiple testing using Benjamini-Hochberg procedure. Color represents the strength of the enrichment: the ratio between the number of proteins in the network that are annotated and the number of proteins that we expect to be annotated with this term in a random network of the same size ($\text{Log}_{10}(\text{observed}/\text{expected})$). Strength values from the downregulated enrichments were multiplied by -1 for visualization purposes.

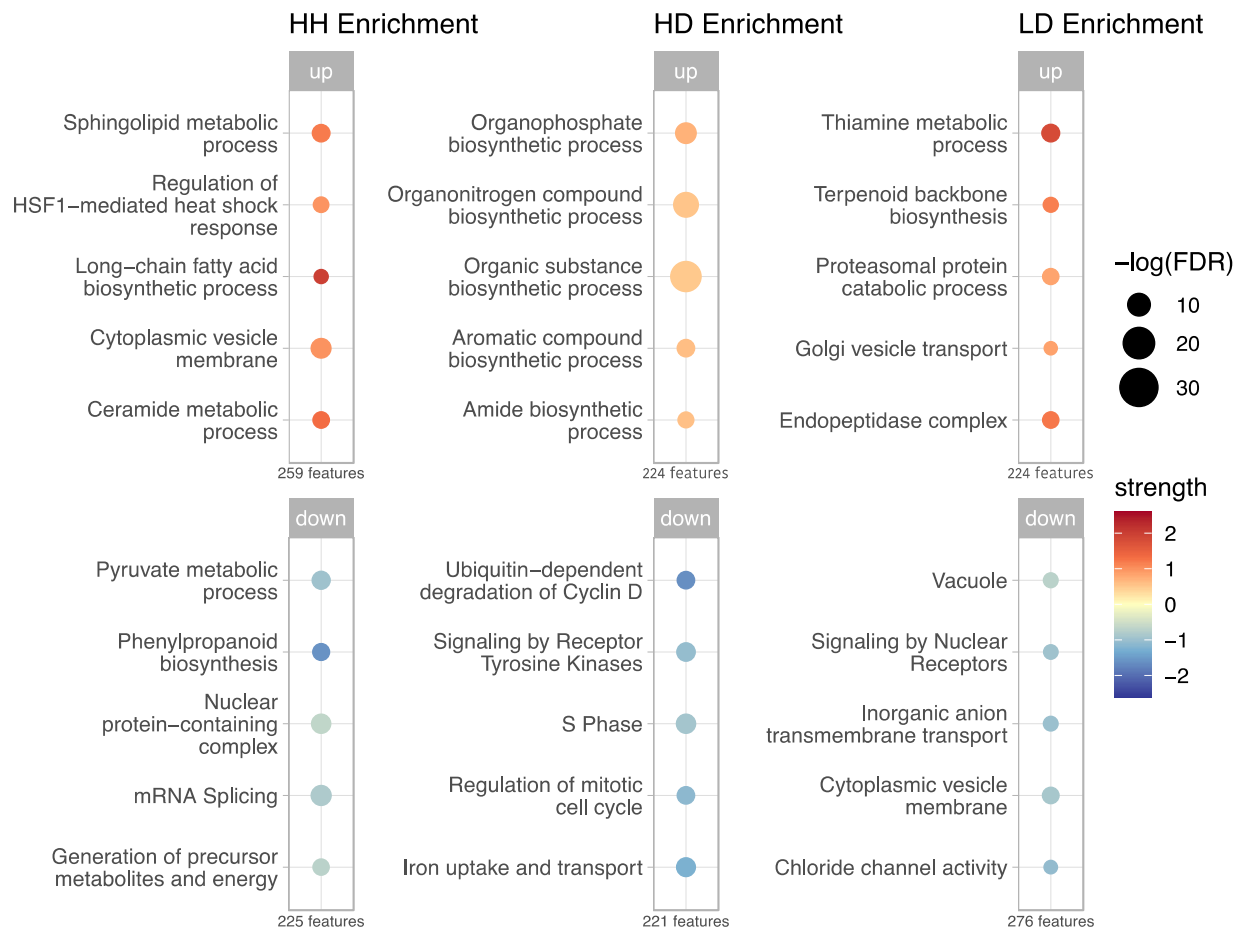


Figure 3: Functional enrichment of up- and downregulated genes within the top 500 *C. goreau* features from each tissue health state. The lists of up- and downregulated genes from each tissue health state were uploaded individually to STRING v. 12.0 using the uploaded proteome of *C. goreau* as the reference organism (STRING ID: STRG0A06ZQW). The number of genes in each list are shown beneath each bubble plot. Upregulated enrichments are shown on the top panel and downregulated enrichments are shown on the bottom panel. Size of bubble represents the $-\log$ transformed false discovery rate for the enrichment, corrected for multiple testing using Benjamini-Hochberg procedure. Color represents the strength of the enrichment: the ratio between the number of proteins in the network that are annotated and the number of proteins that we expect to be annotated with this term in a random network of the same size ($\text{Log}_{10}(\text{observed}/\text{expected})$). Strength values for the downregulated enrichments were multiplied by -1 for visualization purposes.

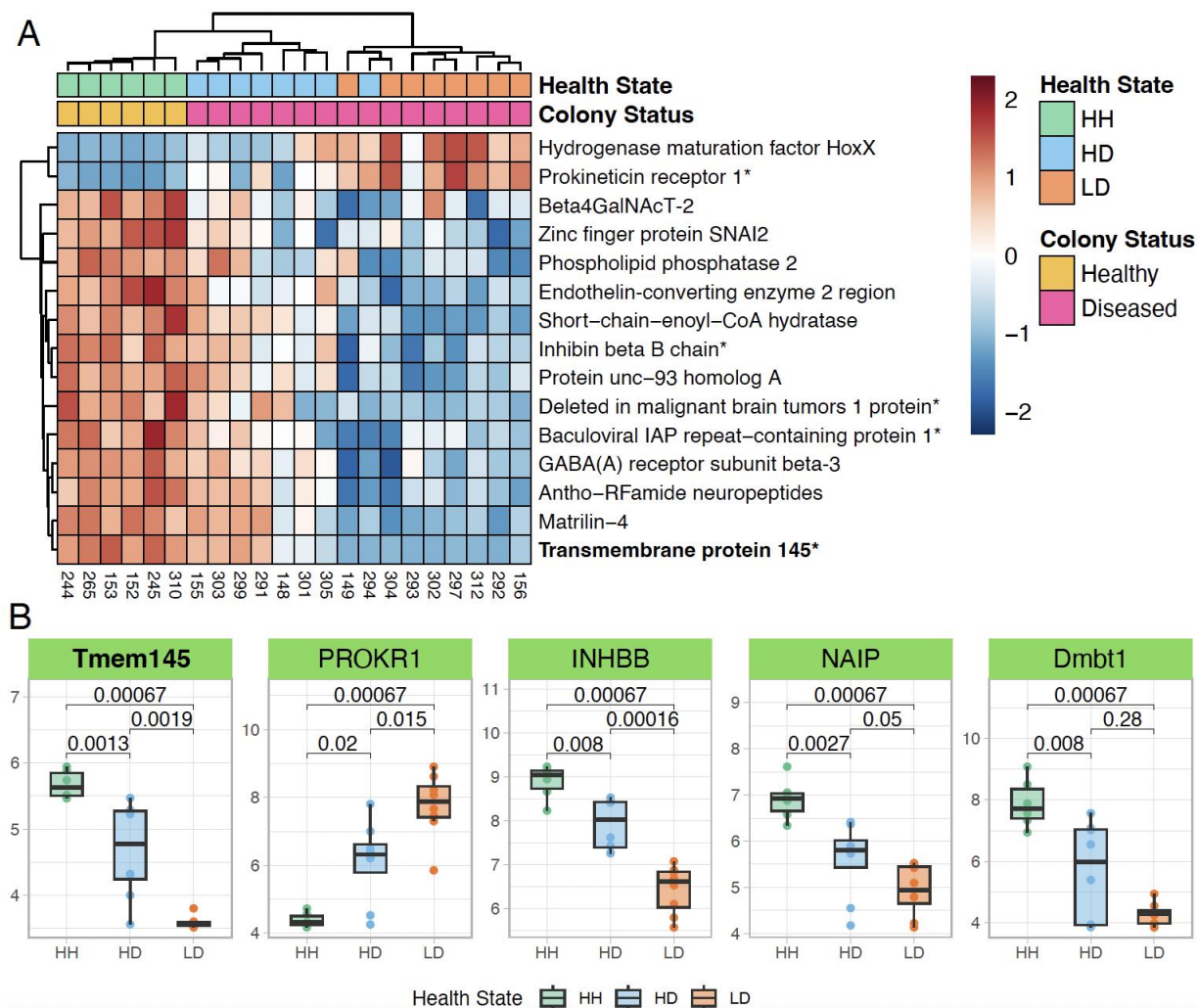


Figure 4: Top features in HH *M. cavernosa*. **A** Relative expression heatmap of the top 15 HH features from *M. cavernosa*. The top feature is shown in bold, and genes plotted in **B** end in an asterisk. **B** Boxplots showing the log transformed expression of five selected features from **A**, organized by tissue health state. *P*-values represent two-sample Wilcoxon test results. Color of boxplots correspond to tissue health state. Boxplot elements: center line, median; box limits, upper and lower quartiles; whiskers, 1.5x interquartile range; points beyond whiskers, outliers.

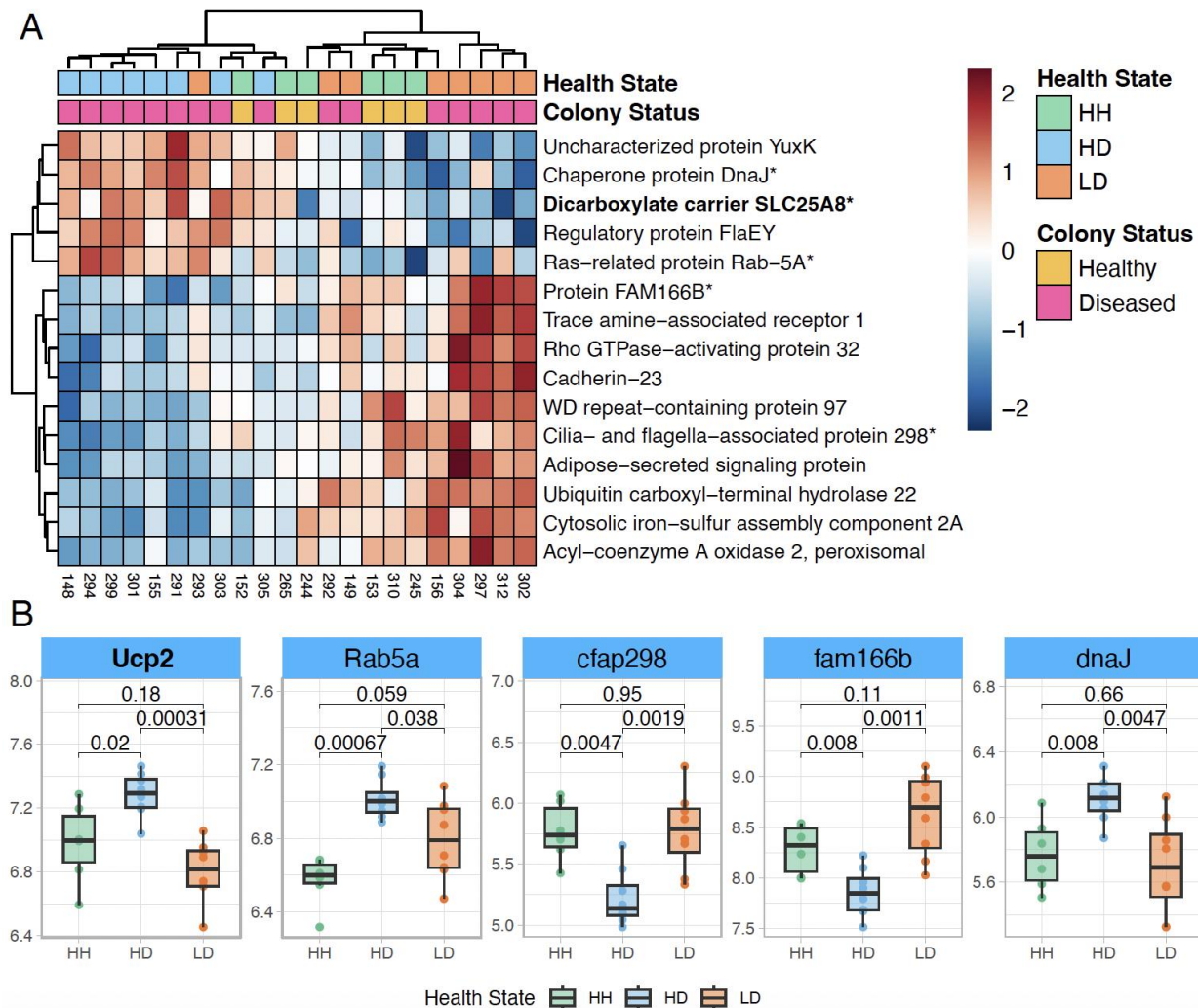


Figure 5: Top features in HD *M. cavernosa*. **A** Relative expression heatmap of the top 15 HD features from *M. cavernosa*. The top feature is shown in bold, and genes plotted in **B** end in an asterisk. **B** Boxplots showing the rlog transformed expression of five selected features from **A**, organized by tissue health state. *P*-values represent two-sample Wilcoxon test results. Color of boxplots correspond to tissue health state. Boxplot elements: center line, median; box limits, upper and lower quartiles; whiskers, 1.5x interquartile range; points beyond whiskers, outliers.

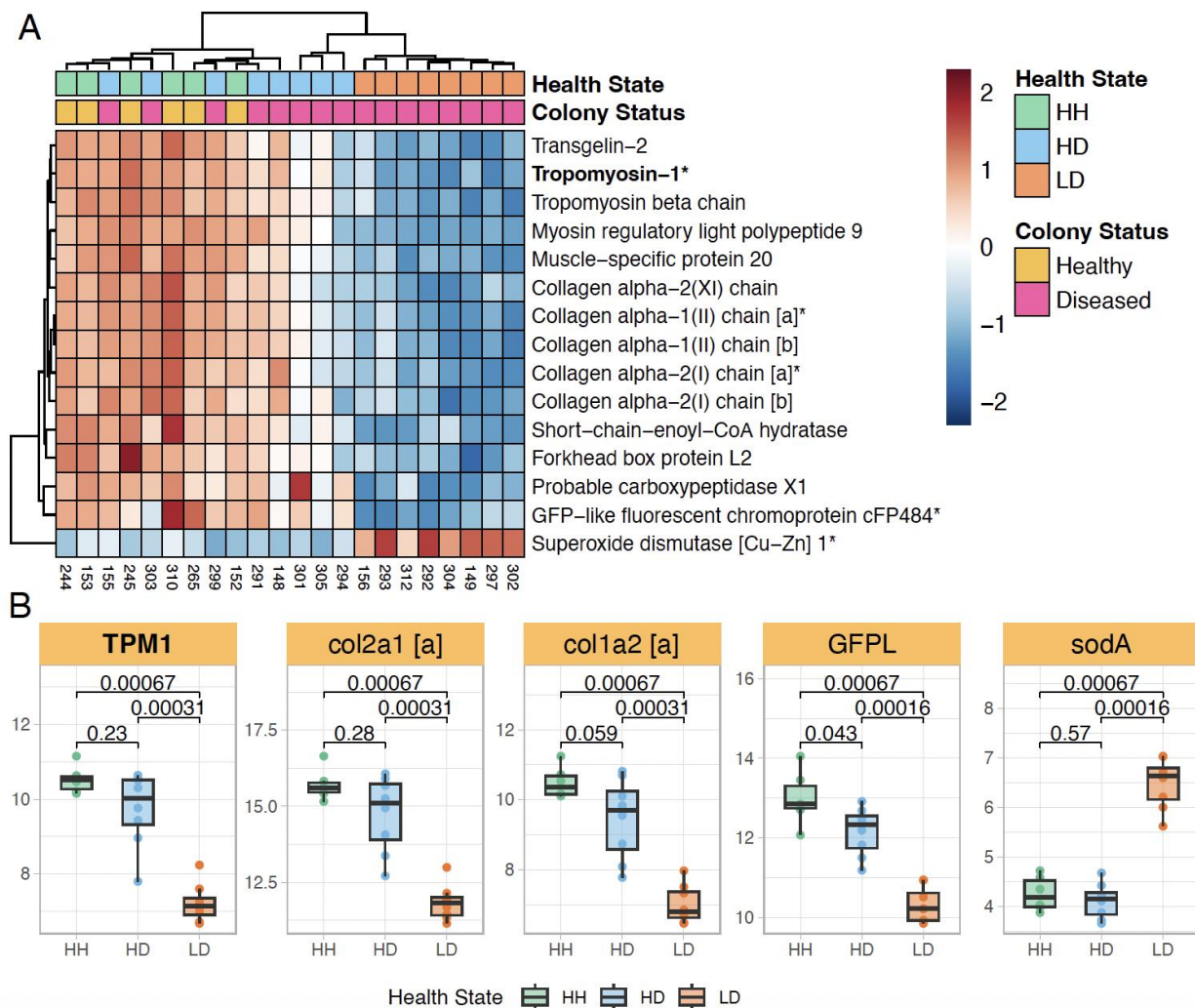
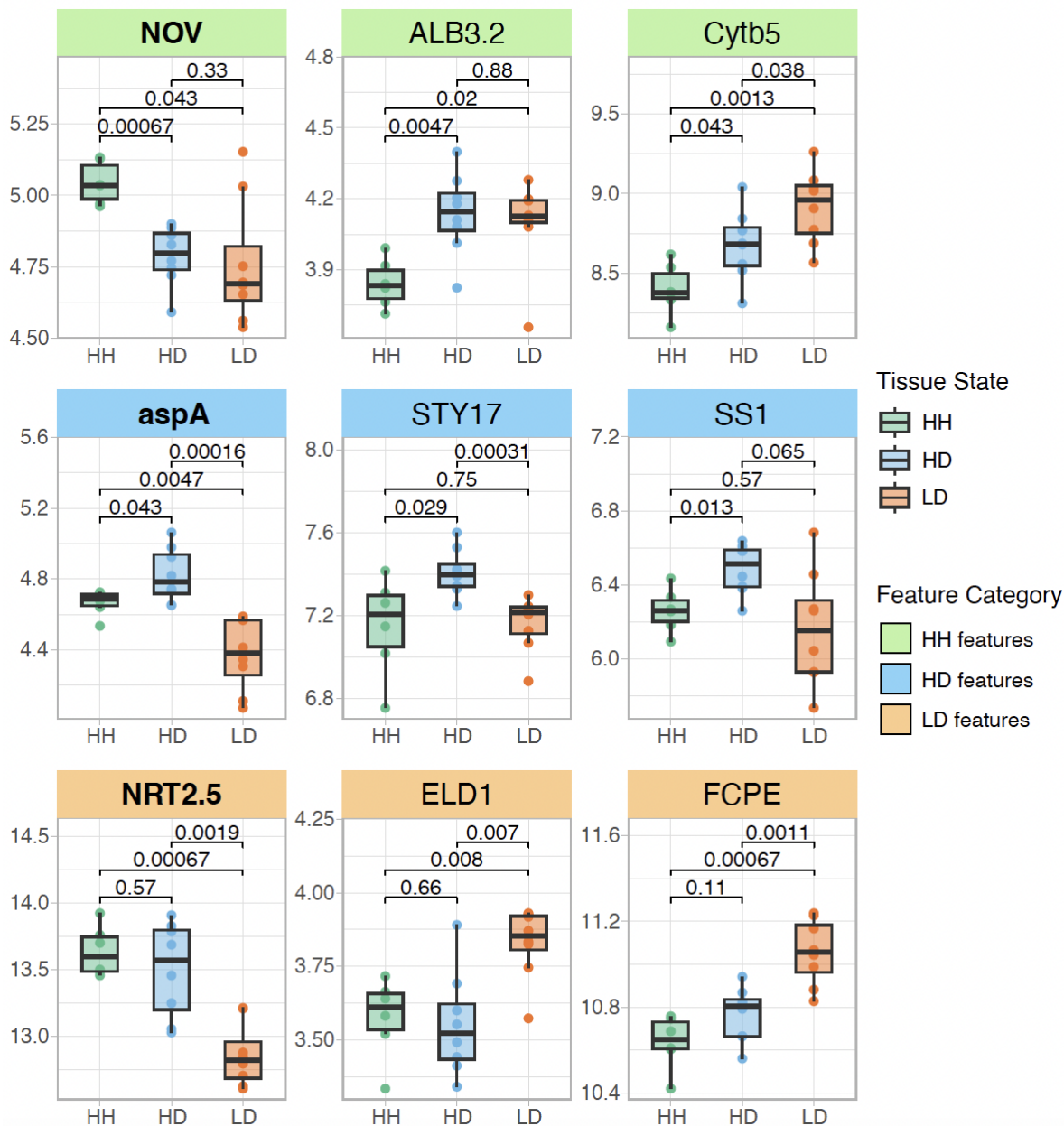


Figure 6: Top features in LD *M. cavernosa*. **A** Relative expression heatmap of the top 15 LD features from *M. cavernosa*. The top feature is shown in bold, and genes plotted in **B** end in an asterisk. **B** Boxplots showing the log transformed expression of five selected features from **A**, organized by tissue health state. *P*-values represent two-sample Wilcoxon test results. Color of boxplots correspond to tissue health state. Boxplot elements: center line, median; box limits, upper and lower quartiles; whiskers, 1.5x interquartile range; points beyond whiskers, outliers.



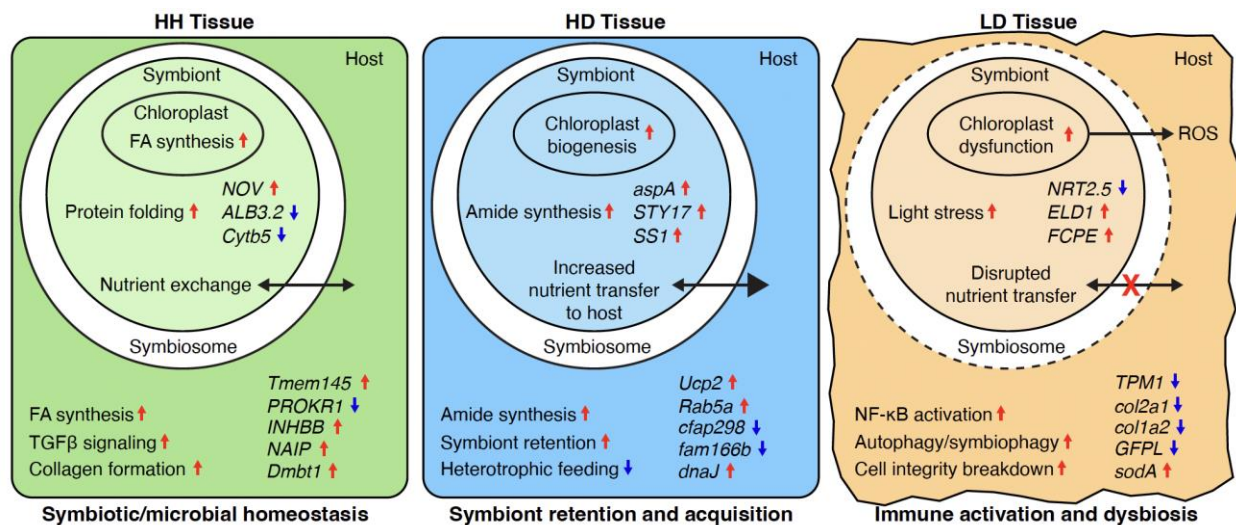


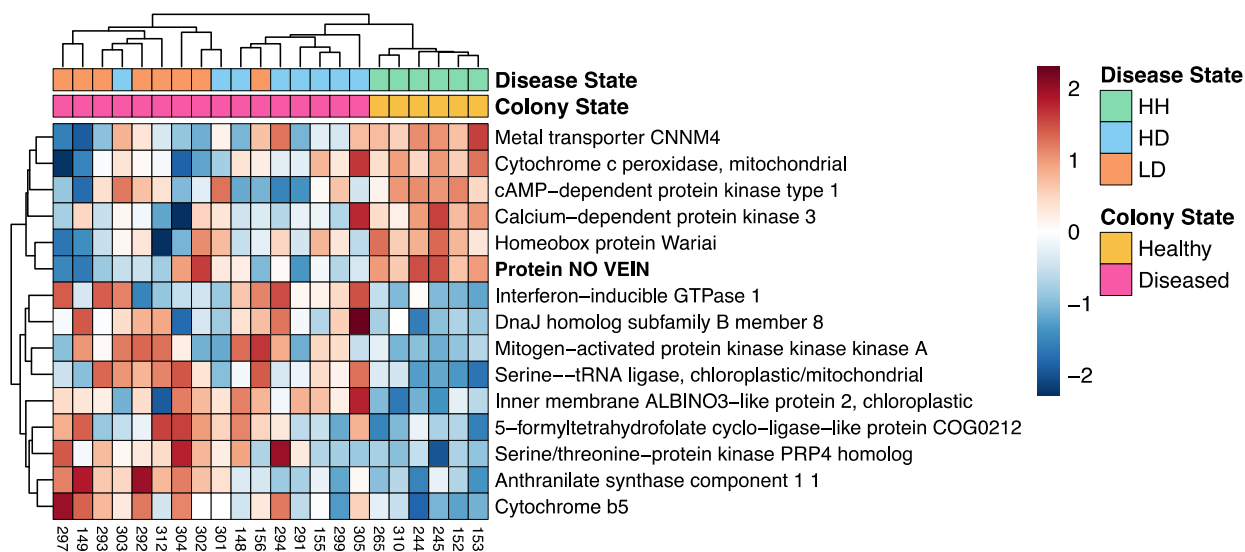
Figure 8: Characterization of SCTLD tissue health states in *M. cavernosa* and *C. goreau*. Processes are shown in regular font and selected features are shown in italic font. Processes are inferred from both functional enrichment of top 500 features and analysis of selected features (genes listed). Upregulated processes/features are denoted with a red arrow and downregulated processes/features are denoted with a blue arrow. (FA, fatty acid; ROS, reactive oxygen species).

Chapter 4 Tables:

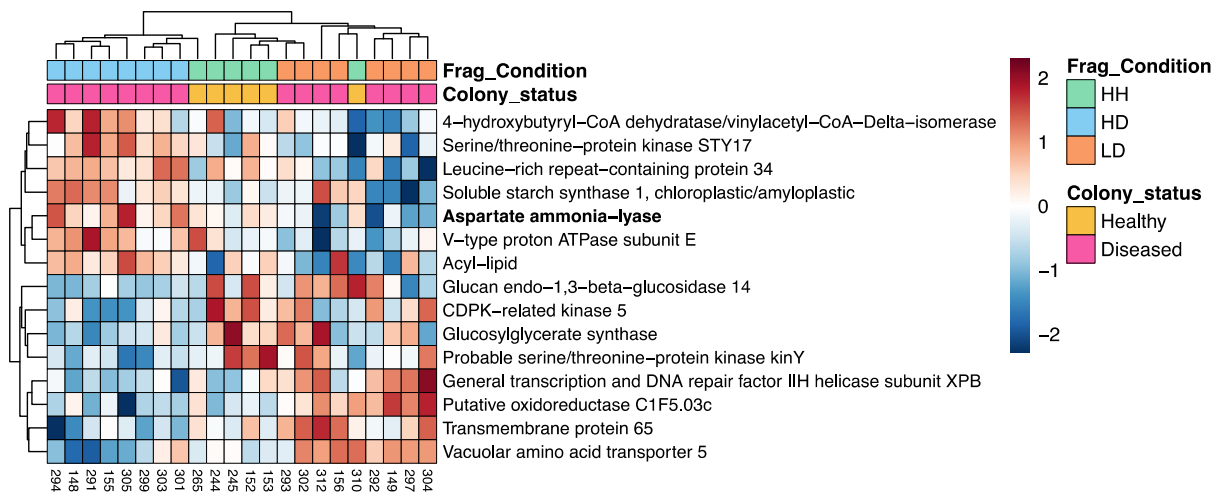
| Type | No. contigs | Complete & Single-Copy (%) | Complete and Duplicated (%) | Fragmented (%) | Missing (%) | N50 |
|--|-------------|----------------------------|-----------------------------|----------------|-------------|--------|
| <i>M. cavernosa assembly metrics based on metazoan reference</i> | | | | | | |
| <i>de novo</i> | 73,047 | 76.0 | 11.3 | 3.1 | 9.6 | 16,467 |
| <i>C. goreau assembly metrics based on eukaryote reference</i> | | | | | | |
| <i>de novo</i> | 48,013 | 52.9 | 16.1 | 7.1 | 23.9 | 13,469 |

Table 1: Reference transcriptome assembly metrics: Assembly completeness was assessed via Benchmarking Universal Single Copy Orthologs (BUSCO) v. 5.2.2 and the “bbstats.sh” script within the BBMap v. 38.90 package^{103,106}.

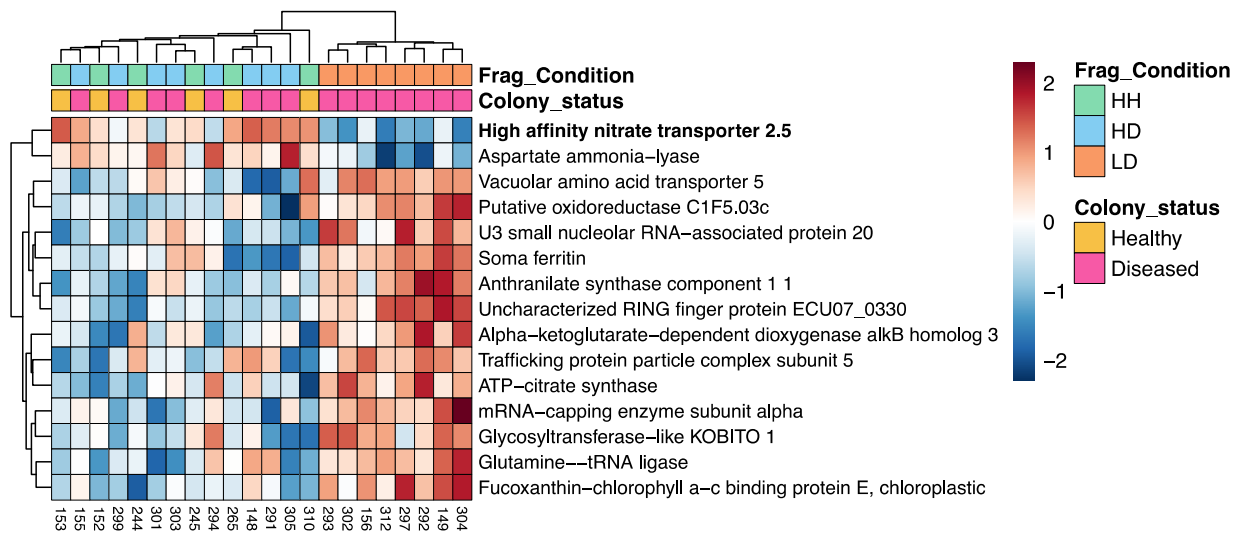
Chapter 4 Supplementary Information:



Supplementary Figure 1: Relative expression heatmap of the top 15 HH features from *C. goreau*. The top feature is shown in bold.



Supplementary Figure 2: Relative expression heatmap of the top 15 HD features from *C. goreauii*. The top feature is shown in bold.



Supplementary Figure 3: Relative expression heatmap of the top 15 LD features from *C. goreauii*. The top feature is shown in bold.

Chapter 5: Conclusion

Coral reefs, one of the most diverse and productive ecosystems on the planet, are in danger. Global climate change and local anthropogenic impacts have fundamentally altered the biodiversity and productivity of coral reefs around the world. This changing environment has also led to a drastic increase in coral disease incidence and severity, which has contributed to large population declines and even functional extinction of certain coral species in relatively short periods of time. SCTLD is one of the most devastating coral disease outbreaks in recorded history and poses a significant threat to Caribbean reef ecosystems.

In this dissertation I present original research contributing valuable insights into the pathogenesis of SCTLD and mechanisms of disease resistance. Our findings reveal that SCTLD triggers shared gene expression signatures across various coral species, including those involved in symbiophagy – the *in situ* degradation of dysfunctional Symbiodiniaceae. Prior to this work, symbiophagy had only been characterized in a bleaching context, where prolonged heat stress triggers the activation of genes that transform the host-derived symbiosome from an arrested state of phagocytosis into a digestive organelle, resulting in the elimination of algal endosymbionts. However, within the context of coral disease, symbiophagy likely represents a host immune response against compromised symbionts. This discovery not only further implicates Symbiodiniaceae in the pathology of SCTLD, but also emphasizes the importance of symbiotic interactions during coral disease outbreaks. By concurrently investigating host and symbiont responses to SCTLD, this dissertation provides a holistic framework for understanding the complexities of coral disease.

In addition, our research provides important insights into the cellular processes involved in SCTLD onset. Using a novel machine learning approach, we identified gene expression signatures unique to the visually healthy tissue on a SCTLD-affected colony in a dominant reef-

building coral, *M. cavernosa*, and its primary algal endosymbiont, *C. goreau*. We found evidence that *M. cavernosa* is attempting to promote and maintain algal endosymbiont retention during the onset of colony infection with SCTL D while also downregulating genes involved in heterotrophic feeding, suggesting a reduction in host nutrient acquisition from the surrounding seawater. Furthermore, *C. goreau* endosymbionts within this tissue state exhibited a simultaneous upregulation of genes involved in chlorophyll assimilation and maintaining photosynthetic capacity. Taken together, these results indicate a metabolic shift in the visually healthy tissue on a SCTL D-affected colony, with an increased reliance on Symbiodiniaceae for energy and nutrient acquisition. These findings align with prior studies that have reported microbiome alterations in this tissue state and sheds light on why antibiotic treatment is effective at halting lesion progression, but ineffective at preventing the emergence of new lesions. If SCTL D is indeed caused by a pathogen of Symbiodiniaceae, this strategy would be detrimental to the coral host, as it promotes increased acquisition of potentially infected endosymbionts.

We also provide evidence that hosting *Durusdinium* spp. may increase susceptibility to and severity of SCTL D. Interestingly, *D. trenchii* is invasive to the Caribbean, but corals that have established a symbiosis with this symbiont tend to be more resilient to heat stress. The accidental introduction of *Durusdinium* spp. to Caribbean reefs has been referred to as “a nugget of hope” for corals²¹⁹, but our research has shown that the heat resilience conferred by *Durusdinium* spp. may come at the cost of increased disease susceptibility and severity. For example, we found evidence of photosynthetic dysfunction in *Breviolum* and *Durusdinium* symbionts, with *Breviolum* spp. downregulating photosystem genes and *Durusdinium* spp. upregulating the same genes in response to SCTL D. Interestingly, the samples dominant in *Durusdinium* spp. exhibited the fastest lesion growth rates out of all the corals in the

transmission experiment, suggesting that *Durusdinium*'s photosystem overexcitation response may lead to worse SCLD outcomes. This response could lead to the overproduction of harmful ROS and leakage into host tissue, increasing the levels of cellular stress in the coral host. Scientists should therefore exercise caution when we refer to *Durusdinium* spp. as a beacon of hope for corals.

This dissertation also examines the cellular phenotypes, Symbiodiniaceae community composition, and shared gene expression patterns contributing to interspecies variation in SCTL D susceptibility. We show that high SCTL D susceptibility is characterized by reduced immune function, increased levels of oxidative stress, and elevated constitutive expression of cellular stress response genes. Conversely, we find that low SCTL D susceptibility is characterized by reduced levels of oxidative stress and elevated constitutive expression of genes involved in immune system regulation and DNA damage responses. These results provide evidence that having a proactive immune system that is primed to respond swiftly against pathogens is protective against SCTL D and likely other coral diseases. We also show that constitutive levels of host gene expression are influenced by the Symbiodiniaceae community structure within a coral, likely affecting disease susceptibility. These findings can be used for the development of targeted disease intervention efforts aimed at preserving the health of coral reef ecosystems.

The research presented in this dissertation has sought to deepen our understanding of SCTL D, offering insights into the cellular processes underlying disease susceptibility and pathogenesis. Through gene expression analyses, histopathology, protein assays, and machine learning techniques, we have discovered key factors contributing to SCTL D susceptibility and disease progression, while also uncovering potential avenues for additional research for

intervention and management. This research highlights the critical role of Symbiodiniaceae in SCTLD and emphasizes the importance of employing holistic approaches to understanding coral disease. By shedding light on the cellular mechanisms involved in SCTLD progression and susceptibility, this research lays the foundation for effective coral disease mitigation and intervention efforts in the face of escalating environmental challenges.

References

1. Knowlton, N. *et al.* Coral Reef Biodiversity. in *Life in the World's Oceans* 65–78 (John Wiley & Sons, Ltd, 2010). doi:<https://doi.org/10.1002/9781444325508.ch4>.
2. Hoegh-Guldberg, O., Pendleton, L. & Kaup, A. People and the changing nature of coral reefs. *Reg. Stud. Mar. Sci.* **30**, 100699 (2019).
3. Woodhead, A. J., Hicks, C. C., Norström, A. V., Williams, G. J. & Graham, N. A. J. Coral reef ecosystem services in the Anthropocene. *Funct. Ecol.* **33**, 1023–1034 (2019).
4. Burke, L., Reytar, K., Spalding, M. & Perry, A. *Reefs at Risk Revisited*. (Washington, DC: World Resources Institute (WRI), 2011).
5. Speers, A. E., Besedin, E. Y., Palardy, J. E. & Moore, C. Impacts of climate change and ocean acidification on coral reef fisheries: An integrated ecological–economic model. *Ecol. Econ.* **128**, 33–43 (2016).
6. Putnam, H. M., Barott, K. L., Ainsworth, T. D. & Gates, R. D. The Vulnerability and Resilience of Reef-Building Corals. *Curr. Biol.* **27**, R528–R540 (2017).
7. Hawthorn, A. *et al.* An introduction to lesions and histology of scleractinian corals. *Vet. Pathol.* 03009858231189289 (2023) doi:10.1177/03009858231189289.
8. Peters, E. C. Diseases of Coral Reef Organisms. in *Coral Reefs in the Anthropocene* (ed. Birkeland, C.) 147–178 (Springer Netherlands, Dordrecht, 2015). doi:10.1007/978-94-017-7249-5_8.
9. Allemand, D., Tambutté, É., Zoccola, D. & Tambutté, S. Coral Calcification, Cells to Reefs. in *Coral Reefs: An Ecosystem in Transition* (ed. Stambler, N.) (Springer, Dordrecht, 2010).

10. Muscatine, L., Pool, R. R. & Trench, R. K. Symbiosis of Algae and Invertebrates: Aspects of the Symbiont Surface and the Host-Symbiont Interface. *Trans. Am. Microsc. Soc.* **94**, 450–469 (1975).
11. Muller-Parker, G., D’Elia, C. F. & Cook, C. B. Interactions Between Corals and Their Symbiotic Algae. in *Coral Reefs in the Anthropocene* (ed. Birkeland, C.) (Springer, Dordrecht, 2015).
12. Sumich, J. L. *An Introduction to the Biology of Marine Life*. (Wm. C. Brown Publishers, 1996).
13. Stanley, G. D. The evolution of modern corals and their early history. *Earth-Sci. Rev.* **60**, 195–225 (2003).
14. Hughes, T. P. *et al.* Coral reefs in the Anthropocene. *Nature* **546**, 82–90 (2017).
15. Eddy, T. D. *et al.* Global decline in capacity of coral reefs to provide ecosystem services. *One Earth* **4**, 1278–1285 (2021).
16. Weis, V. M. Cellular mechanisms of Cnidarian bleaching: stress causes the collapse of symbiosis. *J. Exp. Biol.* **211**, 3059–3066 (2008).
17. Oakley, C. A. & Davy, S. K. Cell Biology of Coral Bleaching. in *Coral Bleaching: Patterns, Processes, Causes and Consequences* (eds. van Oppen, M. J. H. & Lough, J. M.) 189–211 (Springer International Publishing, Cham, 2018). doi:10.1007/978-3-319-75393-5_8.
18. Hughes, T. P. *et al.* Spatial and temporal patterns of mass bleaching of corals in the Anthropocene. *Science* **359**, 80–83 (2018).
19. Hoegh-Guldberg, O. *et al.* Coral Reefs Under Rapid Climate Change and Ocean Acidification. *Science* **318**, 1737–1742 (2007).

20. Pandolfi, J. M., Connolly, S. R., Marshall, D. J. & Cohen, A. L. Projecting Coral Reef Futures Under Global Warming and Ocean Acidification. *Science* **333**, 418–422 (2011).
21. Sully, S., Burkepille, D. E., Donovan, M. K., Hodgson, G. & van Woesik, R. A global analysis of coral bleaching over the past two decades. *Nat. Commun.* **10**, 1264 (2019).
22. Hoegh-Guldberg, O. & Bruno, J. F. The Impact of Climate Change on the World's Marine Ecosystems. *Science* **328**, 1523–1528 (2010).
23. Vega Thurber, R. *et al.* Deciphering Coral Disease Dynamics: Integrating Host, Microbiome, and the Changing Environment. *Front. Ecol. Evol.* **8**, (2020).
24. Burke, S. *et al.* The impact of rising temperatures on the prevalence of coral diseases and its predictability: A global meta-analysis. *Ecol. Lett.* **26**, 1466–1481 (2023).
25. Neely, K. L., Lewis, C. L., Lunz, K. S. & Kabay, L. Rapid Population Decline of the Pillar Coral *Dendrogyra cylindrus* Along the Florida Reef Tract. *Front. Mar. Sci.* **8**, (2021).
26. Papke, E. *et al.* Stony coral tissue loss disease: a review of emergence, impacts, etiology, diagnostics, and intervention. *Front. Mar. Sci.* **10**, (2024).
27. Precht, W. F., Gintert, B. E., Robbart, M. L., Fura, R. & van Woesik, R. Unprecedented Disease-Related Coral Mortality in Southeastern Florida. *Sci. Rep.* **6**, 31374 (2016).
28. Aeby, G. S. *et al.* Pathogenesis of a Tissue Loss Disease Affecting Multiple Species of Corals Along the Florida Reef Tract. *Front. Mar. Sci.* **6**, 678 (2019).
29. Dobbelaere, T., Muller, E. M., Gramer, L. J., Holstein, D. M. & Hanert, E. Coupled Epidemio-Hydrodynamic Modeling to Understand the Spread of a Deadly Coral Disease in Florida. *Front. Mar. Sci.* **7**, (2020).
30. Muller, E. M., Sartor, C., Alcaraz, N. I. & van Woesik, R. Spatial Epidemiology of the Stony-Coral-Tissue-Loss Disease in Florida. *Front. Mar. Sci.* **7**, 163 (2020).

31. Williams, S. D., Walter, C. & Muller, E. M. Fine Scale Temporal and Spatial Dynamics of the Stony Coral Tissue Loss Disease Outbreak Within the Lower Florida Keys. *Front. Mar. Sci.* (2021) doi:10.3389/fmars.2021.631776.
32. Truc, M. *et al.* Evaluating the spread of stony coral tissue loss disease in the Bay Islands, Honduras. *Front. Mar. Sci.* **10**, (2023).
33. Meyer, J. L. *et al.* Microbial Community Shifts Associated With the Ongoing Stony Coral Tissue Loss Disease Outbreak on the Florida Reef Tract. *Front. Microbiol.* **10**, 2244 (2019).
34. Rosales, S. M., Clark, A. S., Huebner, L. K., Ruzicka, R. R. & Muller, E. M. Rhodobacterales and Rhizobiales Are Associated With Stony Coral Tissue Loss Disease and Its Suspected Sources of Transmission. *Front. Microbiol.* **11**, (2020).
35. Becker, C. C., Brandt, M., Miller, C. A. & Apprill, A. Microbial bioindicators of Stony Coral Tissue Loss Disease identified in corals and overlying waters using a rapid field-based sequencing approach. *Environ. Microbiol.* **24**, 1166–1182 (2022).
36. Clark, A. S. *et al.* Characterization of the Microbiome of Corals with Stony Coral Tissue Loss Disease along Florida’s Coral Reef. *Microorganisms* **9**, 2181 (2021).
37. Huntley, N. *et al.* Experimental transmission of Stony Coral Tissue Loss Disease results in differential microbial responses within coral mucus and tissue. *ISME Commun.* **2**, 1–11 (2022).
38. Neely, K. L., Macaulay, K. A., Hower, E. K. & Dobler, M. A. Effectiveness of topical antibiotics in treating corals affected by Stony Coral Tissue Loss Disease. *PeerJ* **8**, (2020).
39. Shilling, E. N., Combs, I. R. & Voss, J. D. Assessing the effectiveness of two intervention methods for stony coral tissue loss disease on *Montastraea cavernosa*. *Sci. Rep.* **11**, 8566 (2021).

40. Walker, B. K., Turner, N. R., Noren, H. K. G., Buckley, S. F. & Pitts, K. A. Optimizing Stony Coral Tissue Loss Disease (SCTLD) Intervention Treatments on *Montastraea cavernosa* in an Endemic Zone. *Front. Mar. Sci.* **8**, (2021).
41. Forrester, G. E., Arton, L., Horton, A., Nickles, K. & Forrester, L. M. Antibiotic Treatment Ameliorates the Impact of Stony Coral Tissue Loss Disease (SCTLD) on Coral Communities. *Front. Mar. Sci.* **9**, (2022).
42. Work, T. M. *et al.* Viral-Like Particles Are Associated With Endosymbiont Pathology in Florida Corals Affected by Stony Coral Tissue Loss Disease. *Front. Mar. Sci.* **8**, 750658 (2021).
43. Veglia, A. J. *et al.* Alphaflexivirus Genomes in Stony Coral Tissue Loss Disease-Affected, Disease-Exposed, and Disease-Unexposed Coral Colonies in the U.S. Virgin Islands. *Microbiol. Resour. Announc.* **11**, e01199-21 (2022).
44. Landsberg, J. H. *et al.* Stony Coral Tissue Loss Disease in Florida Is Associated With Disruption of Host–Zooxanthellae Physiology. *Front. Mar. Sci.* **7**, 576013 (2020).
45. Cróquer, A., Weil, E. & Rogers, C. S. Similarities and Differences Between Two Deadly Caribbean Coral Diseases: White Plague and Stony Coral Tissue Loss Disease. *Front. Mar. Sci.* **8**, (2021).
46. Meiling, S. S., Muller, E. M., Smith, T. B. & Brandt, M. E. 3D Photogrammetry Reveals Dynamics of Stony Coral Tissue Loss Disease (SCTLD) Lesion Progression Across a Thermal Stress Event. *Front. Mar. Sci.* **7**, (2020).
47. Sharp, W. C., Shea, C. P., Maxwell, K. E., Muller, E. M. & Hunt, J. H. Evaluating the small-scale epidemiology of the stony-coral -tissue-loss-disease in the middle Florida Keys. *PLOS ONE* **15**, e0241871 (2020).

48. Hayes, N. K., Walton, C. J. & Gilliam, D. S. Tissue loss disease outbreak significantly alters the Southeast Florida stony coral assemblage. *Front. Mar. Sci.* **9**, (2022).
49. Bruno, J. F. *et al.* Thermal Stress and Coral Cover as Drivers of Coral Disease Outbreaks. *PLOS Biol.* **5**, 1220–1227 (2007).
50. Miller, A. W. & Richardson, L. L. Emerging coral diseases: a temperature-driven process? *Mar. Ecol.* **36**, 278–291 (2015).
51. Howells, E. J., Vaughan, G. O., Work, T. M., Burt, J. A. & Abrego, D. Annual outbreaks of coral disease coincide with extreme seasonal warming. *Coral Reefs* **39**, 771–781 (2020).
52. Pinzón, J. H., Beach-Letendre, J., Weil, E. & Mydlarz, L. D. Relationship between Phylogeny and Immunity Suggests Older Caribbean Coral Lineages Are More Resistant to Disease. *PLoS ONE* **9**, e104787 (2014).
53. Williams, L., Smith, T. B., Burge, C. A. & Brandt, M. E. Species-specific susceptibility to white plague disease in three common Caribbean corals. *Coral Reefs* **39**, 27–31 (2020).
54. Palmer, C. V., Bythell, J. C. & Willis, B. L. Levels of immunity parameters underpin bleaching and disease susceptibility of reef corals. *FASEB J.* **24**, 1935–1946 (2010).
55. Toledo-Hernández, C. & Ruiz-Diaz, C. P. The immune responses of the coral. *Invertebr. Surviv. J.* **11**, 319–328 (2014).
56. Bruno, J. F., Petes, L. E., Drew Harvell, C. & Hettinger, A. Nutrient enrichment can increase the severity of coral diseases. *Ecol. Lett.* **6**, 1056–1061 (2003).
57. Aronson, R. B. & Precht, W. F. White-band disease and the changing face of Caribbean coral reefs. in *The Ecology and Etiology of Newly Emerging Marine Diseases* (ed. Porter, J. W.) 25–38 (Springer Netherlands, Dordrecht, 2001). doi:10.1007/978-94-017-3284-0_2.

58. Jackson, J., Donovan, M., Cramer, K. & Lam, W. *Status and Trends of Caribbean Coral Reefs: 1970-2012*. (Global Coral Reef Monitoring Network, IUCN, Gland, Switzerland, 2014).
59. Egan, S. & Gardiner, M. Microbial Dysbiosis: Rethinking Disease in Marine Ecosystems. *Front. Microbiol.* **7**, (2016).
60. Howe-Kerr, L. I. *et al.* Viruses of a key coral symbiont exhibit temperature-driven productivity across a reefscape. *ISME Commun.* **3**, 1–12 (2023).
61. Marcelino, V. R. & Verbruggen, H. Multi-marker metabarcoding of coral skeletons reveals a rich microbiome and diverse evolutionary origins of endolithic algae. *Sci. Rep.* **6**, 31508 (2016).
62. Hernandez-Agreda, A., Gates, R. D. & Ainsworth, T. D. Defining the Core Microbiome in Corals' Microbial Soup. *Trends Microbiol.* **25**, 125–140 (2017).
63. Brandt, M. E. & McManus, J. W. Dynamics and impact of the coral disease white plague: insights from a simulation model. *Dis. Aquat. Organ.* **87**, 117–133 (2009).
64. NOAA. Stony Coral Tissue Loss Disease Case Definition. (2018).
65. Ushijima, B. *et al.* Disease Diagnostics and Potential Coinfections by *Vibrio coralliilyticus* During an Ongoing Coral Disease Outbreak in Florida. *Front. Microbiol.* **11**, (2020).
66. Meiling, S. S. *et al.* Variable Species Responses to Experimental Stony Coral Tissue Loss Disease (SCTLD) Exposure. *Front. Mar. Sci.* **8**, (2021).
67. Traylor-Knowles, N. *et al.* Gene Expression Response to Stony Coral Tissue Loss Disease Transmission in *M. cavernosa* and *O. faveolata* From Florida. *Front. Mar. Sci.* **8**, 681563 (2021).

68. Dimos, B. A. *et al.* Adaptive variation in homologue number within transcript families promotes expression divergence in reef-building coral. *Mol. Ecol.* **31**, 2594–2510 (2022).
69. Rohlf, R. V. & Nielsen, R. Phylogenetic ANOVA: The Expression Variance and Evolution Model for Quantitative Trait Evolution. *Syst. Biol.* **64**, 695–708 (2015).
70. The UniProt Consortium. UniProt: the universal protein knowledgebase in 2021. *Nucleic Acids Res.* **49**, D480–D489 (2021).
71. Häcker, H., Tseng, P.-H. & Karin, M. Expanding TRAF function: TRAF3 as a tri-faced immune regulator. *Nat. Rev. Immunol.* **11**, 457–468 (2011).
72. Bakshani, C. R. *et al.* Evolutionary conservation of the antimicrobial function of mucus: a first defence against infection. *Npj Biofilms Microbiomes* **4**, 14 (2018).
73. Wright, R. M. *et al.* Intraspecific differences in molecular stress responses and coral pathobiome contribute to mortality under bacterial challenge in *Acropora millepora*. *Sci. Rep.* **7**, 2609 (2017).
74. Jeon, H.-S. *et al.* SMAD6 Contributes to Patient Survival in Non-Small Cell Lung Cancer and Its Knockdown Reestablishes TGF- β Homeostasis in Lung Cancer Cells. *Cancer Res.* **68**, 9686–9692 (2008).
75. Wenger, Y., Buzgariu, W., Reiter, S. & Galliot, B. Injury-induced immune responses in *Hydra*. *Semin. Immunol.* **26**, 277–294 (2014).
76. Mydlarz, L. D., McGinty, E. S. & Harvell, C. D. What are the physiological and immunological responses of coral to climate warming and disease? *J. Exp. Biol.* **213**, 934–945 (2010).
77. Barshis, D. J. *et al.* Genomic basis for coral resilience to climate change. *Proc. Natl. Acad. Sci.* **110**, 1387–1392 (2013).

78. Pincetic, A., Medina, G., Carter, C. & Leis, J. Avian Sarcoma Virus and Human Immunodeficiency Virus, Type 1 Use Different Subsets of ESCRT Proteins to Facilitate the Budding Process. *J. Biol. Chem.* **283**, 29822–29830 (2008).
79. Meng, B., Ip, N. C. Y., Prestwood, L. J., Abbink, T. E. M. & Lever, A. M. L. Evidence that the endosomal sorting complex required for transport-II (ESCRT-II) is required for efficient human immunodeficiency virus-1 (HIV-1) production. *Retrovirology* **12**, 72 (2015).
80. Han, S.-O., Kommaddi, R. P. & Shenoy, S. K. Distinct roles for β -arrestin2 and arrestin-domain-containing proteins in β 2 adrenergic receptor trafficking. *EMBO Rep.* **14**, 164–171 (2013).
81. Radin, J. N. *et al.* β -Arrestin 1 Participates in Platelet-Activating Factor Receptor-Mediated Endocytosis of *Streptococcus pneumoniae*. *Infect. Immun.* **73**, 7827–7835 (2005).
82. Wei, N., Serino, G. & Deng, X.-W. The COP9 signalosome: more than a protease. *Trends Biochem. Sci.* **33**, 592–600 (2008).
83. Schweitzer, K., Bozko, P. M., Dubiel, W. & Naumann, M. CSN controls NF- κ B by deubiquitinylation of I κ B α . *EMBO J.* **26**, 1532–1541 (2007).
84. Chen, M.-C., Cheng, Y.-M., Sung, P.-J., Kuo, C.-E. & Fang, L.-S. Molecular identification of Rab7 (ApRab7) in *Aiptasia pulchella* and its exclusion from phagosomes harboring zooxanthellae. *Biochem. Biophys. Res. Commun.* **308**, 586–595 (2003).
85. Downs, C. A. *et al.* Symbiophagy as a cellular mechanism for coral bleaching. *Autophagy* **5**, 211–216 (2009).
86. Fuess, L. E., Palacio-Castro, A. M., Butler, C. C., Baker, A. C. & Mydlarz, L. D. Increased Algal Symbiont Density Reduces Host Immunity in a Threatened Caribbean Coral Species, *Orbicella faveolata*. *Front. Ecol. Evol.* **8**, (2020).

87. Rosic, N. N., Pernice, M., Dove, S., Dunn, S. & Hoegh-Guldberg, O. Gene expression profiles of cytosolic heat shock proteins Hsp70 and Hsp90 from symbiotic dinoflagellates in response to thermal stress: possible implications for coral bleaching. *Cell Stress Chaperones* **16**, 69–80 (2011).
88. Levy, S. *et al.* A stony coral cell atlas illuminates the molecular and cellular basis of coral symbiosis, calcification, and immunity. *Cell* **184**, 2973–2987.e18 (2021).
89. Mayfield, A. B., Hsiao, Y.-Y., Fan, T.-Y., Chen, C.-S. & Gates, R. D. Evaluating the temporal stability of stress-activated protein kinase and cytoskeleton gene expression in the Pacific reef corals *Pocillopora damicornis* and *Seriatopora hystrix*. *J. Exp. Mar. Biol. Ecol.* **395**, 215–222 (2010).
90. Herman, P. K. Stationary phase in yeast. *Curr. Opin. Microbiol.* **5**, 602–607 (2002).
91. Muscatine, L., R. McCloskey, L. & E. Marian, R. Estimating the daily contribution of carbon from zooxanthellae to coral animal respiration¹. *Limnol. Oceanogr.* **26**, 601–611 (1981).
92. Crossland, C. J., Barnes, D. J. & Borowitzka, M. A. Diurnal lipid and mucus production in the staghorn coral *Acropora acuminata*. *Mar. Biol.* **60**, 81–90 (1980).
93. Crossland, C. J. In situ release of mucus and DOC-lipid from the corals *Acropora variabilis* and *Stylophora pistillata* in different light regimes. *Coral Reefs* **6**, 35–42 (1987).
94. Chen, S., Zhou, Y., Chen, Y. & Gu, J. fastp: an ultra-fast all-in-one FASTQ preprocessor. *Bioinformatics* **34**, i884–i890 (2018).
95. Prada, C. *et al.* Empty Niches after Extinctions Increase Population Sizes of Modern Corals. *Curr. Biol.* **26**, 3190–3194 (2016).

96. Grabherr, M. G. *et al.* Full-length transcriptome assembly from RNA-Seq data without a reference genome. *Nat. Biotechnol.* **29**, 644–652 (2011).
97. Davies, S. W., Marchetti, A., Ries, J. B. & Castillo, K. D. Thermal and pCO₂ Stress Elicit Divergent Transcriptomic Responses in a Resilient Coral. *Front. Mar. Sci.* **3**, (2016).
98. Haas, B. J. *et al.* De novo transcript sequence reconstruction from RNA-seq using the Trinity platform for reference generation and analysis. *Nat. Protoc.* **8**, 1494–1512 (2013).
99. Kirk, N. L., Howells, E. J., Abrego, D., Burt, J. A. & Meyer, E. Genomic and transcriptomic signals of thermal tolerance in heat-tolerant corals (*Platygyra daedalea*) of the Arabian/Persian Gulf. *Mol. Ecol.* **27**, 5180–5194 (2018).
100. Moya, A. *et al.* Whole Transcriptome Analysis of the Coral *Acropora millepora* Reveals Complex Responses to CO₂-driven Acidification during the Initiation of Calcification. *Mol. Ecol.* **21**, 2440–2454 (2012).
101. van de Water, J. A. J. M. *et al.* Antimicrobial and stress responses to increased temperature and bacterial pathogen challenge in the holobiont of a reef-building coral. *Mol. Ecol.* **27**, 1065–1080 (2018).
102. Huang, Y., Niu, B., Gao, Y., Fu, L. & Li, W. CD-HIT Suite: a web server for clustering and comparing biological sequences. *Bioinformatics* **26**, 680–682 (2010).
103. Simão, F. A., Waterhouse, R. M., Ioannidis, P., Kriventseva, E. V. & Zdobnov, E. M. BUSCO: assessing genome assembly and annotation completeness with single-copy orthologs. *Bioinformatics* **31**, 3210–3212 (2015).
104. Database resources of the National Center for Biotechnology Information. *Nucleic Acids Res.* **44**, D7–D19 (2016).

105. Patro, R., Duggal, G., Love, M. I., Irizarry, R. A. & Kingsford, C. Salmon provides fast and bias-aware quantification of transcript expression. *Nat. Methods* **14**, 417–419 (2017).
106. Bushnell, B. *BBMap: A Fast, Accurate, Splice-Aware Aligner*.
<https://www.osti.gov/biblio/1241166> (2014).
107. Sonesson, C., Love, M. I. & Robinson, M. D. Differential analyses for RNA-seq: transcript-level estimates improve gene-level inferences. *F1000Research* **4**, 1521 (2016).
108. Love, M. I., Huber, W. & Anders, S. Moderated estimation of fold change and dispersion for RNA-seq data with DESeq2. *Genome Biol.* **15**, 550 (2014).
109. Blighe, K., Brown, A.-L., Carey, V., Hooiveld, G. & Lun, A. PCAtools: PCAtools: Everything Principal Components Analysis. Bioconductor version: Release (3.15)
<https://doi.org/10.18129/B9.bioc.PCAtools> (2022).
110. Wright, R. M., Aglyamova, G. V., Meyer, E. & Matz, M. V. Gene expression associated with white syndromes in a reef building coral, *Acropora hyacinthus*. *BMC Genomics* **16**, 371 (2015).
111. Walter, W., Sánchez-Cabo, F. & Ricote, M. GOplot: an R package for visually combining expression data with functional analysis. *Bioinformatics* **31**, 2912–2914 (2015).
112. Emms, D. M. & Kelly, S. OrthoFinder: solving fundamental biases in whole genome comparisons dramatically improves orthogroup inference accuracy. *Genome Biol.* **16**, 157 (2015).
113. Rosset, S. L. *et al.* The Molecular Language of the Cnidarian–Dinoflagellate Symbiosis. *Trends Microbiol.* **29**, 320–333 (2021).

114. Maor-Landaw, K., van Oppen, M. J. H. & McFadden, G. I. Symbiotic lifestyle triggers drastic changes in the gene expression of the algal endosymbiont *Breviolum minutum* (Symbiodiniaceae). *Ecol. Evol.* **10**, 451–466 (2019).
115. Collins, T. J. ImageJ for microscopy. *BioTechniques* **43**, S25–S30 (2007).
116. Howe-Kerr, L. I. *et al.* Symbiont community diversity is more variable in corals that respond poorly to stress. *Glob. Change Biol.* **26**, 2220–2234 (2020).
117. Hume, B. C. C. *et al.* An improved primer set and amplification protocol with increased specificity and sensitivity targeting the Symbiodinium ITS2 region. *PeerJ* **6**, e4816 (2018).
118. Hume, B. C. C. *et al.* SymPortal: A novel analytical framework and platform for coral algal symbiont next-generation sequencing ITS2 profiling. *Mol. Ecol. Resour.* **19**, 1063–1080 (2019).
119. Beavers, K. M. Master Coral database used in USVI SCTLTD Transmission Experiment Gene Expression Analysis. Zenodo <https://doi.org/10.5281/zenodo.7838980> (2023).
120. Beavers, K. M. Stony Coral Tissue Loss Disease Induces Transcriptional Signatures of in situ Degradation of Dysfunctional Symbiodiniaceae. Zenodo <https://doi.org/10.5281/zenodo.7839042> (2023).
121. Bayer, T. *et al.* Symbiodinium Transcriptomes: Genome Insights into the Dinoflagellate Symbionts of Reef-Building Corals. *PLoS ONE* **7**, e35269 (2012).
122. Parkinson, J. E. *et al.* Gene Expression Variation Resolves Species and Individual Strains among Coral-Associated Dinoflagellates within the Genus *Symbiodinium*. *Genome Biol. Evol.* **8**, 665–680 (2016).

123. Davies, S. W., Ries, J. B., Marchetti, A. & Castillo, K. D. Symbiodinium Functional Diversity in the Coral *Siderastrea siderea* Is Influenced by Thermal Stress and Reef Environment, but Not Ocean Acidification. *Front. Mar. Sci.* **5**, 150 (2018).
124. Bellantuono, A. J., Dougan, K. E., Granados-Cifuentes, C. & Rodriguez-Lanetty, M. Free-living and symbiotic lifestyles of a thermotolerant coral endosymbiont display profoundly distinct transcriptomes under both stable and heat stress conditions. *Mol. Ecol.* **28**, 5265–5281 (2019).
125. El-Sayed, A. & Kamel, M. Climatic changes and their role in emergence and re-emergence of diseases. *Environ. Sci. Pollut. Res.* **27**, 22336–22352 (2020).
126. Burge, C. A. & Hershberger, P. K. Climate change can drive marine diseases. in *Marine Disease Ecology* (eds. Behringer, D. C., Silliman, B. R. & Lafferty, K. D.) 83–90 (Oxford University Press, 2020).
127. Mydlarz, L. D. & Palmer, C. V. The presence of multiple phenoloxidases in Caribbean reef-building corals. *Comp. Biochem. Physiol. A. Mol. Integr. Physiol.* **159**, 372–378 (2011).
128. Palmer, C. V., Bythell, J. C. & Willis, B. L. Enzyme activity demonstrates multiple pathways of innate immunity in Indo-Pacific anthozoans. *Proc. R. Soc. B Biol. Sci.* **279**, 3879–3887 (2012).
129. Mydlarz, L. D., Holthouse, S. F., Peters, E. C. & Harvell, C. D. Cellular Responses in Sea Fan Corals: Granular Amoebocytes React to Pathogen and Climate Stressors. *PLOS ONE* **3**, e1811 (2008).
130. Petes, L. E., Harvell, C. D., Peters, E. C., Webb, M. a. H. & Mullen, K. M. Pathogens compromise reproduction and induce melanization in Caribbean sea fans. *Mar. Ecol. Prog. Ser.* **264**, 167–171 (2003).

131. Tavassolifar, M. javad, Vodjgani, M., Salehi, Z. & Izad, M. The Influence of Reactive Oxygen Species in the Immune System and Pathogenesis of Multiple Sclerosis. *Autoimmune Dis.* **2020**, 5793817 (2020).
132. Alfadda, A. A. & Sallam, R. M. Reactive Oxygen Species in Health and Disease. *BioMed Res. Int.* **2012**, e936486 (2012).
133. Lesser, M. P. & Shick, J. M. Effects of irradiance and ultraviolet radiation on photoadaptation in the zooxanthellae of *Aiptasia pallida*: primary production, photoinhibition, and enzymic defenses against oxygen toxicity. *Mar. Biol.* **102**, 243–255 (1989).
134. Nii, C. M. & Muscatine, L. Oxidative Stress in the Symbiotic Sea Anemone *Aiptasia pulchella* (Carlgren, 1943): Contribution of the Animal to Superoxide Ion Production at Elevated Temperature. *Biol. Bull.* **192**, 444–456 (1997).
135. Richier, S., Furla, P., Plantivaux, A., Merle, P.-L. & Allemand, D. Symbiosis-induced adaptation to oxidative stress. *J. Exp. Biol.* **208**, 277–285 (2005).
136. Halliwell, B. Reactive Species and Antioxidants. Redox Biology Is a Fundamental Theme of Aerobic Life. *Plant Physiol.* **141**, 312–322 (2006).
137. Krueger, T. *et al.* Differential coral bleaching—Contrasting the activity and response of enzymatic antioxidants in symbiotic partners under thermal stress. *Comp. Biochem. Physiol. A. Mol. Integr. Physiol.* **190**, 15–25 (2015).
138. Estrada-Saldívar, N., Quiroga-García, B. A., Pérez-Cervantes, E., Rivera-Garibay, O. O. & Alvarez-Filip, L. Effects of the Stony Coral Tissue Loss Disease Outbreak on Coral Communities and the Benthic Composition of Cozumel Reefs. *Front. Mar. Sci.* **8**, (2021).

139. Rosales, S. M. *et al.* Bacterial Metabolic Potential and Micro-Eukaryotes Enriched in Stony Coral Tissue Loss Disease Lesions. *Front. Mar. Sci.* **8**, (2022).
140. Traylor-Knowles, N. *et al.* Advances in coral immunity ‘omics in response to disease outbreaks. *Front. Mar. Sci.* **9**, (2022).
141. Studivan, M. S. *et al.* Reef Sediments Can Act As a Stony Coral Tissue Loss Disease Vector. *Front. Mar. Sci.* **8**, (2022).
142. Deutsch, J. M. *et al.* Metabolomics of Healthy and Stony Coral Tissue Loss Disease Affected *Montastraea cavernosa* Corals. *Front. Mar. Sci.* **8**, (2021).
143. Beavers, K. M. *et al.* Stony coral tissue loss disease induces transcriptional signatures of in situ degradation of dysfunctional Symbiodiniaceae. *Nat. Commun.* **14**, 2915 (2023).
144. Studivan, M. S. *et al.* Stony coral tissue loss disease intervention with amoxicillin leads to a reversal of disease-modulated gene expression pathways. *Mol. Ecol.* **32**, 5394–5413 (2023).
145. Fuess, L. E., Pinzón C., J. H., Weil, E. & Mydlarz, L. D. Associations between transcriptional changes and protein phenotypes provide insights into immune regulation in corals. *Dev. Comp. Immunol.* **62**, 17–28 (2016).
146. Changsut, I., Womack, H. R., Shickle, A., Sharp, K. H. & Fuess, L. E. Variation in symbiont density is linked to changes in constitutive immunity in the facultatively symbiotic coral, *Astrangia poculata*. *Biol. Lett.* **18**, 20220273 (2022).
147. Wall, C. B. *et al.* Shifting baselines: Physiological legacies contribute to the response of reef corals to frequent heatwaves. *Funct. Ecol.* **35**, 1366–1378 (2021).
148. R Core Team. R: A language and environment for statistical computing. R Foundation for Statistical Computing, Vienna, Austria (2022).

149. Ogle, D. H., Doll, J. C., Wheeler, A. P. & Dinno, A. *FSA: Simple Fisheries Stock Assessment Methods*. (2023).
150. Langfelder, P. & Horvath, S. WGCNA: an R package for weighted correlation network analysis. *BMC Bioinformatics* **9**, 559 (2008).
151. Szklarczyk, D. *et al.* STRING v11: protein-protein association networks with increased coverage, supporting functional discovery in genome-wide experimental datasets. *Nucleic Acids Res.* **47**, D607–D613 (2019).
152. Kenkel, C. D. & Matz, M. V. Gene expression plasticity as a mechanism of coral adaptation to a variable environment. *Nat. Ecol. Evol.* **1**, 0014 (2017).
153. Alvarez-Filip, L., González-Barrios, F. J., Pérez-Cervantes, E., Molina-Hernández, A. & Estrada-Saldívar, N. Stony coral tissue loss disease decimated Caribbean coral populations and reshaped reef functionality. *Commun. Biol.* **5**, 1–10 (2022).
154. Brandt, M. E. *et al.* The Emergence and Initial Impact of Stony Coral Tissue Loss Disease (SCTLD) in the United States Virgin Islands. *Front. Mar. Sci.* **8**, (2021).
155. Palmer, C. V. *et al.* Patterns of coral ecological immunology: variation in the responses of Caribbean corals to elevated temperature and a pathogen elicitor. *J. Exp. Biol.* **214**, 4240–4249 (2011).
156. Klein, A. M. *et al.* Algal symbiont genera but not coral host genotypes correlate to stony coral tissue loss disease susceptibility among *Orbicella faveolata* colonies in South Florida. *Front. Mar. Sci.* **11**, (2024).
157. Gates, R. D., Baghdasarian, G. & Muscatine, L. Temperature Stress Causes Host Cell Detachment in Symbiotic Cnidarians: Implications for Coral Bleaching. *Biol. Bull.* **182**, 324–332 (1992).

158. Nielsen, D. A., Petrou, K. & Gates, R. D. Coral bleaching from a single cell perspective. *ISME J.* **12**, 1558–1567 (2018).
159. Oakley, C. A. *et al.* Thermal Shock Induces Host Proteostasis Disruption and Endoplasmic Reticulum Stress in the Model Symbiotic Cnidarian *Aiptasia*. *J. Proteome Res.* **16**, 2121–2134 (2017).
160. Kvitt, H., Rosenfeld, H. & Tchernov, D. The regulation of thermal stress induced apoptosis in corals reveals high similarities in gene expression and function to higher animals. *Sci. Rep.* **6**, 30359 (2016).
161. Cunning, R. & Baker, A. C. Thermotolerant coral symbionts modulate heat stress-responsive genes in their hosts. *Mol. Ecol.* **29**, 2940–2950 (2020).
162. Stelzer, G. *et al.* The GeneCards Suite: From Gene Data Mining to Disease Genome Sequence Analyses. *Curr. Protoc. Bioinforma.* **54**, 1.30.1-1.30.33 (2016).
163. Hetz, C., Zhang, K. & Kaufman, R. J. Mechanisms, regulation and functions of the unfolded protein response. *Nat. Rev. Mol. Cell Biol.* **21**, 421–438 (2020).
164. Schneider, C. A., Rasband, W. S. & Eliceiri, K. W. NIH Image to ImageJ: 25 years of image analysis. *Nat. Methods* **9**, 671–675 (2012).
165. Sully, S., Hodgson, G. & van Woesik, R. Present and future bright and dark spots for coral reefs through climate change. *Glob. Change Biol.* **28**, 4509–4522 (2022).
166. Bruno, J. F. & Selig, E. R. Regional Decline of Coral Cover in the Indo-Pacific: Timing, Extent, and Subregional Comparisons. *PLOS ONE* **2**, e711 (2007).
167. Boström-Einarsson, L. *et al.* Coral restoration – A systematic review of current methods, successes, failures and future directions. *PLOS ONE* **15**, e0226631 (2020).

168. Omori, M. Coral restoration research and technical developments: what we have learned so far. *Mar. Biol. Res.* **15**, 377–409 (2019).
169. Vollmer, S. V., Selwyn, J. D., Despard, B. A. & Roesel, C. L. Genomic signatures of disease resistance in endangered staghorn corals. *Science* **381**, 1451–1454 (2023).
170. Mcleod, E. *et al.* The future of resilience-based management in coral reef ecosystems. *J. Environ. Manage.* **233**, 291–301 (2019).
171. van Oppen, M. J. H., Oliver, J. K., Putnam, H. M. & Gates, R. D. Building coral reef resilience through assisted evolution. *PNAS* **112**, 2307–2313 (2015).
172. Kleypas, J. *et al.* Designing a blueprint for coral reef survival. *Biol. Conserv.* **257**, 109107 (2021).
173. Kramer, P. R., Roth, L. & Lang, J. Map of stony coral tissue loss disease outbreak in the Caribbean. (2019).
174. Alvarez-Filip, L., Estrada-Saldívar, N., Pérez-Cervantes, E., Molina-Hernández, A. & González-Barrios, F. J. A rapid spread of the stony coral tissue loss disease outbreak in the Mexican Caribbean. *PeerJ* **7**, e8069 (2019).
175. Weil, E. *et al.* Spread of the new coral disease “SCTLD” into the Caribbean: implications for Puerto Rico. *Reef Encounter* vol. 34 (2019).
176. Evans, J. S., Paul, V. J., Ushijima, B., Pitts, K. A. & Kellogg, C. A. Investigating microbial size classes associated with the transmission of stony coral tissue loss disease (SCTLD). *PeerJ* **11**, e15836 (2023).
177. Gliddon, H. D., Herberg, J. A., Levin, M. & Kaforou, M. Genome-wide host RNA signatures of infectious diseases: discovery and clinical translation. *Immunology* **153**, 171–178 (2018).

178. Das, P., Roychowdhury, A., Das, S., Roychoudhury, S. & Tripathy, S. sigFeature: Novel Significant Feature Selection Method for Classification of Gene Expression Data Using Support Vector Machine and t Statistic. *Front. Genet.* **11**, (2020).
179. Burzykowski, T., Rousseau, A.-J., Geubbelmans, M. & Valkenborg, D. Introduction to machine learning. *Am. J. Orthod. Dentofacial Orthop.* **163**, 732–734 (2023).
180. Bellman, R. & Kalaba, R. On adaptive control processes. *IRE Trans. Autom. Control* **4**, 1–9 (1959).
181. Guyon, I., Weston, J., Barnhill, S. & Vapnik, V. Gene Selection for Cancer Classification using Support Vector Machines. *Mach. Learn.* **46**, 389–422 (2002).
182. Liang, Y. *et al.* Prediction of Drought-Resistant Genes in *Arabidopsis thaliana* Using SVM-RFE. *PLOS ONE* **6**, e21750 (2011).
183. Richhariya, B., Tanveer, M. & Rashid, A. H. Diagnosis of Alzheimer’s disease using universum support vector machine based recursive feature elimination (USVM-RFE). *Biomed. Signal Process. Control* **59**, 101903 (2020).
184. Stanzione, D. *et al.* Frontera: The Evolution of Leadership Computing at the National Science Foundation. in *Practice and Experience in Advanced Research Computing* 106–111 (Association for Computing Machinery, New York, NY, USA, 2020).
doi:10.1145/3311790.3396656.
185. Sayers, E. W. *et al.* Database resources of the National Center for Biotechnology Information. *Nucleic Acids Res.* **50**, D20–D26 (2021).
186. Haas, B.J. TransDecoder. *TransDecoder* <https://github.com/TransDecoder/TransDecoder>.
187. Paysan-Lafosse, T. *et al.* InterPro in 2022. *Nucleic Acids Res.* **51**, D418–D427 (2022).

188. Uddin, S., Khan, A., Hossain, M. E. & Moni, M. A. Comparing different supervised machine learning algorithms for disease prediction. *BMC Med. Inform. Decis. Mak.* **19**, 281 (2019).
189. Imbs, A. B. & Dembitsky, V. M. Coral Lipids. *Mar. Drugs* **21**, 539 (2023).
190. Papina, M., Meziane, T. & van Woesik, R. Symbiotic zooxanthellae provide the host-coral *Montipora digitata* with polyunsaturated fatty acids. *Comp. Biochem. Physiol. B Biochem. Mol. Biol.* **135**, 533–537 (2003).
191. Clark, D. A. & Coker, R. Molecules in focus Transforming growth factor-beta (TGF- β). *Int. J. Biochem. Cell Biol.* **30**, 293–298 (1998).
192. Detournay, O., Schnitzler, C. E., Poole, A. & Weis, V. M. Regulation of cnidarian–dinoflagellate mutualisms: Evidence that activation of a host TGF β innate immune pathway promotes tolerance of the symbiont. *Dev. Comp. Immunol.* **38**, 525–537 (2012).
193. Berthelie, J. *et al.* Implication of the host TGF β pathway in the onset of symbiosis between larvae of the coral *Fungia scutaria* and the dinoflagellate *Symbiodinium* sp. (clade C1f). *Coral Reefs* **36**, 1263–1268 (2017).
194. Fuess, L. E., Mann, W. T., Jinks, L. R., Brinkhuis, V. & Mydlarz, L. D. Transcriptional analyses provide new insight into the late-stage immune response of a diseased Caribbean coral. *R. Soc. Open Sci.* **5**, 172062 (2018).
195. Rosenstiel, P. *et al.* Regulation of *DMBT1* via NOD2 and TLR4 in Intestinal Epithelial Cells Modulates Bacterial Recognition and Invasion. *J. Immunol.* **178**, 8203–8211 (2007).
196. McDowell, I. C. *et al.* Transcriptome of American Oysters, *Crassostrea virginica*, in Response to Bacterial Challenge: Insights into Potential Mechanisms of Disease Resistance. *PLOS ONE* **9**, e105097 (2014).

197. Riesgo, A. *et al.* Transcriptomic analysis of differential host gene expression upon uptake of symbionts: a case study with Symbiodinium and the major bioeroding sponge *Cliona varians*. *BMC Genomics* **15**, 376 (2014).
198. Tsugeki, R. *et al.* NO VEIN Mediates Auxin-Dependent Specification and Patterning in the Arabidopsis Embryo, Shoot, and Root. *Plant Cell* **21**, 3133–3151 (2009).
199. Gonen, N., Meller, A., Sabath, N. & Shalgi, R. Amino Acid Biosynthesis Regulation during Endoplasmic Reticulum Stress Is Coupled to Protein Expression Demands. *iScience* **19**, 204–213 (2019).
200. Howe, R., Kelly, M., Jimah, J., Hodge, D. & Odom, A. R. Isoprenoid Biosynthesis Inhibition Disrupts Rab5 Localization and Food Vacuolar Integrity in Plasmodium falciparum. *Eukaryot. Cell* **12**, 215–223 (2013).
201. Fransolet, D., Roberty, S. & Plumier, J.-C. Establishment of endosymbiosis: The case of cnidarians and Symbiodinium. *J. Exp. Mar. Biol. Ecol.* **420–421**, 1–7 (2012).
202. Chen, M.-C., Cheng, Y.-M., Hong, M.-C. & Fang, L.-S. Molecular cloning of Rab5 (ApRab5) in *Aiptasia pulchella* and its retention in phagosomes harboring live zooxanthellae. *Biochem. Biophys. Res. Commun.* **324**, 1024–1033 (2004).
203. Hashim, S., Mukherjee, K., Raje, M., Basu, S. K. & Mukhopadhyay, A. Live Salmonella Modulate Expression of Rab Proteins to Persist in a Specialized Compartment and Escape Transport to Lysosomes*. *J. Biol. Chem.* **275**, 16281–16288 (2000).
204. Via, L. E. *et al.* Arrest of Mycobacterial Phagosome Maturation Is Caused by a Block in Vesicle Fusion between Stages Controlled by rab5 and rab7*. *J. Biol. Chem.* **272**, 13326–13331 (1997).

205. Alvarez-Dominguez, C., Barbieri, A. M., Berón, W., Wandinger-Ness, A. & Stahl, P. D. Phagocytosed Live *Listeria monocytogenes* Influences Rab5-regulated in Vitro Phagosome-Endosome Fusion*. *J. Biol. Chem.* **271**, 13834–13843 (1996).
206. Brown, B. & Bythell, J. Perspectives on mucus secretion in reef corals. *Mar. Ecol. Prog. Ser.* **296**, 291–309 (2005).
207. Lamberti, G., Gügel, I. L., Meurer, J., Soll, J. & Schwenkert, S. The Cytosolic Kinases STY8, STY17, and STY46 Are Involved in Chloroplast Differentiation in *Arabidopsis*1[W]. *Plant Physiol.* **157**, 70–85 (2011).
208. Brown, G. D., Willment, J. A. & Whitehead, L. C-type lectins in immunity and homeostasis. *Nat. Rev. Immunol.* **18**, 374–389 (2018).
209. Emery, M. A., Dimos, B. A. & Mydlarz, L. D. Cnidarian Pattern Recognition Receptor Repertoires Reflect Both Phylogeny and Life History Traits. *Front. Immunol.* **12**, (2021).
210. Davy, S. K., Allemand, D. & Weis, V. M. Cell Biology of Cnidarian-Dinoflagellate Symbiosis. *Microbiol. Mol. Biol. Rev.* **76**, (2012).
211. Mansfield, K. M. *et al.* Transcription factor NF- κ B is modulated by symbiotic status in a sea anemone model of cnidarian bleaching. *Sci. Rep.* **7**, 16025 (2017).
212. Rivera, H. E. & Davies, S. W. Symbiosis maintenance in the facultative coral, *Oculina arbuscula*, relies on nitrogen cycling, cell cycle modulation, and immunity. *Sci. Rep.* **11**, 21226 (2021).
213. Weis, V. M. Cell Biology of Coral Symbiosis: Foundational Study Can Inform Solutions to the Coral Reef Crisis. *Integr. Comp. Biol.* **59**, 845–855 (2019).
214. Mansfield, K. M. & Gilmore, T. D. Innate immunity and cnidarian-Symbiodiniaceae mutualism. *Dev. Comp. Immunol.* **90**, 199–209 (2019).

215. Zhao, Y. G. & Zhang, H. Autophagosome maturation: An epic journey from the ER to lysosomes. *J. Cell Biol.* **218**, 757–770 (2018).
216. Desalvo, M. K. *et al.* Differential gene expression during thermal stress and bleaching in the Caribbean coral *Montastraea faveolata*. *Mol. Ecol.* **17**, 3952–3971 (2008).
217. Smith, E. G., D'Angelo, C., Salih, A. & Wiedenmann, J. Screening by coral green fluorescent protein (GFP)-like chromoproteins supports a role in photoprotection of zooxanthellae. *Coral Reefs* **32**, 463–474 (2013).
218. Lesser, M. P. Oxidative stress causes coral bleaching during exposure to elevated temperatures. *Coral Reefs* **16**, 187–192 (1997).
219. Berkelmans, R. & van Oppen, M. J. H. The role of zooxanthellae in the thermal tolerance of corals: a 'nugget of hope' for coral reefs in an era of climate change. *Proc. R. Soc. B Biol. Sci.* **273**, 2305–2312 (2006).